COHERENT MANIPULATION OF ATOMS AND MOLECULES BY SEQUENTIAL LASER PULSES

N. V. VITANOV
Helsinki Institute of Physics, PL 9, 00014 University of Helsinki, Finland

M. FLEISCHHAUER
Fachbereich Physik, Universität Kaiserslautern, 67653 Kaiserslautern, Germany

B. W. SHORE
Lawrence Livermore National Laboratory, Livermore, California 94550[1]

K. BERGMANN
Fachbereich Physik, Universität Kaiserslautern, 67653 Kaiserslautern, Germany

I. Introduction 57
A. Early Days of Laser State Selection 59
B. Incoherent Population Transfer Schemes 62
1. Incoherent Excitation of Two-State Systems 62
2. Optical Pumping 63
3. Stimulated Emission Pumping 64
C. Coherent Population Transfer 64
1. Resonant Coherent Excitation: Rabi Oscillations 65
2. Three-State Systems 66
II. Principles of Coherent Excitation 67
A. Coherent Excitation 67
B. Partial Coherence: The Density Matrix 68
C. Two States 69
1. The Rotating Wave Approximation (RWA) 69
2. Rabi Cycling 70
3. Probability Loss 71
4. Adiabatic States and Adiabatic Following 72
5. Rapid Adiabatic Passage 73
6. Estimating Transition Probabilities 75

N. V. Vitanov is also affiliated with the Department of Physics, Sofia University, James Boucher 5 blvd., 1126 Sofia, Bulgaria, and Institute of Solid State Physics, Bulgarian Academy of Sciences, 1784 Sofia, Bulgaria.

[1]Retired.

ISBN 0-12-003846-3/ISSN 1049-250X/01 $35.00

D. Three States 76
1. The Three-State RWA Hamiltonian 76
2. Pulse Sequences 77
3. Adiabatic Elimination 78
4. Autler-Townes Splitting 79
III. Three-State STIRAP: Theory 82
A. Basic Properties of STIRAP 82
1. Basic Equations and Definitions 82
2. Adiabatic States 83
3. The STIRAP Mechanism 85
4. Five-Stage Description of STIRAP 86
5. Intermediate-State Population: Importance of the Null Eigenvalue . . 88
6. Intuitive versus Counterintuitive Pulse Sequences 89
7. Adiabatic Condition: Local and Global Criteria 90
8. Nonadiabatic Transitions 92
B. Sensitivity of STIRAP to Interaction Parameters. 93
1. Sensitivity to Delay 93
2. Sensitivity to Rabi Frequency and Pulse Width. 94
3. Sensitivity to Single-Photon Detuning 94
4. Sensitivity to Two-Photon Detuning. 95
5. Sensitivity to Losses from the Intermediate State 97
6. Sensitivity to Beam Geometry 100
7. Multiple Intermediate States 101
8. STIRAP Beyond the RWA. 102
IV. Three-State STIRAP: Experiments 103
A. Experimental Demonstrations with CW Lasers 103
1. Sodium Dimers 103
2. Metastable Neon Atoms 104
B. Experimental Demonstrations with Pulsed Lasers 107
1. General Considerations for Pulsed Lasers 107
2. Nitrous Oxide Molecules 108
3. Sulfur Dioxide Molecules 109
4. STIRAP in a Ladder System: Rubidium Atoms 111
C. STIRAP with Degenerate or Nearly Degenerate States. 111
V. STIRAP-Like Population Transfer in Multistate Chains 117
A. Resonantly Driven Chains with Odd Number of States. 118
B. Resonantly Driven Chains with Even Number of States 120
C. The Off-Resonance Case 121
D. Optimization of Multistate STIRAP: Dressed-State Picture 124
VI. Adiabatic Momentum Transfer 126
A. Coherent Matter-Wave Manipulation 127
1. Atomic Mirrors 127
2. Atomic Beam Splitters 130
3. Atomic Interferometers 131
B. Coherent Manipulation of Laser-Cooled and Trapped Atoms. 133
C. Measurement of Weak Magnetic Fields with Larmor Velocity Filter . . . 134
VII. Branched-Chain Excitation 135
A. Branched Linkage Patterns 135
B. The Tripod Linkage. 136
1. Concept 136

2. The Tripod Linkage . . . 136
3. Adiabatic Evolution . . . 137
C. Experimental Demonstration . . . 141
VIII. Population Transfer via a Continuum of Intermediate States . . . 143
A. Laser-Induced Continuum Structure . . . 145
1. LICS Equations . . . 145
2. Coherent and Incoherent Channels . . . 146
3. Fano Profile . . . 146
4. Population Trapping: Dark and Bright States . . . 149
B. Population Transfer via a Continuum . . . 150
1. Population Transfer in the Ideal Case . . . 150
2. Satisfying the Trapping Condition . . . 151
3. Suppressing Incoherent Ionization . . . 152
C. Tripod Coupling via a Continuum . . . 155
IX. Extensions and Applications of STIRAP . . . 156
A. Control of Chemical Reactions . . . 156
B. Hyper-Raman STIRAP (STIHRAP) . . . 156
C. Stark-Chirped Rapid Adiabatic Passage . . . 157
1. Theory . . . 158
2. Experimental Demonstration . . . 160
D. Adiabatic Passage by Light-Induced Potentials (APLIP) . . . 161
E. Photoassociative STIRAP as a Source for Cold Molecules . . . 161
X. Propagation Phenomena . . . 162
A. Electromagnetically Induced Transparency (EIT) . . . 163
1. Complete Decoupling of Light and Matter . . . 163
2. Elimination of Absorption; Slow Light . . . 165
B. Adiabatons . . . 167
C. Matched Pulses . . . 168
D. Coherence Transfer between Matter and Light . . . 170
XI. Applications of STIRAP in Quantum Optics and Quantum Information . . . 173
A. Single-Atom Cavity Quantum Electrodynamics . . . 173
B. Quantum Logic Gates Based on Cavity QED . . . 175
C. Quantum Networking . . . 177
D. Many-Atom Systems . . . 177
XII. Summary and Outlook . . . 179
XIII. Acknowledgments . . . 180
XIV. References . . . 180

I. Introduction

Many branches of contemporary physics require atoms or molecules prepared in specified quantum states—not only for traditional studies of state-to-state collision dynamics, isotope separation, or laser-controlled chemical reactions, but also in more recently developing research areas of atom optics and quantum information. Of greatest interest is the fraction of all atoms or molecules in a specific state, a time-varying probability here termed the *population* $P(t)$. Schemes for transferring population selectively (i.e., to a single predetermined quantum state), such as

excitation with frequency-swept pulses and stimulated Raman adiabatic passage (STIRAP), have opened new opportunities for coherent control of atomic and molecular processes. With the growing interest in quantum information, there is also concern with creating and controlling specified coherent superpositions of quantum states. These more general properties of an ensemble of atoms or molecules are embodied in the time-varying state vector $\Psi(t)$.

This chapter describes the basic principles underlying a variety of techniques that can be used to control state vectors and, in particular, to transfer population, selectively, between quantum states of atoms or molecules. We also describe experimental demonstrations of the various principles. (Aspects of these population transfer schemes have been reviewed by Vitanov *et al.*, 2001.) All the methods share a common reliance on adiabatic time evolution, induced by a sequence of delayed, but partially overlapping, laser pulses. They begin with an ensemble of atoms or molecules in which the population is in a specified discrete quantum state. Then the sequence of laser pulses forces the population into a desired target state. Only highly monochromatized light can provide the selectivity needed to isolate a single final state—broadband light or charged particle pulses cannot so discriminate. The control of phase imposes further constraints; it requires coherent radiation, available only from a laser.

One goal of the theory of coherent excitation is to predict, for a given set of radiation pulses, the probability that atoms will undergo a transition between the initial state and the desired target state (the population *transfer efficiency*). More generally, theory can predict the changes of a state vector $\Psi(t)$ produced by specified radiation. Alternatively, theory can provide a prescription for pulses that will produce a desired population transfer or state vector change.

We begin our discussion, in Section I.A, with a brief summary of the historical background for the subsequent discussions of adiabatic transfer schemes. Although the excitation techniques described in this chapter require coherent radiation, incoherent light, such as that from filtered atomic vapor lamps or from broadband lasers with poor coherence properties, also has very useful applications for selective excitation, some of which are described briefly in Section I.B. Coherent excitation differs qualitatively from incoherent excitation. To emphasize this difference, Section I.C contrasts some simple examples.

Starting with Section II, we develop the general mathematical principles needed to describe coherent excitation and adiabatic time evolution of quantum systems. In Section III we apply this to the basic STIRAP process, wherein adiabatic evolution produces complete population transfer in a three-state Raman system. Section IV discusses various experimental demonstrations of the STIRAP technique. Sections V–VIII describe various theoretical and experimental extensions of the original three-state STIRAP. Although our primary concern is with the effect of prescribed fields on atoms, the atomic excitation creates localized polarization which alters the radiation as it propagates; Section X discusses some of the effects to be found by treating the field and the atoms together. Section XI

discusses some applications of the STIRAP principles in the rapidly growing area of quantum information and in the general area of quantum optics. Section XII offers a summary and comments on possible future work.

A. Early Days of Laser State Selection

The use of lasers to address individual states in atoms or molecules dates back more than 30 years [for reviews see Bergmann (1988), Rubahn and Bergmann (1990)]. The early work, taking advantage of the small bandwidth and high spectral power density of laser radiation, employed lasers to populate individual rotational-vibrational levels in an electronically excited state of molecules, as preparation for collision studies (Kurzel and Steinfeld 1970; Bergmann and Demtröder, 1971) or for spectroscopic analysis (Demtröder *et al.*, 1969). Later, individual thermally populated states in the electronic ground state were labeled through population depletion by optical pumping (Bergmann *et al.*, 1978; Gottwald *et al.*, 1986). That work paved the way for detailed studies in crossed molecular beams involving molecules in preselected rotational (Hefter *et al.*, 1981) or individual vibrational states (Ziegler *et al.*, 1988) colliding with atoms (Gottwald *et al.*, 1987) or electrons (Ziegler *et al.*, 1987). By 1986 laser state selection by population depletion had even been developed sufficiently to allow collision studies of molecules in individual magnetic sublevels (Mattheus *et al.*, 1986; Hefter *et al.*, 1986) with high resolution of the scattering angle.

State selection by population depletion through optical pumping is limited to thermally populated levels. Access to higher lying vibrationally excited levels in the electronic ground state was gained by the Franck–Condon pumping method (Rubahn and Bergmann, 1990) whereby excitation, from thermally populated levels (j'', v''), into a suitably chosen rovibrational level (j', v') in the electronically excited state, followed by spontaneous decay back to the electronic ground state, establishes a distribution $f_{v'}(v'')$ of population over vibrationally excited levels v''. Within the limits given by the optical transition rates, the distribution $f_{v'}(v'')$ can be controlled by a suitable choice of the level v'.

In the early 1980s, high-power pulsed lasers became more readily available and a variety of other schemes for laser state selection, in particular for the population of vibrationally excited levels in the electronic ground state, such as overtone pumping (OTP) (Crim, 1984) or off-resonance stimulated Raman scattering (ORSRS) (Orr *et al.*, 1984; Meier *et al.*, 1986), were developed. In OTP, levels $v'' > 1$ are directly excited from $v'' = 0$ in a single photon transition. High laser power is needed because the transition probability decreases rapidly with $\Delta v''$. Only a small fraction of the molecules are typically excited to high-lying levels. In ORSRS the frequency difference between a strong (possibly fixed frequency) laser and a tunable laser matches the transition frequency between rotational levels in the vibrational states $v'' = 0$ and $v'' = 1$. A substantial fraction (<50%) of the molecules in a given state $(j'', v'' = 0)$ can be excited to $v'' = 1$.

Another two-step process, *stimulated emission pumping* (SEP) (Kittrell *et al.*, 1981), has proven to be a flexible and very successful method for population transfer. In SEP a suitable level in an electronic state is excited. Rather than allowing spontaneous emission to distribute the population over many vibrational levels, another laser, the frequency of which is tuned to resonance with the desired target state, forces as much as 50% of the electronically exited molecules into that state. However, about 50% of the population will remain in the excited electronic state and will subsequently be distributed by spontaneous emission over other vibrational levels v''.

In the context of this early work the coherence properties of the radiation were not essential. It was therefore natural, in seeking to improve the flexibility of state selection, to look for schemes which also exploit coherence properties of lasers. Of particular interest were methods that would efficiently and selectively populate high-lying vibrational levels of molecules, which otherwise were not accessible for detailed collision studies.

The attempts to *selectively* populate high-lying levels in the electronic ground state led to the development of a Raman laser that utilized a molecular beam as a gain medium (Jones *et al.*, 1983; Hefter *et al.*, 1985). In that work, a ring cavity was built around a molecular beam whose axis coincided with the waist of the cavity (Fig. 1). The directional flow carried molecules into and out of the active region of

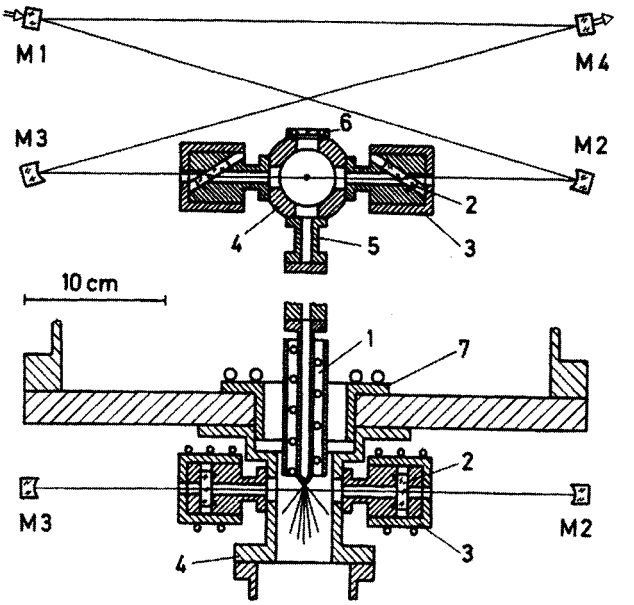

FIG. 1. Raman laser with molecular beam and ring cavity. Top and side view. (From P. L. Jones, U. Gaubatz, U. Hefter, B. Wellegehausen, and K. Bergmann. An optically pumped sodium-dimer supersonic beam laser. *Appl. Phys. Lett.* 1983;42:222–224.)

the laser cavity. A pump laser, propagating along the cavity axis, coupled thermally populated levels (j'', $v'' = 0$) to near resonance with levels v' in an electronically excited state. When implemented with a beam of sodium dimers, the rotational degree of freedom was cooled to a temperature of the order of $T_{\text{rot}} = 20\,\text{K}$ by supersonic expansion. Therefore the density of molecules in levels (j'', $v'' = 0$) with $j'' < 15$ was sufficiently high to provide a substantial gain. Thus, driven by the pump laser, Stokes radiation was generated in the cavity. Intracavity filters restricted laser oscillation to a single vibrational band $v' \rightarrow v''$, thereby providing the desired selectivity. Indeed, it was found (Becker *et al.*, 1987) that up to 70% of the molecules in (j'', $v'' = 0$) could be transferred to a specific level (j'', $v'' = 5$).

Further analysis of the scheme revealed, however, that the coincidence of the axis of the pump beam and the generated Stokes beam limited the achievable transfer efficiency for the following reason (see Fig. 2). The transit time of the molecules across the waist of the cavity was about an order of magnitude longer than the radiative lifetime in the electronically excited state. Near the axis of the cavity, the Stokes radiation (established during the prior buildup of laser oscillation) was sufficiently strong to compete successfully with spontaneous emission and thus to force the molecules into the desired state v'' by a Raman process. However, detrimental processes are unavoidable as the molecules enter or leave the cavity. When entering the cavity, the molecules are exposed to pump radiation while the Stokes radiation is still weak. Therefore, the latter cannot yet compete with the spontaneous emission and a fraction of the molecules is lost by optical pumping to other vibrational levels. Detuning the pump laser from resonance with the level v' would not cure the problem: although detuning would reduce the loss rate, the gain would be reduced as well. As the molecules, placed into a level $v'' \gg 1$ near the center of the pump and Stokes beams, leave the cavity, they are still exposed to the Stokes radiation. This, again, leads to some loss of molecules due to optical pumping.

Obviously, the detrimental losses due to spontaneous emission could be reduced when the axis of the Stokes laser beam, provided by an external source rather than generated in the cavity, would be shifted upstream of the axis of the pump laser,

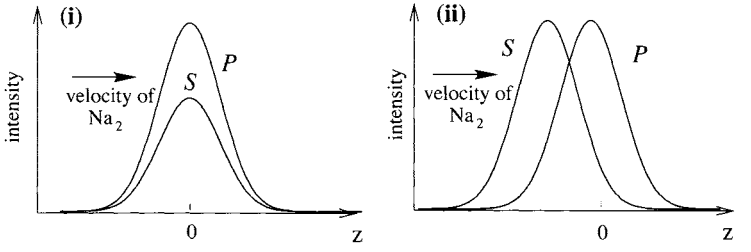

FIG. 2. (i) Profile of pump and Stokes laser intensities. The z axis is parallel to the axis of the molecular beam; $z = 0$ corresponds to the intersection with the cavity waist. (ii) Same as (i) but with Stokes field shifted somewhat upstream.

while retaining some overlap of the beams. Although that reasoning aimed at the reduction of the losses due to incoherent processes, it led quickly to the development of the stimulated Raman adiabatic passage process (STIRAP). Encouraging results were obtained from numerical studies, including incoherent processes, and were supported by first experimental evidence (Gaubatz *et al.*, 1988), before the basic theory and experimental technique was fully developed (Gaubatz *et al.*, 1990).

It is important to note that already in 1984, Oreg *et al.* had published theoretical work that included the essential elements of the consequences of sequential pulse interaction, namely, 100% transfer efficiency when the Stokes radiation interacts first. However, the practical relevance of the result of that work remained unrecognized until the phenomenon was independently rediscovered and the method developed in Kaiserslautern.

B. Incoherent Population Transfer Schemes

1. Incoherent Excitation of Two-State Systems

Until the advent of laser light sources, theoretical descriptions of radiative excitation followed the lead of Einstein, who treated two-state atoms within a radiation-filled cavity (Einstein, 1917). With this approach one postulates a set of equations for the rate of change in atomic populations exposed to beams of light, the *radiative rate equations,*

$$\frac{d}{dt}P_n(t) = \sum_m R_{n,m}(t)P_m(t), \tag{1}$$

linking the various changes in probabilities $P_n(t)$ by a matrix of rate coefficients $R_{n,m}(t)$ in which excitation and stimulated emission rates for two-state atoms are proportional to the instantaneous radiation intensity $I(t)$ (power per unit area) and to the Einstein–Milne B coefficient, and in which spontaneous emission from the excited state (level 2) takes place at a rate A (cf. Shore, 1990, sect. 2.2). When all the two-level atoms are initially (at time $t \to -\infty$) unexcited (in state 1), when the radiation is sufficiently intense (the *saturated* regime in which spontaneous emission has a negligible effect, $BI \gg A$), and when the two levels have the same degeneracy, then the excited-state population at time t is

$$P_2(t) = \tfrac{1}{2}\left[1 - e^{-BF(t)}\right], \tag{2}$$

where $F(t) = \int_{-\infty}^{t} I(t')\,dt'$ is the pulsed radiation *fluence* (energy per unit area) up to time t. As this expression shows, an increase of pulse fluence always increases the excited-state population, which approaches monotonically the saturation value of 50%. This is the best population-transfer efficiency achievable with incoherent

light. Once the radiation ceases, the atoms will spontaneously emit radiation and return (with exponential decay at rate A) to lower-lying levels. Eventually no excitation will remain; any excitation must be maintained by radiation.

2. *Optical Pumping*

The presence of spontaneous emission hinders direct excitation by providing an ever-present deexcitation rate. However, when one deals with more than two levels, spontaneous emission offers a mechanism for creating complete population transfer. The procedure can be understood from Fig. 3a: a radiation beam resonantly couples the initially populated state ψ_1 to the excited state ψ_2, from which spontaneous emission occurs. This uncontrolled radiative decay not only returns population to state ψ_1, it also takes some population into a third state ψ_3 that is unaffected by the radiation beam. (Either its energy lies far from resonance with the initial state or it is prevented from interacting by selection rules based on polarization of the light.) Each time an atom in state ψ_1 absorbs a photon, there is a chance that the resulting decay of excited state ψ_2 will carry population into state ψ_3. Once population is in state ψ_3 it is immune to further action by the radiation. If there are no other decay options than those to ψ_1 and ψ_3, the resulting population transfer, *optical pumping,* will eventually place all population into state ψ_3.

The simplicity of optical pumping has led to widespread use as a means of preparing atoms or molecules in a well-defined ground or metastable state—it requires only a single light source, which need not be a laser. Its main limitation is the lack of selectivity: the spontaneous emission step will generally place population in a mixture of final states—all the states into which the pump-excited state ψ_2 can decay. The distribution of final populations is determined by the relative decay rates that link each final state with the excited state. For vibrational transitions in molecules these rates are proportional to Franck–Condon factors. These rarely exceed a few percent, and so the selectivity is correspondingly low. Furthermore,

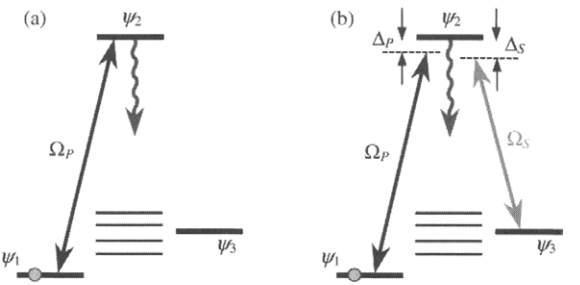

FIG. 3. (a) Linkage diagram for optical pumping. A pump field (not necessarily a laser) excites state ψ_2, which spontaneously decays either back to state ψ_1, or to state ψ_3, or possibly to some other states. (b) Linkage diagram for stimulated emission pumping. A pump field populates state ψ_2, and a subsequent Stokes (or dump) field populates state ψ_3.

optical pumping has limited use in optically thick vapors: subsequent absorption of the spontaneous-emission photons will reexcite the atoms, via the transition ψ_3 to ψ_2. Finally, the buildup of population in the target state takes place gradually, at a rate fixed by the A coefficient. It is therefore not possible to use optical pumping to move population more rapidly than this.

3. *Stimulated Emission Pumping*

Although optical pumping uses only a single light source, the overall population transfer involves two photons, as a Raman process: a *pump* photon from the imposed light source followed by a spontaneously emitted *Stokes* photon. It is natural to consider a *stimulated* Raman process in which externally supplied fields drive both transitions. A strong stimulated emission field will induce a transition to a selected final state, rather than to the mixture that would occur with spontaneous emission.

In one form of this two-photon process of population transfer, *stimulated emission pumping* (SEP) (Dai and Field, 1995), a pump field first places population from the initial state ψ_1 into the excited state ψ_2. Some time later a Stokes (or dump) field transfers population into the desired final state ψ_3 (hence the names *pump and dump*). Figure 3b depicts the relevant Λ-type linkage.

Because of its simplicity, the SEP technique has enjoyed widespread application in collision dynamics and spectroscopy (Hamilton *et al.*, 1986; Dai and Field, 1995). Its main limitation is the low efficiency: typically the transfer efficiency does not exceeds 10%, but this is quite adequate for many spectroscopic studies.

The reason for low efficiency is readily understood. If the intensity of the pump laser is sufficiently strong to saturate the $\psi_1 \leftrightarrow \psi_2$ transition, then, as suggested by the solution to the two-level rate equations, at most 50% of the population will be transferred from state ψ_1 to state ψ_2. If the Stokes laser is also sufficiently strong to saturate its transition, then half of the population in state ψ_2 will be subsequently transferred to the target state ψ_3. Therefore at most one-quarter of the population can be transferred to the target state. Half of the population remains in the initial state, and the remaining quarter is distributed according to the branching of spontaneous emission from state ψ_2.

SEP efficiency can be improved slightly if the pump and Stokes pulses are applied simultaneously, rather than successively. If they are sufficiently strong to saturate the transitions, thereby equalizing the populations, then one-third of the population can be transferred to the target state ψ_3.

C. Coherent Population Transfer

The response of a quantum system to coherent (laser) radiation differs significantly from its response to light from a lamp, even a very monochromatic lamp. Whereas the sudden application of *incoherent* radiation to an atom or molecule typically

results in a monotonic approach to some equilibrium excitation, the sudden application of steady *coherent* radiation typically produces oscillating populations. These differences are clearly seen in the behavior of two-state systems, as noted below. They are equally evident in multilevel systems.

1. Resonant Coherent Excitation: Rabi Oscillations

The excited population $P_2(t)$ of a two-state system exposed to steady coherent radiation does not follow any monotonically increasing pattern, such as Eq. (2). Instead it oscillates sinusoidally (*Rabi oscillations*). When the radiation is resonant (the carrier frequency equal to the Bohr frequency), the result is

$$P_2(t) = \tfrac{1}{2}[1 - \cos(\Omega t)]. \tag{3}$$

The frequency of population oscillation, the *Rabi frequency* Ω, will be associated below with the strength of the atom–radiation interaction. As will be shown, it is proportional to the square root of the laser intensity.

When the radiation intensity varies, then so does the Rabi frequency $\Omega(t)$, and the cosine argument Ωt is replaced by the so-called *pulse area* $A(t)$, or time integral of the Rabi frequency,

$$\Omega t \rightarrow \int_{-\infty}^{t} \Omega(t')\, dt' \equiv A(t). \tag{4}$$

Unlike the monotonic approach to a steady saturation value observed for incoherent excitation, here the excited-state population oscillates between 0 and 1. At times when the pulse area $A(t)$ is an odd multiple of π (odd-π pulses) the population resides entirely in the excited state: the population is completely *inverted*. (Recall that with incoherent excitation, no more than half the population can be excited.) For pulse areas equal to even multiples of π (even-π pulses), the system returns to the initial state.

Although it is useful to consider single stationary atoms, in practice one must deal with an ensemble of atoms or molecules, often with a distribution of velocities. Atoms that move in the direction of a traveling wave experience a Doppler-shifted laser field, so their excitation is not exactly resonant. As noted in Eq. (18), their population oscillations are more rapid and have smaller peak values than do those of resonant atoms. Atoms that move across a laser beam will experience a pulse area that is dependent on the duration of their transit time across the beam, and hence on their velocity. These velocity-dependent interactions, and the presence of fluctuations in the laser intensity, require an averaging over excitation probabilities. The result is an effective excitation probability that has less pronounced oscillations; in extreme cases the averaging can bring the excitation probability to 0.5, the same as with incoherent excitation.

2. Three-State Systems

The oscillatory Rabi cycling characteristic of two-state systems can also be found in multistate systems. One example is a coherently driven three-state system subjected to the same pulse sequence as in SEP: first the pump pulse, followed after its completion (without overlap) by the Stokes pulse. Then the excitation can still be considered as a two-step process, but the probabilities for each step are different from those in SEP. In the case of exact single-photon resonances the transition probabilities P_{12} from state ψ_1 to state ψ_2 and P_{23} from state ψ_2 to state ψ_3 are

$$P_{12} = \tfrac{1}{2}(1 - \cos A_p), \qquad P_{23} = \tfrac{1}{2}(1 - \cos A_s). \tag{5}$$

where A_p and A_s are the pump and Stokes pulse areas [as in Eq. (3)]. If the system is initially in state ψ_1, then the population of state ψ_3 after the excitation is the product of the two probabilities,

$$P_{13} = \tfrac{1}{4}(1 - \cos A_p)(1 - \cos A_s). \tag{6}$$

Hence, when the pulse areas are both equal to odd multiples of π, there occurs complete population transfer from state ψ_1 to state ψ_3. However, the transfer efficiency depends strongly on the pulse areas, and it can even vanish (when A_p or A_s is an even multiple of π).

When the pump and Stokes pulses share a common time dependence, the population changes can no longer be separated into two consecutive independent two-state transitions. Nevertheless, an exact analytic expression can still be derived. If the system is initially in state ψ_1 and the two lasers are each resonantly tuned, then the population of state ψ_3 at the end of the excitation pulse is

$$P_{13} = \frac{A_p A_s}{A}\left(1 - \cos \tfrac{1}{2}A\right), \tag{7}$$

where $A = \sqrt{A_p^2 + A_s^2}$. Here again, the transfer efficiency depends on the pulse areas: complete population transfer from state ψ_1 to state ψ_3 occurs whenever $A = 2(2k + 1)\pi$ $(k = 0, 1, 2, \ldots)$ and $A_p = A_s$, while complete population return to the initial state ψ_1 takes place when $A = 4k\pi$.

Just as with two-state Rabi oscillations, intensity fluctuations or a distribution of velocities will tend to average out the population oscillations and to lower the transfer efficiency. Moreover, because the population passes through the intermediate state ψ_2 during the transfer process, inevitable spontaneous emission will lead to population losses unless the excitation time is much shorter than the lifetime of ψ_2.

Rabi cycling is but one of the ways in which coherent laser pulses can induce population changes. Another class of change, the central theme of this chapter, *adiabatic evolution,* can occur when the Hamiltonian changes sufficiently slowly.

Section II explains the basic principles of adiabatic population transfer in terms of energy-level crossings, and Section III describes adiabatic population transfer by sequential laser pulses.

II. Principles of Coherent Excitation

A. Coherent Excitation

The quantum mechanical description of the internal excitation of an atom (or molecule) is embodied in a time-dependent state vector, $\Psi(t)$, and in a fixed set of basis states $\psi_1, \psi_2, \ldots$, associated with likely energy states of the atom in the absence of any radiation pulses. These basis states serve as a fixed coordinate system (in a Hilbert space) wherein one can express the state vector as a time-varying superposition, which we take to be

$$\Psi(t) = \sum_{n=1}^{N} C_n(t) \exp[-i\zeta_n(t)]\hat{\psi}_n \equiv \sum_{n=1}^{N} C_n(t)\psi_n(t), \tag{8}$$

where $\hat{\psi}_n$ is the static bare physical state. Hereafter, we write ψ_n for $\psi_n(t)$, the bare state with RWA phase factor $\exp[-i\zeta_n(t)]$. The real-valued phase $\zeta_n(t)$ is specified a priori, usually for mathematical convenience (as will be noted below), and the complex-valued function of time $C_n(t)$ is a *probability amplitude,* whose absolute square is the probability (or population) $P_n(t)$ that the atom will be found in state ψ_n at time t:

$$P_n(t) = |C_n(t)|^2 = |\langle\psi_n|\Psi(t)\rangle|^2. \tag{9}$$

As the latter part of the equation indicates, the probability amplitude can be regarded (apart from a phase) as the projection of the state vector onto one of the coordinate axes of the Hilbert space.

Changes in the state vector are governed by the time-dependent Schrödinger equation,

$$\hbar\frac{\partial}{\partial t}\Psi(t) = -i\mathcal{H}(t)\Psi(t). \tag{10}$$

For all the excitation processes discussed here (those produced by laser pulses whose frequencies lie in the optical or infrared region of the spectrum), the Hamiltonian operator $\mathcal{H}(t)$ varies with time as a result of the interaction energy $\mathbf{d} \cdot \mathbf{E}(t)$ of atomic dipole transition moment operator $\mathbf{d}$ with the electric field vector evaluated at the center of mass of the atom, $\mathbf{E}(t)$. In the simplest examples the

electric field has the form of a periodic variation at a carrier frequency (the optical frequency ω) and a more slowly varying envelope, $\mathcal{E}(t)$:

$$\begin{aligned}\mathbf{E}(t) &= \mathbf{e}\mathcal{E}(t)\cos(\omega t + \phi) \\ &= \tfrac{1}{2}\mathbf{e}\mathcal{E}(t)\,[\exp(i\omega t + i\phi) + \exp(-i\omega t - i\phi)].\end{aligned} \tag{11}$$

Here $\mathbf{e}$ is a unit vector defining the direction of the electric field, i.e., the polarization direction. The connection between the electric field envelope and the intensity of the radiation $I(t)$ is

$$\mathcal{E}(t)[\mathrm{V/cm}] = 27.4682\sqrt{I(t)[\mathrm{W/cm^2}]}.$$

When the state-vector expansion of Eq. (8) is used with the time-dependent Schrödinger equation (10), there results a coupled set of ordinary differential equations. These may be written in vector form as

$$\hbar\frac{d}{dt}\mathbf{C}(t) = -i\mathsf{H}(t)\mathbf{C}(t), \tag{12}$$

where $\mathbf{C}(t) = [C_1(t), C_2(t), \ldots, C_N(t)]^T$ is an N-component column vector of (complex-valued) probability amplitudes. The elements of the $N \times N$ Hamiltonian matrix $\mathsf{H}(t)$ depend on how the phases are chosen in Eq. (8), as will be noted subsequently.

B. Partial Coherence: The Density Matrix

We shall be concerned in this chapter only with excitation by purely coherent radiation. Obviously, this is an idealization that cannot hold under all circumstances. In practice, a variety of uncontrollable stochastic events, ranging from spontaneous emission to atomic collisions and laser fluctuations, all cause irreversible changes. To treat such situations one must formulate quantum mechanics in terms of a *density matrix* $\rho(t)$ rather than a state vector $\Psi(t)$ (cf. Shore, 1990, chap. 6). In brief, probabilities are obtained as diagonal elements of this matrix,

$$P_n(t) = \rho_{n,n}(t) = \langle\psi_n|\rho(t)|\psi_n\rangle, \tag{13}$$

and the off-diagonal elements represent coherences. Instead of the Schrödinger equation, one deals with the equation of motion,

$$\hbar\frac{d}{dt}\rho(t) = -i\mathsf{H}(t)\rho(t) + i\rho(t)\mathsf{H}(t) - \mathcal{R}(t)\rho(t). \tag{14}$$

The Hamiltonian matrix $\mathsf{H}(t)$ is identical to what occurs with the Schrödinger equation; the operator $\mathcal{R}(t)$ incorporates the various stochastic processes which are not present with purely coherent excitation.

The density matrix can also be used to treat purely coherent excitation of an ensemble in which the initial state is not expressible as a single state vector, as in the example

$$\rho(0) = |\psi_1\rangle \cos\theta \langle\psi_1| + |\psi_2\rangle \sin\theta \langle\psi_2|. \tag{15}$$

In this case there is no stochastic operator, $\mathcal{R}(t) = 0$, and the evolution is equivalent to that predicted by the Schrödinger equation.

For simplicity we will not consider the density matrix, although many of the papers treating STIRAP do discuss it, and realistic modelings often require using it.

C. Two States

For a simple two-state atom $\mathbf{C}(t) = [C_1(t), C_2(t)]^T$ is a two-component column vector whose elements are the probability amplitudes of the two states ψ_1 and ψ_2. The precise appearance of the matrix elements of the Hamiltonian $\mathsf{H}(t)$ depends on the choice of phases $\zeta_n(t)$. Were we to set the phases to zero (the Schrödinger picture), then the diagonal elements of $\mathsf{H}(t)$ would be the energies of the two states, E_1 and E_2, and the off-diagonal elements would contain the laser–atom dipole interaction energy, including the carrier-frequency oscillations from $\cos(\omega t + \phi)$.

1. The Rotating Wave Approximation (RWA)

It proves more convenient to incorporate the state energies and the carrier frequency ω as phases (the rotating-wave picture): $\zeta_1(t) = E_1 t$ and $\zeta_2(t) = \zeta_1(t) + \omega t$. By so doing we can make the first of the diagonal elements of the Hamiltonian matrix zero; the second diagonal element, the *detuning* Δ, is the difference between the Bohr frequency and the carrier frequency:

$$\hbar\Delta = E_2 - E_1 - \hbar\omega.$$

As presented here, the detuning is constant in time. More generally, the laser pulses induce time-varying Stark shifts of the energy levels (see Section II.D.3), and the detuning then becomes explicitly time-dependent.

The off-diagonal matrix element acquires a factor $\exp(-i\omega t)$ which cancels one part of the rapid carrier variation of the electric field—one of the two exponentials shown in Eq. (11). The remaining exponential is then $\exp(+i2\omega t)$. For most near-resonant excitation situations this factor varies much more rapidly than any changes of the probability amplitudes, and it is then permissible to neglect this

term (thereby making the *rotating wave approximation,* RWA). When this is done, and the detuning is allowed to vary in time, the Hamiltonian matrix reads (Shore, 1990)

$$\mathsf{H}(t) = \hbar \begin{bmatrix} 0 & \frac{1}{2}\Omega(t) \\ \frac{1}{2}\Omega(t) & \Delta(t) \end{bmatrix}. \tag{16}$$

The off-diagonal element $\Omega(t)$, the *Rabi frequency*, parameterizes the strength of the atom–laser interaction; it is proportional to the component of the atomic transition dipole moment in the direction of the electric-field vector, d_{12}, and to the laser electric-field amplitude $\mathcal{E}(t)$; i.e.,

$$\hbar\Omega(t) = d_{12}\mathcal{E}(t). \tag{17}$$

As long as the phase ϕ of the electric field (11) remains constant, it is always possible to choose the expansion phases $\zeta_n(t)$ so that the Rabi frequency is real-valued and positive (Shore, 1990). The diagonal elements of $\mathsf{H}(t)$ are the two RWA energies: the zero element is the energy of state ψ_1 lifted (dressed) by the photon energy $\hbar\omega$ and used as the reference energy level, while the energy $\hbar\Delta$ is the frequency offset (detuning) of state ψ_2.

For the RWA to be valid it is necessary that both the frequencies $\Omega(t)$ and $\Delta(t)$ be much smaller than the carrier frequency ω, and that the pulse duration be many optical cycles. For a discussion of deviations from the RWA, see Section III.B.8.

We have presented the RWA as a combination of choosing phases and neglecting high-frequency oscillations. A more physical picture is possible (Series, 1978). The presence of the phases in the expansion (8) is equivalent to the introduction of a time-varying coordinate system in the two-dimensional Hilbert space spanned by the states ψ_1 and ψ_2. Indeed, this is a rotation at a steady rate ω, the carrier frequency of the laser. In this rotating coordinate system one term of the interaction energy is slowly varying (it varies only with the varying intensity envelope), while the second term oscillates at twice the carrier frequency. The neglect of this "counterrotating" term leads to the RWA.

2. *Rabi Cycling*

The simple periodic solution to the resonant RWA equations reveals the connection of the frequency of population oscillations and the strength of the interaction to be the Rabi frequency. For numerical estimates of this frequency the following formula is useful,

$$|\Omega[\text{rad/ns}]| = 0.22068 \left(\frac{d_{12}}{ea_0}\right) \sqrt{I[\text{W/cm}^2]},$$

where e is the electron charge and a_0 is the Bohr radius, so that ea_0 is the atomic unit of dipole moment.

An analytic solution for two-state excitation exists not only for resonant excitation but for detuned excitation, when the radiation remains steady. The excitation probability is then

$$P_e(t) = \frac{1}{2}\left(\frac{\Omega}{\tilde{\Omega}}\right)^2 [1 - \cos(\tilde{\Omega}t)], \tag{18}$$

where $\tilde{\Omega} = \sqrt{\Omega^2 + \Delta^2}$ is the *nonresonant flopping frequency*. As can be seen, when detuning grows, the population oscillations become more rapid and less complete—population never resides entirely in the excited state.

The solution (18) predicts that, at the termination of a pulse of constant-intensity radiation, some population may remain in the excited state. When one treats pulses that turn on and off more gradually, this tends not to be the case. Instead, a detuned, slowly varying pulse will return the population to the initial state—a process often termed *coherent population return* (Vitanov, 1995; Vitanov and Knight, 1995; Kuhn *et al.*, 1998).

3. *Probability Loss*

The model of a two-state system is an idealization that, however useful, is never completely correct. Real atoms have an infinite number of bound states lying below the ionization continuum and molecules have numerous vibrational and rotational levels below each dissociation limit. When the radiation is very close to resonance between the ground state and a single excited state, the remaining levels hold little probability; primarily their influence comes indirectly, through providing the polarizability that appears as Stark shifts of the two energy levels of interest.

However, one effect of additional energy levels can become important: the excited state can always undergo spontaneous emission (over a time interval comparable to the inverse of the spontaneous emission time). When this emission leads to levels other than the ground state, then population is lost from the two-state system. To account correctly for this loss, one should really include not only additional levels in the description of the system, but one should base the mathematics on a density matrix rather than a state vector (cf. Section II.B). One simple way of accounting for probability loss out of the system of interest, occurring from state ψ_2 at a rate Γ, is to take the state energy to be a complex number. The resulting detuning is

$$\hbar\Delta = E_2 - \hbar\omega - i\tfrac{1}{2}\Gamma.$$

Under the influence of such a non-Hermitian Hamiltonian, probability is not conserved. The probabilities $P_n(t)$ will in general approach zero at long times.

4. Adiabatic States and Adiabatic Following

Theoretical discussion of time-evolving quantum systems is greatly facilitated by introducing instantaneous eigenstates $\Phi_k(t)$ of the time-varying Hamiltonian matrix,

$$\mathsf{H}(t)\Phi_k(t) = \hbar\varepsilon_k(t)\Phi_k(t). \tag{19}$$

Because the Hamiltonian changes with time, both the eigenvalues $\hbar\varepsilon_k(t)$ and the eigenvectors, the *adiabatic states* $\Phi_k(t)$, will change with time. The adiabatic states are time-dependent superpositions of the unperturbed states ψ_1 and ψ_2 (known also as *diabatic states*) (Shore, 1990),

$$\Phi_+(t) = \psi_1 \sin\Theta(t) + \psi_2 \cos\Theta(t), \tag{20a}$$

$$\Phi_-(t) = \psi_1 \cos\Theta(t) - \psi_2 \sin\Theta(t), \tag{20b}$$

where the mixing angle $\Theta(t)$ is defined (modulo π) as

$$\Theta(t) = \frac{1}{2}\arctan\left[\frac{\Omega(t)}{\Delta(t)}\right].$$

The energies of the adiabatic states are the two eigenvalues of $\mathsf{H}(t)$,

$$\varepsilon_\pm(t) = \tfrac{1}{2}[\Delta(t) \pm \sqrt{\Delta^2(t) + \Omega^2(t)}]. \tag{21}$$

What we here term *adiabatic states* are known also as *dressed states,* implying that the field interaction has clothed the atom in photons; the original (physical) states ψ_n are termed *bare states.*

The adiabatic states can serve as a moving coordinate system in which to place the state vector $\mathbf{\Psi}(t)$ as it changes under the influence of the coherent radiation pulse. Such coordinates are most useful when the elements of the Hamiltonian—the Rabi frequency and the detuning—change sufficiently slowly (i.e., adiabatically); then the state vector remains fixed in the adiabatic coordinates space. Mathematically, adiabatic evolution requires that the coupling between the adiabatic states be negligible compared to the difference between their eigenfrequencies (Shore, 1990; Messiah, 1962; Crisp, 1973), viz.,

$$|\langle\dot{\Phi}_+|\Phi_-\rangle| \ll |\varepsilon_+ - \varepsilon_-|, \tag{22}$$

where the dot denotes a time derivative (note that $\langle\dot{\Phi}_+|\Phi_-\rangle = -\langle\Phi_+|\dot{\Phi}\rangle$). Explicitly, the two-state *adiabatic condition* reads

$$\tfrac{1}{2}|\dot{\Omega}\Delta - \Omega\dot{\Delta}| \ll (\Omega^2 + \Delta^2)^{3/2}. \tag{23}$$

According to Eq. (23), adiabatic evolution requires a smooth pulse, long interaction time, and large Rabi frequency and/or large detuning.

When the adiabatic condition holds, there are no transitions between the adiabatic states and their populations are conserved. That is, the state vector $\Psi(t)$ remains fixed in the time-varying coordinate system of adiabatic states, as the latter move with respect to the fixed basis ψ_1 and ψ_2. In particular, if the state vector $\Psi(t)$ coincides with a single adiabatic state $\Phi(t)$ at some time t, then it will remain in that adiabatic state as long as the evolution is adiabatic: the state vector $\Psi(t)$ will *adiabatically follow* the state $\Phi(t)$. The relationship of the single adiabatic state $\Phi(t)$ [and of the state vector $\Psi(t)$] to the diabatic (bare) states will change if the mixing angle $\Theta(t)$ changes, and so adiabatic evolution can produce population transfer between those diabatic states.

Generally speaking, successful population transfer means that the state vector $\Psi(t)$ connects to the initial state ψ_1 at early times, and connects to a specified target state ψ_N at late times. Under appropriate conditions, this connection can be provided by a single adiabatic state. Such a state is termed an *adiabatic transfer* (AT) state. One refers to these asymptotic connections with initial and target states as *connectivity*.

5. *Rapid Adiabatic Passage*

When discussing adiabatic time evolution it is useful to plot the values of the adiabatic energies as a function of time, and to view carefully the time intervals during which the curves are close together—it is during these intervals that the adiabatic condition is most likely to be violated. There are two distinct types of adiabatic population changes, distinguished by the behavior of the diabatic energies 0 and $\hbar\Delta(t)$. The *no-crossing* case is depicted in Fig. 4 (top left frame) in the particular case of constant detuning; then the diabatic energy curves are parallel to each other during the interaction. In the absence of interaction the adiabatic energies coincide with the diabatic ones, but the (pulsed) interaction $\Omega(t)$ pushes them away from each other. As Eqs. (20) show, at early and late times each adiabatic state is identified with the same diabatic state: $\Phi_-(t \to \pm\infty) = \psi_1, \Phi_+(t \to \pm\infty) = \psi_2$, while at intermediate times it is a superposition of diabatic states. Consequently, starting from the ground state ψ_1 initially, the population makes a partial excursion into the excited state ψ_2 at intermediate times and eventually returns to ψ_1 in the end (bottom left frame). Hence in the no-crossing case adiabatic evolution leads to *complete population return*.

A rather different situation occurs when the detuning $\Delta(t)$ sweeps slowly from some very large negative value to some very large positive value (or vice versa), as shown in Fig. 4 (top right frame). That is, the Hamiltonian at the end of the pulse differs from the Hamiltonian at the beginning, because of the detuning change. Large in this context means much larger than the Rabi frequency $\Omega(t)$. The two

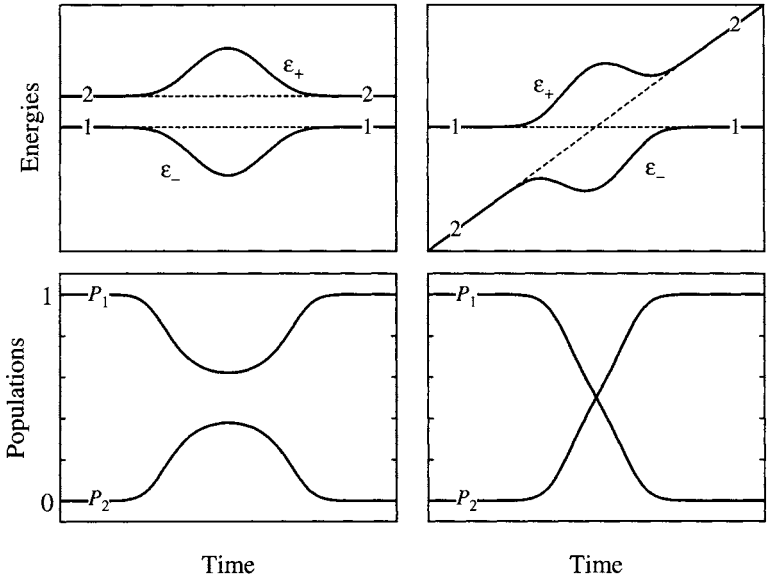

FIG. 4. Time evolution of the energies (upper frames) and the populations (lower frames) in a two-state system. In the upper plots, the dashed lines show the unperturbed (diabatic) energies, and the solid curves show the adiabatic energies. The left-hand frames are for the no-crossing case, while the right-hand frames are for the level-crossing case.

diabatic energies 0 and $\hbar\Delta(t)$ intersect at time t_0 when the detuning is zero. The adiabatic energies approach the diabatic energies when $\Delta(t)$ is large (at early and late times), but the presence of interaction prevents their intersection—the adiabatic energies have an *avoided crossing*. Indeed, as Eq. (21) shows, the eigenenergy separation $\hbar\varepsilon_+(t) - \hbar\varepsilon_+(t) = \hbar\sqrt{\Delta^2(t) + \Omega^2(t)}$ is equal to $\hbar\Omega(t_0)$ at the crossing. For constant $\Omega(t)$ this is the minimum value of the eigenvalue separation, while for pulse-shaped $\Omega(t)$ (as in Fig. 4), there are two minima near t_0. At very early and late times the ratio $\Delta(t)/\Omega(t) \overset{t\to\pm\infty}{\longrightarrow} \pm\infty$. Hence, during the excitation the mixing angle $\Theta(t)$ rotates clockwise from $\Theta(-\infty) = \pi/2$ to $\Theta(+\infty) = 0$ and the composition of the adiabatic states changes accordingly. Asymptotically, each adiabatic state becomes uniquely identified with a single unperturbed state,

$$\psi_1 \overset{-\infty\leftarrow t}{\longleftarrow} \Phi_+(t) \overset{t\to+\infty}{\longrightarrow} \psi_2, \tag{24a}$$

$$-\psi_2 \overset{-\infty\leftarrow t}{\longleftarrow} \Phi_-(t) \overset{t\to+\infty}{\longrightarrow} \psi_1. \tag{24b}$$

Consequently, starting from state ψ_1 initially, the system follows adiabatically the adiabatic state $\Phi_+(t)$ and eventually ends up in state ψ_2. The laser pulse, with

detuning sweep, has produced *complete population transfer,* a process known as adiabatic passage or, because it must occur in a time shorter than the radiative lifetime of the excited state, as *rapid adiabatic passage.* We emphasize that adiabatic passage in a two-state system does not depend on the sign of the detuning slope: it takes place for both $\dot{\Delta}(t) > 0$ (as was assumed above) and $\dot{\Delta}(t) < 0$.

The adiabatic condition (23) expresses a constraint at each moment; it is a "local" condition. A "global" condition can be obtained from the expression $\langle \dot{\Phi}_+ | \Phi_- \rangle = \dot{\Theta}$. The average value of this angle, as it increases from 0 to $\pi/2$ is $\pi/4$. For resonant excitation the time-integrated difference of the two eigenvalues is just the time integral of the Rabi frequency, i.e., the pulse area. Hence one finds the commonly used rule of thumb that the pulse area must be very large,

$$A = \int_{-\infty}^{+\infty} dt\, \Omega(t) \gg 1.$$

Adiabatic passage offers significant advantages over Rabi cycling as a means of producing complete population transfer in an ensemble of atoms. Unlike Rabi cycling, adiabatic passage is robust against small-to-moderate variations in the laser intensity, detuning, and interaction time. Therefore it can produce uniform excitation for a broad range of Doppler shifts.

6. *Estimating Transition Probabilities*

A popular tool for estimating the transition probability between two crossing *diabatic* states is the Landau–Zener formula (Landau, 1932; Zener, 1932),

$$P = 1 - p, \qquad p = \exp\left[-\frac{\pi \Omega^2(t_0)}{2|\dot{\Delta}(t_0)|}\right], \tag{25}$$

where $\dot{\Delta}(t_0)$ is the rate of change in the detuning evaluated at the crossing time t_0 and $\Omega(t_0)$ is the value of the Rabi frequency at t_0. This formula is exact only for a constant Rabi frequency and a linearly varying detuning over an infinite time interval, so it is only an approximation to any actual probability for adiabatic passage. Nevertheless, it correctly identifies the importance of the ratio of Ω^2 to $\dot{\Delta}$ as a measure of the likelihood of population transfer. We note here that the probability for (nonadiabatic) transition between the *adiabatic* states is $p = 1 - P$.

There exist other models of level-crossing excitation, more realistic because they allow pulsed interactions. The Allen–Eberly–Hioe model (Allen and Eberly, 1975; Hioe, 1984) assumes a hyperbolic-secant pulse and a hyperbolic-tangent chirp. The Demkov–Kunike model (Demkov and Kunike, 1969; Suominen and Garraway, 1992) adds a static detuning to this model.

D. Three States

1. The Three-State RWA Hamiltonian

The usual situation with three discrete quantum states can be regarded as a linkage chain $\psi_1 \leftrightarrow \psi_2 \leftrightarrow \psi_3$ in which one of the states, the intermediate state ψ_2, is coupled by radiative interaction to two other states, which have no radiative coupling between them. (When the excitation is only by means of electric dipole radiation, the parity selection rule forbids the 3–1 linkage for free atoms or molecules.) Typically, each of the two linkages originates in a separate laser pulse, whose carrier frequency is close to the relevant Bohr frequency. The following variants of this chain occur, distinguished by the ordering of their unperturbed energies E_j (see Fig. 5):

- The states may form a *ladder,* in which successive energies lie higher than the predecessors. Population begins in state ψ_1. The ladder configuration occurs when one has interest in stepwise excitation toward ionization. It readily generalizes to multiple levels, each more highly excited.
- The linkage may form a *lambda*, in which the middle state, ψ_2, has unperturbed energy lying above either other state (the relative energy ranking of ψ_1 and ψ_3 is not significant). Again, population begins in state ψ_1. The lambda configuration exemplifies a Raman process.
- The linkage may form a *vee*, in which the middle state has lowest unperturbed energy, and initially holds the population. The vee configuration has interesting quantum-beat interference patterns between the two excitation branches leading to and from a single state.

In all of these cases the phases $\zeta_n(t)$ of the state vector expansion (8) can be chosen to place a zero as one of the diagonal elements of the Hamiltonian matrix, and to permit a generalized rotating wave approximation in which time variations

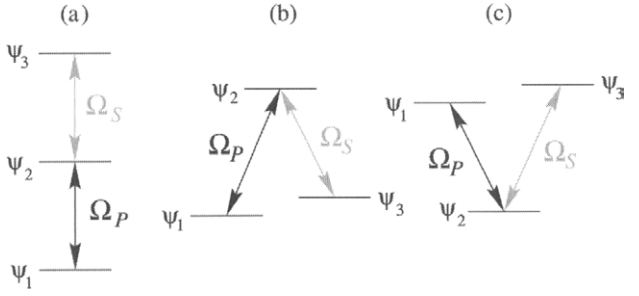

FIG. 5. Linkages for three-state coupling: (a) ladder configuration; (b) Λ configuration; (c) V configuration.

at the carrier frequencies have been eliminated. When the zero goes into the first element, the pattern is

$$\mathsf{H}(t) = \hbar \begin{bmatrix} 0 & \frac{1}{2}\Omega_1(t) & 0 \\ \frac{1}{2}\Omega_1(t) & \Delta_2 & \frac{1}{2}\Omega_2(t) \\ 0 & \frac{1}{2}\Omega_2(t) & \Delta_3 \end{bmatrix}. \tag{26}$$

The off-diagonal elements are the Rabi frequencies $\Omega_j(t)$, related to transition-dipole moments and electric-field envelopes by the relationships

$$\hbar\Omega_1(t) = d_{12} \cdot \mathcal{E}_1(t), \qquad \hbar\Omega_2(t) = d_{23} \cdot \mathcal{E}_2(t). \tag{27}$$

The expressions for the detunings $\Delta_j(t)$ depend on whether the Hamiltonian describes a ladder, a lambda, or a vee linkage. For the ladder arrangement one has

$$\hbar\Delta_2 = E_2 - E_1 - \hbar\omega_1, \tag{28a}$$

$$\hbar\Delta_3 = E_3 - E_1 - \hbar\omega_1 - \hbar\omega_2, \tag{28b}$$

while for the lambda the formulas read

$$\hbar\Delta_2 = E_2 - E_1 - \hbar\omega_1, \tag{29a}$$

$$\hbar\Delta_3 = E_3 - E_1 - \hbar\omega_1 + \hbar\omega_2. \tag{29b}$$

It is not difficult to obtain numerical solutions to the set of coupled ordinary differential equations, from which one can make plots of populations as a function of time or, for time fixed at the end of both pulses, as a function of other parameters. Some special limiting cases have properties that are of particular importance for population transfer.

2. *Pulse Sequences*

Much of the early theoretical work on three-state systems involved steady fields. Although population transfer can take place under such circumstances, all population changes are periodic, and so there is a regular return of population into the initial state, just as with the two-state atom. Of greater interest are various sequences of pulse pairs, one associated with each of the two transitions. These typically fall into two classes: when the first pulse introduces a coupling between the initial state and the next state of the chain, the sequence is often called "intuitive" ordering of pulses, because intuition suggests that one should start moving population by acting on a populated state. As will be noted in the sections on

STIRAP, a "counterintuitive" sequence, acting first on an unpopulated state, often is a better choice.

There are two possibilities for causing individual atoms (or molecules) to experience a sequence of pulses. The atoms may be relatively stationary, say in a vapor cell, and be exposed to pulsed lasers. Alternatively, the atoms may be moving together, say in an atomic beam, and pass across beams from steady lasers. What matters for excitation is the timing of the fields in the rest frame of each atom.

3. *Adiabatic Elimination*

An important special case of three-state excitation occurs when the detuning Δ from the intermediate state ψ_2 is very large, but the two-photon detuning δ between states ψ_1 and ψ_3 is small. This situation implies nearly resonant two-photon excitation without having a single-photon resonance. The RWA Hamiltonian of Eq. (26) provides the following equation for the amplitude in the intermediate state, ψ_2:

$$i\frac{d}{dt}C_2(t) = \tfrac{1}{2}\Omega_1 C_1(t) + \Delta_2 C_2 + \tfrac{1}{2}\Omega_2 C_3(t). \tag{30}$$

When Δ_2 is very large, rapid oscillations of amplitude $C_2(t)$ will occur, at this frequency. These variations are much more rapid than any changes of interest. One can average over many such oscillation periods (i.e., over a time interval $\Delta t \gg \Delta_2^{-1}$) to obtain more slowly varying amplitudes, $\bar{C}_n(t)$, for which the time variation of $\bar{C}_2(t)$ vanishes. By setting $(d/dt)\bar{C}_2 = 0$, we obtain from Eq. (30) that

$$\bar{C}_2(t) = \frac{-\Omega_1}{2\Delta_2}\bar{C}_1(t)\frac{-\Omega_2}{2\Delta_2}\bar{C}_3(t). \tag{31}$$

This approximation, known as *adiabatic elimination,* relates the intermediate-state amplitude $\bar{C}_2(t)$ to those of the other two states. Because Δ_2 is large (in order that adiabatic elimination be valid), the amplitude $\bar{C}_2(t)$ is small, and the population is confined to the two states ψ_1 and ψ_3. The two-state Hamiltonian that results from adiabatic elimination,

$$\mathsf{H}(t) = \hbar\begin{bmatrix} S_1(t) & \frac{1}{2}\bar{\Omega}(t) \\ \frac{1}{2}\bar{\Omega}(t) & \Delta_3(t) + S_3(t) \end{bmatrix}, \tag{32}$$

is similar to the simple two-state equation (16), but the interaction term—the Rabi frequency—now involves the product of two interactions,

$$\bar{\Omega}(t) = \frac{-\Omega_1(t)\Omega_2(t)}{2\Delta_2}, \tag{33}$$

and the diagonal elements have acquired dynamic Stark shifts,

$$S_1(t) = \frac{-|\Omega_1(t)|^2}{4\Delta_2}, \qquad S_3(t) = \frac{-|\Omega_2(t)|^2}{4\Delta_2}. \tag{34}$$

By incorporating $S_1(t)$ into the phase $\zeta_k(t)$, the Hamiltonian can be made to appear as in Eq. (16). The detuning then involves the difference between Stark-shifted Bohr frequencies and the carrier frequency,

$$\hbar\Delta(t) = E_3 + \hbar S_3(t) - E_1 - \hbar S_1(t) - \hbar\omega.$$

The preceding formulas give the essential properties of two-photon interactions. For more accurate results one should include a larger number of possible intermediate states (ideally an infinite number). In so doing one should avoid making the RWA at an early stage, and should treat the full Hamiltonian (cf. Shore, 1990, sect.14.8).

The two-photon Rabi frequency and the dynamic Stark shifts are both consequences of the presence of additional energy states that do not participate strongly in the excitation because they are far off resonance. The electric field interacts not only with any permanent dipole transition moments, as embodied in the operator **d,** but also with an induced dipole moment. The proportionality between this induced moment and the electric field is the complex-valued frequency-dependent *polarizability* tensor $\mathsf{Q}(\omega)$. The polarizability contributes to the Hamiltonian an interaction energy (Shore, 1990, sect. 14.9; Yatsenko *et al.,* 1998),

$$\mathcal{H}^{int}(t) = -\tfrac{1}{2}\mathbf{E}(t) \cdot \mathsf{Q}(\omega) \cdot \mathbf{E}(t). \tag{35}$$

The Hamiltonian matrix of such an interaction has both diagonal elements (acting as dynamic Stark shifts) and off-diagonal elements (acting as two-photon Rabi frequencies.)

4. Autler-Townes Splitting

Another important situation occurs when the coupling between two states (taken here to be Ω_2 between ψ_2 and ψ_3) is strong, whereas the coupling to the first state, Ω_1, is weak. For simplicity, let the fields be steady, not pulsed, and let the strong 2–3 transition be resonant with field of frequency ω_2 while the weak field has tunable frequency ω. It is natural to diagonalize the strong-coupling portion of the Hamiltonian, which is a two-level system. This leads to the dressed states Φ_- and Φ_+, whose composition is identical to that given above, and to the following

expression for the state vector:

$$\Psi(t) = \psi_1 C_1(t) e^{-i\omega t} + \Phi_- B_-(t) + \Phi_+ B_+(t). \tag{36}$$

The RWA Hamiltonian takes the form

$$\mathsf{H}(t) = \hbar \begin{bmatrix} \Delta & \frac{1}{2}\Omega_- & \frac{1}{2}\Omega_+ \\ \frac{1}{2}\Omega_- & -\varepsilon & 0 \\ \frac{1}{2}\Omega_+ & 0 & +\varepsilon \end{bmatrix}, \tag{37}$$

where the dressed eigenvalues are $\pm\varepsilon = \pm\frac{1}{2}|\Omega_2|$, the detuning is $\Delta = (E_2 - E_1)/\hbar - \omega$, and the Rabi frequencies $\Omega_\pm$ are expressible in terms of the components of the dressed states. The situations of interest are when there occur two identical diagonal elements of this Hamiltonian, i.e., there is a degeneracy of diabatic energies; such a situation is one in which the excitation is dominated by Rabi oscillations between the degenerate states. There are two choices of probe frequency that make two diagonal element identical:

$$\hbar\omega = E_2 - E_1 \pm \hbar\varepsilon = E_2 - E_1 \pm \tfrac{1}{2}\hbar|\Omega_2|. \tag{38}$$

That is, there are two weak-field detunings for which there will be appreciable coupling between state ψ_1 and the strongly driven two-state system. In essence, the strong field has split the energy level accessed by the third state into two levels, separated by the *Autler–Townes* splitting $2\varepsilon = \hbar|\Omega_2|$ (Autler and Townes, 1955).

The Autler–Townes effect manifests itself in the absorption spectrum in the form of a splitting of the resonance. There is, however, another interesting feature when the lifetime of state ψ_3 is much longer than that of the excited state ψ_2. In this case one observes that the absorption exactly vanishes when the weak field is tuned midway between the two dressed energy levels (38). This is a result of an interference between the two absorption channels starting from the ground state ψ_1 via the two dressed states $\Phi_\pm$ with subsequent decay out of the system (Imamoglu *et al.*, 1989; Lounis and Cohen-Tannoudji, 1992; Fleischhauer *et al.*, 1992), as illustrated in Figs. 6 and 7. The interference of the decay channels becomes apparent if we include decay rates Γ_2 and Γ_3 in the above analysis. After the partial diagonalization we find

$$\mathsf{H}(t) = \frac{\hbar}{2} \begin{bmatrix} 2\Delta & \Omega_- & \Omega_+ \\ \Omega_- & -2\varepsilon - \frac{i}{2}(\Gamma_2 + \Gamma_3) & i(\Gamma_3 - \Gamma_2) \\ \Omega_+ & i(\Gamma_3 - \Gamma_2) & 2\varepsilon - \frac{i}{2}(\Gamma_2 + \Gamma_3) \end{bmatrix}. \tag{39}$$

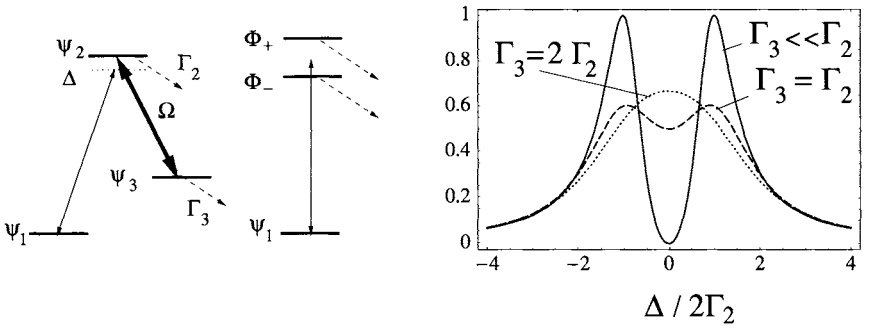

FIG. 6. *Left:* Diagonalization of strong, resonant coupling of levels ψ_2 and ψ_3 leads to symmetrically split Autler–Townes doublett $\Phi_\pm$. *Right:* Absorption of weak probe field as function of detuning Δ for $\Omega = 2\Gamma_2$. Destructive interference of absorption pathways for $\Gamma_3 \ll \Gamma_2$ leads to cancellation of absorption on resonance. Interference is absent for $\Gamma_3 = \Gamma_2$ and constructive for $\Gamma_3 > \Gamma_2$.

Three cases are of interest:

- If $\Gamma_3 \ll \Gamma_2$, i.e., if the decay out of state ψ_3 can be disregarded, the two absorption channels start and end in the same states and there is destructive interference. When $\Gamma_3 = 0$ there is complete cancellation of the absorption. This case, termed electromagnetically induced transparency (EIT) (Boller *et al.*, 1991), has a number of important implications (cf. Section XA).
- If $\Gamma_3 \gg \Gamma_2$, the interference is constructive and there is an enhanced absorption compared to a simple sum of two Lorentzian line profiles.
- Finally, if $\Gamma_3 \sim \Gamma_2$, the interference effect almost vanishes and only the splitting remains.

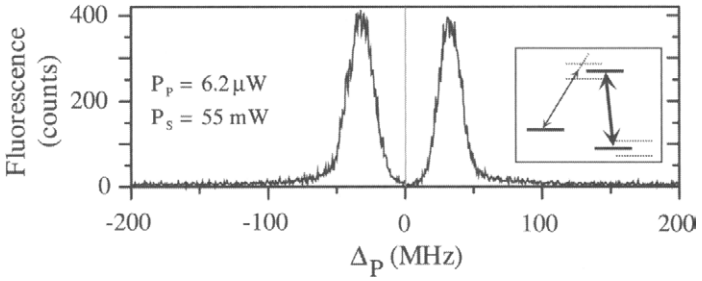

FIG. 7. Experimental demonstration of Autler–Townes splitting in neon. The Stokes (dressing) laser intensity is 55 mW and the probe laser intensity is 0.62 μW. From Bergmann *et al.* (1998).

III. Three-State STIRAP: Theory

A. Basic Properties of STIRAP

When the three-state linkage forms a lambda pattern (see Fig. 3b), one has a typical stimulated-Raman excitation scheme. The field acting on the initial state ψ_1 is termed the *pump* field, and the interaction leading to the final (target) state ψ_3 is termed the *Stokes*.

It is intuitively evident that population transfer between states ψ_1 and ψ_3 can take place, as in SEP, when the pump pulse precedes the Stokes pulse. Simultaneous and steady pulses can also produce complete population transfer, if the pulse areas are carefully chosen. What may not be obvious at first is that even more satisfactory population transfer can be produced if the Stokes pulse occurs first—the pulses then arrive in a "counterintuitive" ordering. This is the basis for a process now called stimulated Raman adiabatic passage (STIRAP) (Oreg *et al.*, 1984; Kuklinski *et al.*, 1989; Gaubatz *et al.*, 1990; Bergmann and Shore, 1995; Shore, 1995; Bergmann *et al.*, 1998, Vitanov *et al.*, 2001).

The STIRAP technique uses the coherence of two pulsed laser fields to achieve a (nearly) complete population transfer from an initially populated state ψ_1 to a target state ψ_3 via an intermediate state ψ_2 (see Fig. 3b). If a two-photon resonance between ψ_1 and ψ_3 is maintained, if there is sufficient overlap of the two pulses, and if the pulses are sufficiently strong that the time evolution is adiabatic, then (almost) complete population transfer occurs between states ψ_1 and ψ_3. Furthermore, there is almost no population in the (usually decaying) intermediate state ψ_2 at any time. The following sections offer explanations for this remarkable result.

1. Basic Equations and Definitions

The mathematical description of STIRAP derives from the Schrödinger equation (12) with $\mathbf{C}(t)$ a three-component column vector. Initially the population resides entirely in state ψ_1, meaning $\mathbf{C}(-\infty) = [1, 0, 0]^T$. The objective is to transfer population into state ψ_3, meaning $\mathbf{C}(+\infty) = [0, 0, 1]^T$.

With the rotating wave approximation, the Hamiltonian $\mathsf{H}(t)$ for purely coherent excitation has the form

$$\mathsf{H}(t) = \hbar \begin{bmatrix} 0 & \frac{1}{2}\Omega_p(t) & 0 \\ \frac{1}{2}\Omega_p(t) & \Delta_p & \frac{1}{2}\Omega_s(t) \\ 0 & \frac{1}{2}\Omega_s(t) & \Delta_p - \Delta_s \end{bmatrix}. \tag{40}$$

Here $\Omega_p(t)$ and $\Omega_s(t)$ are the (real-valued) Rabi frequencies of the pump and Stokes pulses, respectively,

$$\hbar\Omega_p(t) = d_{12}\mathcal{E}_p(t), \qquad \hbar\Omega_s(t) = d_{23}\mathcal{E}_s(t).$$

The diagonal elements of this matrix involve the single-photon detunings of the pump and Stokes lasers from their respective transitions,

$$\hbar\Delta_p = E_2 - E_1 - \hbar\omega_p, \qquad \hbar\Delta_s = E_2 - E_3 - \hbar\omega_s. \tag{41}$$

An essential condition for STIRAP is that there be two-photon resonance between states ψ_1 and ψ_3, meaning $\Delta_p = \Delta_s \equiv \Delta$, or

$$\delta \equiv \Delta_p - \Delta_s = 0. \tag{42}$$

The single-photon detuning Δ has relatively little effect on STIRAP; Section III.B.3 will discuss its effect.

Although the definitions of Eq. (14) pertain to excitation in the absence of any incoherent processes, it is easy to include the possibility of loss from state ψ_2 at a rate Γ by making the replacement $E_2 \to E_2 - \frac{1}{2}i\Gamma$. In this way it is possible to model the effect of spontaneous emission out of state ψ_2 into states *other than* ψ_1 or ψ_2. As long as the excitation is adiabatic, the presence of a complex-valued detuning has no effect on the STIRAP process, because population never is found in state ψ_2. However, as the detuning and the loss rate increase, adiabaticity deteriorates, which eventually reduces the transfer efficiency; for further discussion see Sections III.B.3 and III.B.5.

In practice, a part of the spontaneous emission acts to repopulate states ψ_1 and ψ_3. Such effects cannot be treated within the Schrödinger equation; they require a density matrix treatment.

2. *Adiabatic States*

The population transfer mechanism in STIRAP is most easily understood in a Hilbert space whose coordinate basis vectors are instantaneous eigenstates of the time-varying Hamiltonian (i.e., a basis of adiabatic states). When the two-photon resonance condition (42) is fulfilled, the eigenvalues of $\mathsf{H}(t)$, which represent the energies of the adiabatic states, are $\hbar\varepsilon_-$, $\hbar\varepsilon_0$, and $\hbar\varepsilon_+$, where

$$\varepsilon_+(t) = \tfrac{1}{2}[\Delta + \sqrt{\Delta^2 + \Omega^2(t)}] = \tfrac{1}{2}\Omega(t)\cot\varphi(t), \tag{43a}$$

$$\varepsilon_0(t) = 0, \tag{43b}$$

$$\varepsilon_-(t) = \tfrac{1}{2}[\Delta - \sqrt{\Delta^2 + \Omega^2(t)}] = -\tfrac{1}{2}\Omega(t)\tan\varphi(t). \tag{43c}$$

The presence of a null eigenvalue follows from the choice of energy zero point [and the phases $\zeta_n(t)$], which here reckons all energies as excitation from the initial state ψ_1.

The corresponding eigenstates $\Phi_+(t)$, $\Phi_0(t)$, and $\Phi_-(t)$ of $\mathsf{H}(t)$ are connected to the bare (diabatic) states ψ_1, ψ_2, and ψ_3 by the relations

$$\Phi_+(t) = \psi_1 \sin\vartheta(t) \sin\varphi(t) + \psi_2 \cos\varphi(t) + \psi_3 \cos\vartheta(t) \sin\varphi(t), \quad (44a)$$

$$\Phi_0(t) = \psi_1 \cos\vartheta(t) - \psi_3 \sin\vartheta(t), \quad (44b)$$

$$\Phi_-(t) = \psi_1 \sin\vartheta(t) \cos\varphi(t) - \psi_2 \sin\varphi(t) + \psi_3 \cos\vartheta(t) \cos\varphi(t), \quad (44c)$$

where the time-dependent mixing angles $\vartheta(t)$ and $\varphi(t)$ are defined as

$$\tan\vartheta(t) = \frac{\Omega_p(t)}{\Omega_s(t)}, \qquad \tan 2\varphi(t) = \frac{\Omega(t)}{\Delta}, \quad (45)$$

with $\Omega(t)$ the root-mean-square (RMS) field

$$\Omega(t) = \sqrt{\Omega_p^2(t) + \Omega_s^2(t)}. \quad (46)$$

The adiabatic state $\Phi_0(t)$ associated with the null eigenvalue has particular importance: it has no component of the excited state ψ_2. The latter state can undergo spontaneous emission back to state ψ_1, state ψ_3 (in the Λ configuration), and in most cases it can also decay to other states. By avoiding the possibility of such loss, the state $\Phi_0(t)$ acts to trap population; it is known as a *trapped state* (Alzetta *et al.*, 1976, 1979; Arimondo and Orriols, 1976; Gray *et al.*, 1978; Arimondo, 1996).

We introduce the diabatic or adiabatic bases by writing one of the two expansions

$$\Psi(t) = \sum_n \hat{\psi}_n C_n(t) \exp[-i\zeta_n(t)]$$

$$= \sum_k \Phi_k(t) B_k(t). \quad (47)$$

According to Eqs. (44), the probability amplitudes of the adiabatic states $\mathbf{B}(t) = [B_+(t), B_0(t), B_-(t)]^T$ are connected to the diabatic-state (or bare-state) amplitudes $\mathbf{C}(t)$ by the orthogonal transformation

$$\mathbf{C}(t) = \mathsf{R}(t)\mathbf{B}(t), \quad (48)$$

where the rotation matrix $\mathsf{R}(t)$ is given by

$$\mathsf{R}(t) = \begin{bmatrix} \sin\vartheta\sin\varphi & \cos\vartheta & \sin\vartheta\cos\varphi \\ \cos\varphi & 0 & -\sin\varphi \\ \cos\vartheta\sin\varphi & -\sin\vartheta & \cos\vartheta\cos\varphi \end{bmatrix}. \tag{49}$$

The Schrödinger equation in the adiabatic representation is obtained from Eqs. (12), (48), and (49) and is given by

$$\hbar\frac{d}{dt}\mathbf{B}(t) = -i\mathsf{H}_b(t)\mathbf{B}(t), \tag{50}$$

with the Hamiltonian given by $\mathsf{H}_b = \mathsf{R}^{-1}\mathsf{H}\mathsf{R} - i\hbar\mathsf{R}^{-1}\dot{\mathsf{R}}$, or explicitly,

$$\mathsf{H}_b = \hbar\begin{bmatrix} \frac{1}{2}\Omega\cot\varphi & i\dot{\vartheta}\sin\varphi & i\dot{\varphi} \\ -i\dot{\vartheta}\sin\varphi & 0 & -i\dot{\vartheta}\cos\varphi \\ -i\dot{\varphi} & i\dot{\vartheta}\cos\varphi & -\frac{1}{2}\Omega\tan\varphi \end{bmatrix}, \tag{51}$$

where an overdot means a time derivative.

3. The STIRAP Mechanism

STIRAP is based on tying the state vector $\Psi(t)$ to the zero-eigenvalue adiabatic state $\Phi_0(t)$, which is a coherent superposition of the initial state ψ_1 and the final state ψ_3 only. For the counterintuitive pulse ordering the relations $\Omega_p(t)/\Omega_s(t) \overset{t\to-\infty}{\longrightarrow} 0$ and $\Omega_p(t)/\Omega_s(t) \overset{t\to+\infty}{\longrightarrow} \infty$ apply; hence, as time progresses from $-\infty$ to $+\infty$, the mixing angle $\vartheta(t)$ rises from 0 to $\pi/2$. Consequently, the adiabatic state $\Phi_0(t)$ evolves from the bare state ψ_1 initially to a superposition of states ψ_1 and ψ_3 at intermediate times and finally to the target state ψ_3 at the end of the interaction; thus, state $\Phi_0(t)$ links adiabatically the initial state ψ_1 to the target state ψ_3. Since the Hamiltonian is explicitly time dependent, the derivative terms in Eq. (51) (the nonadiabatic couplings) are nonzero and, consequently, diabatic transitions between the adiabatic states will occur. The goal is to reduce the diabatic transition rates to negligibly small values, i.e., to ensure adiabatic evolution. Then the system can be forced to stay in the trapped state at all times, and a complete population transfer from ψ_1 to ψ_3 will be achieved, as shown in Fig. 8. Moreover, because the intermediate state ψ_2 does not participate in the trapped state Φ_0, it does not participate in the population transfer either and remains unpopulated throughout the interaction. Hence, as long as the excitation is adiabatic, its properties, such as radiative decay, do not influence STIRAP. From another viewpoint, when the Stokes pulse is stronger (in the beginning) the population is predominantly in state ψ_1, and when the pump pulse is stronger (in the end) the population is

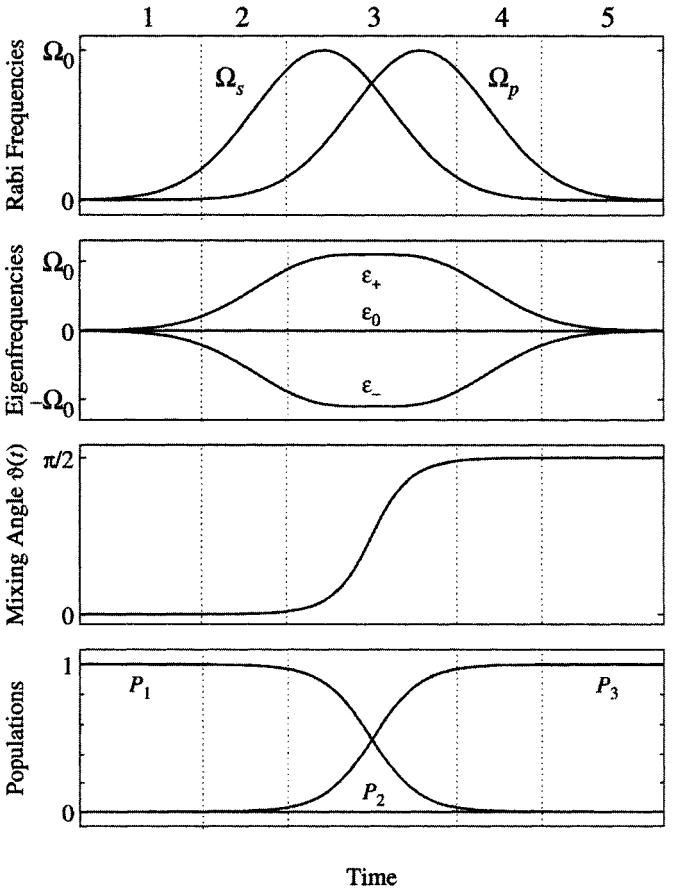

FIG. 8. Time dependencies of the pump and Stokes Rabi frequencies, the eigenfrequencies, the mixing angle and the populations in three-state STIRAP. Dotted lines separate five phases of STIRAP; see Section III.A.4.

predomonantly in state ψ_3; thus the intermediate state is always weakly coupled to the more populated state, which provides another explanation why this state is bypassed by STIRAP during the transfer. A vector picture of the STIRAP process is shown in Fig. 9.

4. Five-Stage Description of STIRAP

The STIRAP process can be viewed as comprising five stages, each defined by the relative strengths of the two fields (Fig. 8). For each stage, coherence is essential.

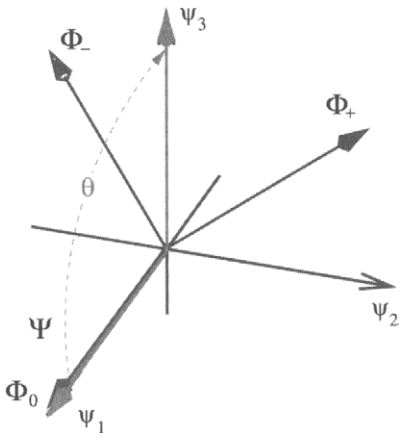

FIG. 9. Vector picture of STIRAP. ψ_1, ψ_2, and ψ_3 are bare atomic eigenstates or diabatic states. Φ_0, Φ_+, and Φ_- are the adiabatic dressed states. The trapped state Φ_0 is rotated from ψ_1 to ψ_3. Under adiabatic conditions, the state vector Ψ follows the evolution of Φ_0.

- *Phase 1:* Only the Stokes pulse is present; its intensity increases steadily. The pump laser does not act yet, i.e., the population in state ψ_1 is not perturbed yet, the mixing angle remains zero, and the state vector remains parallel to state ψ_1. The Stokes pulse prepares for the lossless transfer process in the sense that it provides the Autler–Townes splitting of levels, needed in phase 2. This phase is therefore the *Stokes-induced Autler–Townes phase*. Its purpose is to line up the state vector Ψ with the state Φ_0, i.e., $|\langle\Psi|\Phi_0\rangle| = 1$.
- *Phase 2:* The Stokes pulse has nearly reached the maximum intensity, but the pump pulse is still weak. The state vector deviates only by a very small angle from state ψ_1. One might ask: why is the pump laser radiation not absorbed? Here the Autler–Townes effect leads to a cancellation of the transition rate from the ground state to the two Autler–Townes states. This is the same mechanism that leads to EIT. The effect of the Stokes-induced Autler–Townes splitting is very obvious here. This phase is therefore the *Stokes-induced EIT phase*.
- *Phase 3:* The Stokes pulse decreases and the pump pulse increases. Now the essential part of the population dynamics starts. The pump pulse couples state ψ_1 strongly to the other levels. The mixing angle increases and the state vector departs from the state ψ_1 direction toward state $-\psi_3$, while remaining in the $\psi_1\psi_3$ plane and leaving state ψ_2 unpopulated. This phase is the *adiabatic passage (AP) phase*, with Stokes and pump acting on equal footing, because it is the ratio of these two Rabi frequencies which determines the dynamics.

- *Phase 4:* The population is now almost completely deposited into state ψ_3, but the Stokes pulse is still not zero. Why is there no loss due to optical pumping out of state ψ_3 by the Stokes field? The answer is that the pump field protects the population in state ψ_3 by inducing Autler–Townes splitting and interference (coupling of states ψ_1 and ψ_2). This is the *pump-induced EIT phase.*
- *Phase 5:* The Stokes pulse intensity is zero and the pump-induced Autler–Townes splitting must be reduced to zero. This phase is the *pump-induced Autler–Townes phase.*

We emphasize that the phenomena of Autler–Townes splitting, EIT, and adiabatic passage all depend on the coherence of the radiation. Phase fluctuations would cause the state vector to "jiggle arround," thereby causing strong nonadiabatic coupling.

5. *Intermediate-State Population: Importance of the Null Eigenvalue*

Once the conditions for STIRAP are fulfilled—two-photon resonance between states ψ_1 and ψ_3, counterintuitive pulse ordering, and adiabatic evolution—a complete population transfer from ψ_1 to ψ_3 is guaranteed. Moreover, because the adiabatic transfer (AT) state (44b) does not involve the intermediate state ψ_2, the latter remains unpopulated during the transfer: the AT state is a *dark state.* This means that its properties have little impact on the transfer efficiency. For example, this remarkable feature of STIRAP allows efficient population transfer on time scales exceeding the lifetime of the intermediate state, which usually can decay on the nanosecond scale.

For example, such a situation arises in the implementation of STIRAP with continuous lasers, when the atomic or molecular beam crosses two spatially displaced and partially overlapping continuous-wave (CW) laser beams at right angles (Gaubatz *et al.,* 1990; Theuer and Bergmann, 1998). The time it takes for the atoms or molecules to cross the laser beams is often two orders of magnitude longer than the lifetime of the excited state. It would be impossible to achieve any population transfer by intermediate storage in the excited state, e.g., by stimulated emission pumping. STIRAP, however, produces a transfer efficiency of nearly 100%, because the upper state is never populated appreciably.

It is readily shown that only on two-photon resonance ($\delta = 0$) does there exist a trapped state, without a contribution from the intermediate state ψ_2. Indeed, it follows from the Hamiltonian (40) that the components of any of the eigenstates of H must obey the relation

$$\tfrac{1}{2}\Omega_s C_2 = (\varepsilon - \delta)C_3.$$

Because on two-photon resonance ($\delta = 0$) one of the eigenvalues is zero ($\varepsilon = 0$),

the right hand side (RHS) of the above equation vanishes and the corresponding eigenstate—the trapped state—has no component from the intermediate state, $C_2 = 0$. Off two-photon resonance ($\delta \neq 0$), one can easily show that no eigenvalue is equal to δ ($\varepsilon \neq \delta$) and thus the RHS does not vanish; the implication is a nonzero component $C_2 \neq 0$ from the intermediate state.

6. *Intuitive versus Counterintuitive Pulse Sequences*

When both the pump and Stokes lasers are on resonance with their respective transitions, the two opposite pulse sequences lead to qualitatively different results. While, as explained above, the counterintuitive sequence induces complete population transfer to state ψ_3, the intuitive sequence produces generalized Rabi oscillations in the populations of all three states (He *et al.*, 1990; Shore *et al.*, 1992a,b; Vitanov and Stenholm, 1997b). This is readily seen by noting that for $\Delta = 0$, we have $\varphi \equiv \pi/4$. Because for the intuitive ordering $\vartheta(-\infty) = \pi/2$ and $\vartheta(+\infty) = 0$, we find that the adiabatic states behave as

$$\tfrac{1}{\sqrt{2}}(\psi_1 + \psi_2) \xleftarrow{-\infty} \Phi_+(t) \xrightarrow{+\infty} \tfrac{1}{\sqrt{2}}(\psi_2 + \psi_3), \tag{52a}$$

$$-\psi_3 \xleftarrow{-\infty} \Phi_0(t) \xrightarrow{+\infty} \psi_1, \tag{52b}$$

$$\tfrac{1}{\sqrt{2}}(\psi_1 - \psi_2) \xleftarrow{-\infty} \Phi_-(t) \xrightarrow{+\infty} \tfrac{1}{\sqrt{2}}(-\psi_2 + \psi_3). \tag{52c}$$

It follows from the above equations that initially both states $\Phi_+(t)$ and $\Phi_-(t)$ are populated. Because of the interference between the two different paths from state ψ_1 to state ψ_3, the final population of state ψ_3 will oscillate (Vitanov and Stenholm, 1997b),

$$P_1 = 0, \qquad P_2 = \sin^2 \tfrac{1}{2}A, \qquad P_3 = \cos^2 \tfrac{1}{2}A, \tag{53}$$

with $A = \int_{-\infty}^{+\infty} \Omega(t)\, dt$. Thus, only for certain values of the RMS pulse area (generalized π pulses) is it possible to obtain complete population transfer from state ψ_1 to state ψ_3 with a resonant intuitive pulse sequence. However, in such a setup, the intermediate state would receive appreciable transient population and considerable population losses would occur, unless the pulse durations are much shorter than the intermediate-state lifetime.

When the two lasers are tuned away from the respective single-photon resonances, while maintaining the two-photon resonance, adiabatic evolution produces complete population transfer from ψ_1 to ψ_3 for both pulse sequences (Shore *et al.*, 1992b; Vitanov and Stenholm, 1997b). For the counterintuitive sequence (Stokes before pump), this occurs because, as emphasized above, the trapped state does not

depend on the single-photon detuning Δ. For the intuitive sequence (pump before Stokes), the adiabatic transfer is carried out through the adiabatic state $\Phi_-(t)$. Indeed, for the intuitive ordering, the relations $\vartheta(-\infty) = \pi/2$, $\vartheta(+\infty) = 0$, and $\varphi(-\infty) = \varphi(+\infty) = 0$ apply; then the adiabatic state $\Phi_-(t)$ has the following asymptotic behavior:

$$\psi_1 \xleftarrow{-\infty} \Phi_-(t) \xrightarrow{+\infty} \psi_3. \tag{54}$$

Thus the adiabatic state $\Phi_-(t)$ provides adiabatic connection between states ψ_1 and ψ_3. However, unlike the counterintuitive ordering, here the intermediate state receives a significant transient population, $P_e = \sin^2 \varphi(t)$. Hence, if the lifetime of state ψ_2 is comparable or shorter than the excitation duration, then efficient population transfer can be achieved only with the counterintuitive pulse sequence.

The similarity of population transfer by the two pulse sequences in the off-resonant case ($\Delta \neq 0$) is easily explained when the single-photon detuning Δ is large ($|\Delta| \gg \Omega_p, \Omega_s$); then the intermediate state ψ_2 can be eliminated adiabatically (Shore *et al.*, 1992b; Vitanov and Stenholm, 1997b). As shown in Section II.D.3, the resulting effective two-state model involves a coupling $\Omega_{\text{eff}} = -\Omega_p \Omega_s / 2\Delta$ and a detuning $\Delta_{\text{eff}} = \left(\Omega_p^2 - \Omega_s^2\right)/4\Delta$. Obviously, for sequential pulses the detuning $\Delta_{\text{eff}}(t)$ passes through resonance at the time t_0 when $\Omega_p(t_0) = \Omega_s(t_0)$; this level crossing leads, in the adiabatic limit, to complete population transfer for both pulse orderings, because the ordering reversal leads to the unimportant change of sign in Δ_{eff}, and does not affect Ω_{eff}.

Finally, another interesting feature of STIRAP is that the population P_1 of the initial state ψ_1 does not depend on the pulse order, as can be inferred from the symmetric dependence of P_1 on the pulse delay τ in Fig. 10. This symmetry can be deduced rigorously (Vitanov, 1999).

7. Adiabatic Condition: Local and Global Criteria

For adiabatic evolution, the coupling between each pair of adiabatic states should be negligible compared to the difference between the energies of these states. With respect to the trapped state $\Phi_0(t)$ the adiabatic condition reads (Messiah, 1962; Crisp, 1973; Shore, 1990)

$$|\langle \dot{\Phi}_0 | \Phi_\pm \rangle| \ll |\varepsilon_0 - \varepsilon_\pm|, \tag{55}$$

(note that $\langle \Phi_0 | \dot{\Phi}_\pm \rangle = -\langle \dot{\Phi}_0 | \Phi_\pm \rangle$) or, explicitly (Vitanov and Stenholm 1997a,b),

$$\left| \dot{\vartheta} \frac{\sin^2 \varphi}{\cos \varphi} \right| \ll \tfrac{1}{2}\Omega, \qquad \left| \dot{\vartheta} \frac{\cos^2 \varphi}{\sin \varphi} \right| \ll \tfrac{1}{2}\Omega. \tag{56}$$

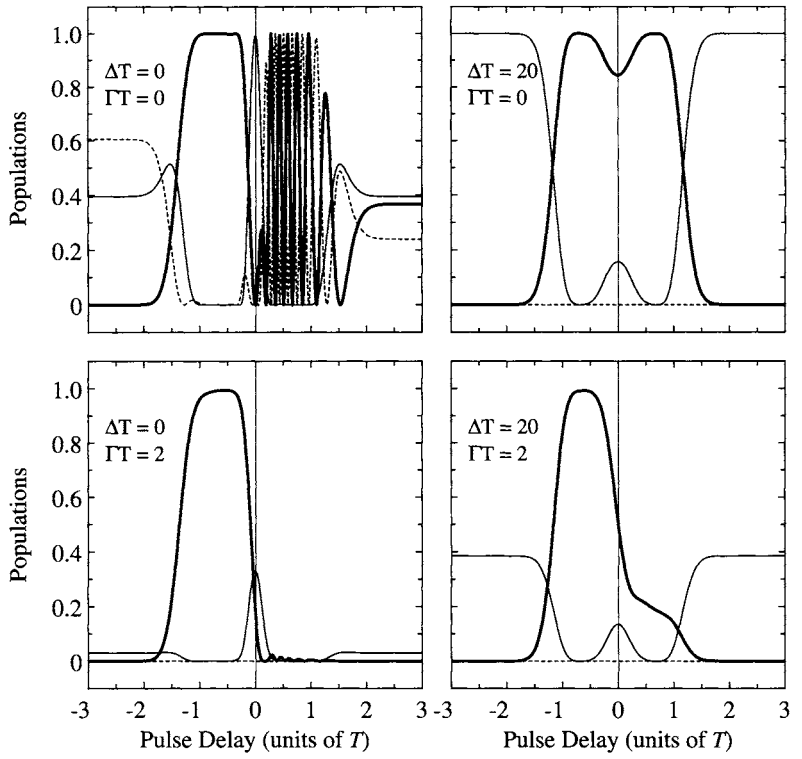

FIG. 10. Numerically calculated populations of the initial state (thin solid line), the intermediate state (dashed line), and the final state (thick solid line) plotted against the pulse delay for different single-photon detuning Δ and loss rate Γ, whose values are denoted in each frame. We have assumed Gaussian pulse shapes, $\Omega_p(t) = \Omega_0 \exp[-(t-\tau)^2/T^2]$, $\Omega_s(t) = \Omega_0 \exp[-(t+\tau)^2/T^2]$, with $\Omega_0 T = 40$.

On one-photon resonance ($\Delta = 0$), we have $\varphi = \pi/4$ and the adiabaticity condition simplifies (Gaubatz *et al.*, 1990),

$$\Omega \gg |\dot{\vartheta}| \propto T^{-1},$$

where T is the pulse width. Assuming that the pump and Stokes pulses are sufficiently smooth and have the same peak Rabi frequency Ω_0, this condition can be written as

$$\Omega_0 T \gg 1. \tag{57}$$

On the left-hand side of this inequality we have the factor $\Omega_0 T$, which, up to an unimportant pulse-shape-dependent factor of the order of unity, is essentially the pulse area. Hence adiabaticity demands a large pulse area. In terms of incoherent

excitation, the large pulse area means saturation of the transitions. In practical applications, the pulse area should exceed 10 to provide efficient population transfer, $\Omega_0 T > 10$.

The above adiabatic criteria (56) and (57) are directly applicable to STIRAP with continuous-wave lasers in the crossed-beam geometry (atomic beam crossing two spatially displaced CW laser beams), because CW lasers have almost perfect coherence properties. For pulsed lasers, the adiabatic conditions need to be modified. For perfectly coherent pulsed lasers, the adiabatic condition is essentially the same, but it is more conveniently written in the equivalent form

$$\Omega_0^2 T > \frac{100}{T}. \tag{58}$$

This condition imposes a lower limit on the pulse energy (which is proportional to $\Omega_0^2 T$) for a given pulse duration T; obviously, the needed laser energy grows rapidly when the pulse duration decreases.

Pulsed lasers, however, often suffer from phase fluctuations, i.e., the actual linewidth $\Delta\omega$ deviates from the transform limit $\omega_{\mathrm{TL}} = 1/T$. A careful analysis of the effect of imperfect laser coherence on the STIRAP efficiency leads to the modified adiabaticity condition (Kuhn *et al.*, 1992),

$$\Omega_0 T \gg \left[1 + \left(\frac{\Delta\omega}{\Delta\omega_{\mathrm{TL}}}\right)^2\right]^{1/2}. \tag{59}$$

The adverse effect of imperfect laser coherence derives from the fact that both phase fluctuations and frequency chirp correspond to time-dependent changes in the laser frequencies. Unless these changes are correlated (e.g., if the pump and Stokes pulses are derived from the same laser), they will result in time-dependent detuning from two-photon resonance. The two-photon detuning induces nonadiabatic couplings between the dark state and the other adiabatic states that reduce the transfer efficiency. These population losses can be reduced by increasing the laser intensity, thereby suppressing nonadiabatic transitions. This problem is discussed in more detail in Section IV.B.

8. Nonadiabatic Transitions

An important subject of theoretical investigation is the behavior of the system away from the adiabatic limit. Of particular interest is here the question in what manner the adiabatic limit is approached.

For smooth, ramped pump, and Stokes pulses, diabatic corrections are exponentially small in the inverse adiabaticity parameter (Elk, 1995). This behavior is

very similar to the classic result by Dykhne (1962) and Davis and Pechukas (1976) for two-level systems. For many STIRAP models this is not the case, however, and there is a power-law dependence (Laine and Stenholm, 1996; Vitanov and Stenholm, 1996; Drese and Holthaus, 1998).

The following section discusses various other factors that affect adiabaticity.

B. Sensitivity of STIRAP to Interaction Parameters

1. Sensitivity to Delay

The following considerations affect the choice of an optimum delay between the Stokes and pump pulses.

- *Coincident pulses:* In this case the mixing angle ϑ is constant and the evolution is fully adiabatic because the nonadiabatic coupling vanishes ($\dot{\vartheta} = 0$). However, the initial projection of the state vector $\mathbf{\Psi}$ onto the trapped state $\Phi_0(t)$ is incomplete, i.e., the trapped state is not the only adiabatic state populated initially and the interference between different evolution paths from ψ_1 to ψ_3 lead to oscillations in the final population of the target state ψ_3 (Vitanov, 1998b), rather than to complete population transfer. Hence this regime presents the "good adiabaticity argument" but the "bad projection argument."
- *Small delay, very large overlap:* For delayed and counterintuitively ordered pulses, the initial projection of the state vector onto Φ_0 is unity. When the pulses are only slightly delayed, the mixing angle ϑ is nearly constant during most of the overlap and hence $\dot{\vartheta} \approx 0$ ("good adiabaticity argument"); if the pump and Stokes peak Rabi frequencies are equal, then $\vartheta \approx \pi/4$ during the overlap. However, ϑ rises too quickly from 0 to about $\pi/4$ during the short interval between the arrivals of the Stokes and pump pulses, and then again rises too quickly from $\pi/4$ to $\pi/2$ during the short interval between the disappearance of the two pulses. During these two time intervals, the nonadiabatic coupling (which is $\propto \dot{\vartheta}$) can reach significant values and can cause nonadiabatic transitions to the other adiabatic states Φ_+ and Φ_-. Thus when the system enters the pulse overlap region the state vector $\mathbf{\Psi}$ is not parallel to the trapped state Φ_0, i.e., we have "bad projection." The presence of two nonadiabatic zones eventually leads to interference and oscillations in the transfer efficiency, as for coincident pulses. Hence this regime presents the "good adiabaticity argument" during the pulse overlap, but the "bad projection argument" at the entry and the exit of the overlap region.
- *Large delay, very small overlap:* The initial projection of the state vector onto Φ_0 is unity. However, the mixing angle ϑ stays nearly constant for most

of the excitation (≈ 0 early when only the Stokes pulse is present and $\approx \pi/2$ at late times when only the pump pulse is present) and rises from 0 to $\pi/2$ during only a very short period when the pulses overlap; during this period the nonadiabatic coupling ($\propto \dot{\vartheta}$) is very large and causes transitions to the other adiabatic states Φ_+ and Φ_-, resulting in loss of transfer efficiency. Hence this regime presents the "good projection argument" but the "bad adiabaticity argument" during the pulse overlap.

- *Optimum delay:* The optimal pulse delay, which must lead to maximal transfer efficiency, can be determined by maximizing adiabaticity. For maximal adiabaticity, the mixing angle $\vartheta(t)$ must change slowly and smoothly in time, so that the nonadiabatic coupling ($\propto \dot{\vartheta}$) remains small, without pronounced peaks. As follows from the above discussion, the optimal adiabaticity occurs for a certain range of moderate delays, when both the two-peak time dependence of $\dot{\vartheta}$ appearing for small delay and the sharp-single-peak time dependence appearing for large delay, are absent. The particular optimal value of τ depends on the pulse shapes. For Gaussian pulses, the optimum occurs when the delay is nearly equal to the pulse width, $\tau_{\text{opt}} \approx T$.

2. *Sensitivity to Rabi Frequency and Pulse Width*

It is best to have intensities adjusted such that when combined with the given dipole transition moments rates the two peak Rabi frequencies are about equal. If the maximum Rabi frequencies are very different, and the pulse widths are about the same, than the projection of the state vector onto the adiabatic transfer state is very good early (or late) but necessarily less good late (or early), i.e., "good projection" cannot be achieved both early *and* late, and consequently the transfer efficiency will be small. It is interesting to note that in this case the population which does not end up in state ψ_3 returns to state ψ_1, i.e., the transfer efficiency is not limited by spontaneous emission losses. The same reasoning leads to the conclusion that the pump and Stokes pulse widths should also be about equal.

It should be noted that with large pulse areas those prescriptions are not in conflict with the claim that the method is robust. For large pulse areas, small deviations from the optimum do not lead to significant drop in transfer efficiency. Using equal peak Rabi frequencies and equal pulse widths allows to reduce the necessary pulse areas and hence facilitates efficient population transfer.

3. *Sensitivity to Single-Photon Detuning*

Typical STIRAP experiments permit measurement of the population transfer probability for various choices of the two carrier frequencies. Because a plot of transfer probability versus frequency appears similar to a plot of emission or absorption

intensity versus frequency (a *spectral line profile*), the full-width at half-maximum (FWHM) profile is termed the line width.

Two profiles are of interest. Variation of both the pump and Stokes frequencies, while maintaining the two-photon resonance condition, presents a *single-photon* profile, $P_3(\Delta)$. Alternatively, variation of either carrier frequency, while keeping the other fixed, will cause a change in the two-photon detuning, and will lead to a two-photon profile, $P_3(\delta)$.

As is evident from Eqs. (44), the single-photon detuning Δ does not affect the formation or the composition of the trapping state (as long as two-photon resonance is maintained), because the mixing angle ϑ does not depend on Δ. However, the other mixing angle φ depends on Δ and therefore the detuning affects the adiabatic conditions (56). Since $|\varphi| \leq \pi/4$, and hence $|\sin\varphi| \leq \cos\varphi$, the latter of conditions (56) is more stringent. Because φ is a decreasing function of Δ [cf. Eq. (45)], the LHS of this condition increases with Δ. This implies that STIRAP works best on single-photon resonance; when the single-photon detuning Δ increases, adiabaticity deteriorates and the transfer efficiency decreases.

We can easily derive the scaling properties of the FWHM $\Delta_{1/2}$ of the single-photon line profile $P_3(\Delta)$. For large Δ, when Δ begins to affect adiabaticity, we have $\varphi \approx \Omega/2\Delta$ and condition (56) becomes $\frac{1}{4}\Omega^2 \gg |\Delta\dot{\vartheta}|$. Because $\dot{\vartheta}$ depends only on the pulse delay τ and the pulse shapes [cf Eq. (45)], but not on Δ or on the peak Rabi frequency Ω_0, the width $\Delta_{1/2}$ must scale with Ω_0^2. Upon introducing a pulse-delay dependent proportionality factor $D(\tau)$, one may write (Vitanov and Stenholm, 1997a)

$$\Delta_{1/2} = D(\tau)\Omega_0^2. \tag{60}$$

Because the Rabi frequency is proportional to the electric field amplitude, the single-photon width $\Delta_{1/2}$ is proportional to the peak intensity.

4. Sensitivity to Two-Photon Detuning

It is also possible to derive a simple scaling relationship for the sensitivity of population transfer to the two-photon detuning $\delta = \Delta_p - \Delta_s$ (Danileiko *et al.*, 1994; Romanenko and Yatsenko, 1997; Fewell *et al.*, 1997; Vitanov, 2001). The detuning from two-photon resonance is much more crucial for STIRAP than the single-photon detuning, because the two-photon detuning prevents the exclusive population of the trapped state.

The sensitivity of the transfer efficiency to the two-photon detuning δ can be quantified by examining the behavior of the three eigenstates of the Hamiltonian (40), which are no longer given by Eqs. (44) (Danileiko *et al.*, 1994; Romanenko and Yatsenko, 1997; Fewell *et al.*, 1997). In particular, the trapped state $\Phi_0(t)$ is no longer an eigenstate of $\mathsf{H}(t)$. For nonzero δ, each of the three eigenstates of the

Hamiltonian (40) connects to *the same* bare state at both $t = -\infty$ and $t = +\infty$, and hence there is no adiabatic transfer state providing an adiabatic connection from state ψ_1 to state ψ_3, as does the trapped state Φ_0 for $\delta = 0$. Thus adiabatic evolution leads to complete population return of the system to its initial state ψ_1, i.e., to zero transfer efficiency. The only mechanism by which some population transfer to state ψ_3 can occur is by nonadiabatic transitions between the adiabatic states. Such transitions can take place for small values of δ when there are narrow avoided crossings between the adiabatic eigenvalues. This is illustrated in Fig. 11. By using the Landau–Zener formula (Landau, 1932; Zener, 1932) to evaluate the nonadiabatic transitions at these avoided crossings, analytic expressions for the two-photon linewidth have been derived (Danileiko *et al.*, 1994; Romanenko and Yatsenko, 1997).

An alternative approach to estimating the two-photon line width makes use of the adiabatic condition (Vitanov, 2001). We assume for simplicity single-photon resonance, $\Delta = 0$. From the initial bare-state basis we make a transformation to the basis of the states (44), which are the eigenstates of $\mathsf{H}(t)$ for $\delta = 0$, rather than to the genuine $\delta \neq 0$ adiabatic basis. In the basis (44), the effect of nonzero two-photon detuning δ shows up in additional terms in the respective Hamiltonian proportional to δ (Vitanov 2001),

$$\mathsf{H}_b(\delta) = \mathsf{H}_b(\delta = 0) + \frac{1}{2}\hbar\delta\cos^2\vartheta \begin{bmatrix} 1 & -\sqrt{2}\tan\vartheta & 1 \\ -\sqrt{2}\tan\vartheta & 2\tan^2\vartheta & -\sqrt{2}\tan\vartheta \\ 1 & -\sqrt{2}\tan\vartheta & 1 \end{bmatrix}, \quad (61)$$

where $\mathsf{H}_b(\delta = 0)$ is given by Eq. (51). If we now assume that the evolution is adiabatic for $\delta = 0$ (i.e., that we have unity transfer efficiency on two-photon resonance), we can neglect all nondiagonal terms in $\mathsf{H}_b(\delta = 0)$. We can also neglect

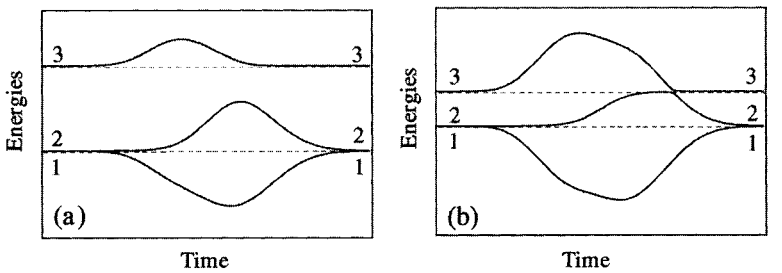

FIG. 11. Time evolution of the energies in a three-state system with two-photon detuning: (a) large two-photon detuning (no transfer); (b) narrow avoided crossings for small two-photon detuning (transfer through diabatic transitions).

all δ terms in the diagonal elements of $\mathsf{H}_b(\delta)$, unless the two-photon detuning is comparable with the eigenvalue separation (then the transfer efficiency would be virtually zero). Then the effect of the nonzero two-photon detuning δ shows up as additional nonadiabatic couplings (which do not vanish in the adiabatic limit) between the $\delta = 0$ adiabatic states (44). Considerable population transfer between states ψ_1 and ψ_3 can still be realized if the Λ system is forced to stay in the trapped state Φ_0. This requirement leads to the condition

$$\delta \sin\vartheta \cos\vartheta \ll \tfrac{1}{\sqrt{2}}\Omega.$$

Because, as we emphasized above, the mixing angle ϑ does not depend on the peak Rabi frequency Ω_0 but only on the ratio Ω_p/Ω_s, i.e., on the pulse delay τ and the pulse shapes, the width $\delta_{1/2}$ of the two-photon line profile $P_3(\delta)$ must scale with Ω_0. By introducing a pulse-delay dependent proportionality factor $d(\tau)$, one may write (Vitanov 2001)

$$\delta_{1/2} = d(\tau)\Omega_0. \tag{62}$$

By contrast with the single-photon width $\Delta_{1/2}$, the two-photon width $\delta_{1/2}$ varies in proportion to the Rabi frequency, meaning the square root of the peak intensity.

In conclusion, STIRAP efficiency is much less sensitive to single-photon detuning (because the single-photon linewidth grows with the square of the pulse area, $\Delta_{1/2} \propto (\Omega_0 T)^2$) than to two-photon detuning (where the linewidth increases only linearly with the pulse area, $\delta_{1/2} \propto \Omega_0 T$). A numerical example is shown in Fig. 12 and experimental results in Fig. 13.

5. Sensitivity to Losses from the Intermediate State

As we emphasized above, in the adiabatic limit, no population resides in state ψ_2, and spontaneous emission from ψ_2 is not detrimental to successful population transfer. However, a strong decay from state ψ_2 may reduce adiabaticity and demands larger laser intensity for high transfer efficiency. The influence of spontaneous emission from the intermediate state ψ_2 both within the Λ system (back to states ψ_1 and ψ_3) (Band and Julienne, 1991a, 1992) and to other states (Glushko and Kryzhanovsky, 1992; Fleischhauer and Manka, 1996; Vitanov and Stenholm, 1997d) has been studied. Modeling spontaneous emission within the Λ system requires using the Liouville density-matrix equation and it is hard to derive analytic estimates, while population losses to states outside the Λ system allow analytic treatment (Fleischhauer and Manka, 1996; Vitanov and Stenholm, 1997d) using the Schrödinger equation.

The effect of irreversible losses is most conveniently estimated in the lossless ($\Gamma = 0$) adiabatic basis (51), where the effect of the loss rate shows as additional

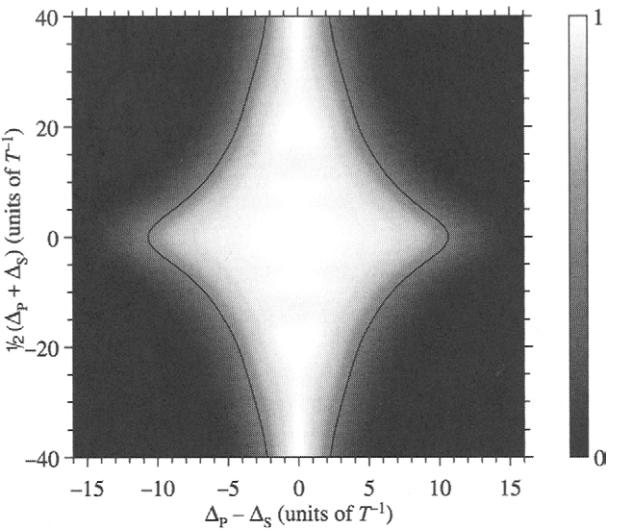

FIG. 12. Numerically calculated transfer efficiency in STIRAP plotted versus the sum and the difference of the pump and Stokes detunings (i.e., versus the single-photon and two-photon detunings) for Gaussian pulse shapes, $\Omega_p = \Omega_0 \exp[-(t-\tau)^2/T^2]$, $\Omega_s = \Omega_0 \exp[-(t+\tau)^2/T^2]$, with $\Omega_0 T = 20$, $\tau = 0.5T$. The curves show the $P_3 = 0.5$ value.

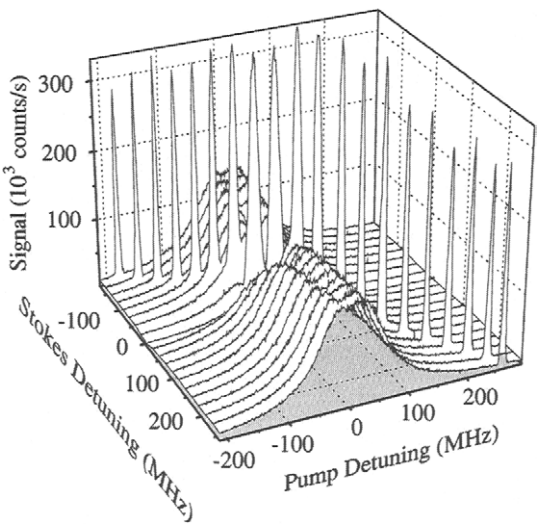

FIG. 13. Experimentally measured transfer efficiency of STIRAP plotted versus the pump and Stokes detunings. (From J. Martin, B. W. Shore, and K. Bergmann. Coherent population transfer in multilevel systems with magnetic sublevels. III. Algebraic analysis. *Phys. Rev. A* 1996;54:1556–1569.)

imaginary terms (Vitanov and Stenholm, 1997d) in the Hamiltonian

$$\mathsf{H}_b(\Gamma) = \mathsf{H}_b(\Gamma = 0) + \frac{1}{2} i\Gamma \begin{bmatrix} -\cos^2\varphi & 0 & \frac{1}{2}\sin 2\varphi \\ 0 & 0 & 0 \\ \frac{1}{2}\sin 2\varphi & 0 & -\sin^2\varphi \end{bmatrix}, \tag{63}$$

where $\mathsf{H}_b(\Gamma = 0)$ is given by Eq. (51). Obviously, the losses affect much more strongly population transfer by the intuitive pulse ordering because then the decaying intermediate state may receive considerable transient population. Since then the population is transferred via the adiabatic state Φ_-, which decays with a rate $\frac{1}{2}\Gamma \sin^2\varphi$, the transfer efficiency decreases exponentially with Γ.

For the counterintuitive pulse ordering, the population losses occur by two mechanisms. The first mechanism, which dominates at small to medium decay rates, is by dissipation of population that visits state ψ_2 due to imperfect adiabaticity. In the adiabatic basis, imperfect adiabaticity leads to nonadiabatic transitions from the nondecaying dark state Φ_0 to the other, decaying adiabatic states Φ_+ and Φ_-, from which population losses occur. The second mechanism is quantum overdamping, which dominates for large Γ and leads to effective decoupling of the three-state system from the laser fields. These two mechanisms lead to different damping of the transfer efficiency with Γ: exponential at small Γ (but with a much smaller effective loss rate than for the intuitive pulse ordering) and polynomial at large Γ.

By using a similar approach as for the estimation of the single-photon line width $\Delta_{1/2}$ (Section III.B.3), one can show that the "linewidth" $\Gamma_{1/2}$, the loss rate value at which the transfer efficiency drops to $\frac{1}{2}$, is proportional to the squared pulse area (Vitanov and Stenholm, 1997d),

$$\Gamma_{1/2} \approx G\left(\frac{\tau}{T}\right)(\Omega_0 T)^2, \tag{64}$$

where $G(\tau/T)$ is a coefficient that depends on the pulse delay τ (and on the specific pulse shapes) but not on $\Omega_0 T$. In the case of Gaussians, an analytic approximation for the coefficient $G(\tau/T)$ reads (Vitanov and Stenholm, 1997d)

$$G(\tau/T) \approx \frac{3(\tau/T)\ln 2}{8(\tau/T)^2 + \pi/2} e^{-2(\tau/T)^2}. \tag{65}$$

Formula (65) suggests that $G(\tau/T)$ rises from zero at $\tau = 0$ to its maximum value of about 0.23 at $\tau \approx 0.302T$ and then decreases in a near-Gaussian fashion with τ. The decrease of $G(\tau/T)$ at small τ/T is because then the loss rates of states Φ_+ and Φ_- increase and larger pulse area is needed to suppress them. The decrease of $G(\tau/T)$ at large τ/T is due to the larger nonadiabatic coupling between the dark

state Φ_0 and the other adiabatic states Φ_+ and Φ_-, which again requires larger pulse area to ensure sufficient adiabaticity.

6. *Sensitivity to Beam Geometry*

The optimum geometry of the laser beams (circular or cylindrical with different orientations of the ellipsoid) depends on the purpose of the excitation. For scattering experiments it is desirable to maximize the flux of atoms which crosses the laser beams in regions that allow adiabatic evolution. In other applications, one may want to manipulate a highly collimated beam, and the laser power may be at the limit of what is needed; in that case, one wants to increase the interaction time to improve the adiabatic evolution.

Given the nonspherical intensity distribution according to

$$\vec{E}(x, y, t) = \tfrac{1}{2}\vec{e}\mathcal{E}_0 e^{i\omega t} e^{-(x/w_x)^2-(y/w_y)^2} + \text{c.c.}, \tag{66}$$

the intensity $I(x, y)$ and power P are given by $I(x, y) = \frac{1}{2}c\epsilon_0\vec{E}^2(x, y)$ and $P = \int_{x,y} dx\, dy I(x, y) = \frac{\pi}{2} w_x w_y I_0$, respectively. From these one obtains the Rabi frequency,

$$\Omega = \frac{d}{\hbar}\sqrt{\frac{4}{c\pi\epsilon_0}}\sqrt{\frac{P}{w_x w_y}}. \tag{67}$$

The global adiabaticity criterion can be written in a form which contains the shape parameters of the laser beam,

$$\frac{4d}{\hbar v}\sqrt{\frac{1}{c\pi\epsilon_0}}\sqrt{\frac{w_x P}{w_y}} \gg 1, \tag{68}$$

where v is the atom velocity.

It is interesting to note that the adiabaticity criterion is independent of the laser beam diameter D for circular beam geometry! This is because the interaction time increases linearly with D, while the local (and maximum) Rabi frequency decreases inversely proportional to D. Thus, the dependence on D cancels.

As illustrated in Fig. 14, a laser beam focused cylindrically with the long axis perpendicular to the particle beam axis allows one to manipulate a relatively large flux, but the Rabi frequency increases less than the interaction time decreases (given the same power of the laser beam, of course). Thus the price for a high flux of manipulated (excited) atoms or molecules is a higher intensity.

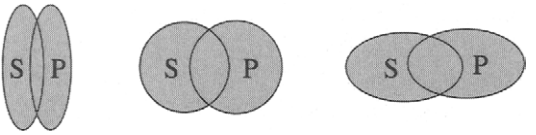

FIG. 14. Laser beam geometries for STIRAP.

A cylindrical focus with the long axis parallel to the particle beam axis reduces the flux of manipulated particles. However, since the interaction time increases more than the Rabi frequency decreases, the required intensity is smaller.

Given these considerations it is interesting to ask: how large can we allow the cylindrical focus to be? One obvious limitation is that the interaction time can not be increased indefinitely. Increasing the interaction time makes the transfer process more sensitive to the detrimental phase fluctuations during the adiabatic passage process. Thus the transit time through the overlap region should be small compared to the inverse of the laser linewidth.

7. *Multiple Intermediate States*

In the standard three-state STIRAP, the Raman linkage between the initial state ψ_1 and the final state ψ_3 takes place via a single intermediate state ψ_2. In real atoms, and particularly in molecules, it may happen that there are multiple intermediate states strongly coupled to ψ_1 and ψ_3 by the pump and Stokes fields, thus forming a parallel multi-Λ system. Such couplings may be present because, while very sensitive to the two-photon resonance, STIRAP is relatively insensitive to the single-photon detuning from the intermediate state. Coulston and Bergmann (1992) were the first to consider the effects of multiple intermediate states in the simplest case of $N=2$ states and equal couplings $\Omega_p(t)$ to state ψ_1 and equal couplings $\Omega_s(t)$ to state ψ_3. Vitanov and Stenholm (1999) studied the general case of unequal couplings and unevenly distributed, N intermediate states. It has been concluded that the dark state (44b) remains a zero-eigenvalue eigenstate of the Hamiltonian only when, for each intermediate state ψ_k, the ratio $\Omega_p^{(k)}(t)/\Omega_s^{(k)}(t)$ between the couplings to the initial and target states is the same and does not depend on k. Then the multi-Λ system behaves very similarly to the single-Λ system in STIRAP, and complete population transfer with no transient population in any intermediate state can take place for adiabatic evolution. When this proportionality condition is not fulfilled, a dark state does not exist but a more general adiabatic transfer state, which links adiabatically the initial and target states, may exist under certain conditions on the single-photon detunings and the relative coupling strengths. This AT state, unlike the dark state, contains contributions from the intermediate states which therefore acquire transient populations during the transfer.

It has been shown (Vitanov and Stenholm, 1999) that when the pump and Stokes frequencies are scanned across a manifold of N intermediate states (while maintaining the two-photon resonance), the target-state population passes through N regions of high transfer efficiency (unity in the adiabatic limit) and $N-1$ regions of low efficiency (zero in the adiabatic limit). It is most appropriate to tune the pump and Stokes lasers either just below or just above all intermediate states because there the AT state always exists, the adiabatic regime is achieved more quickly, the transfer is more robust against laser fluctuations, and the transient intermediate-state populations, which are inversely proportional to squared single-photon detunings, can easily be suppressed.

8. STIRAP Beyond the RWA

Conventional STIRAP assumes applicability of the rotating-wave approximation. This approximation requires that the two Rabi frequencies and the single-photon detunings are much smaller than the Bohr transition frequencies. In most experiments, these conditions are well satisfied.

Several extensions of conventional STIRAP beyond the RWA have been explored. In the most extreme case, Guérin and Jauslin (1998) have examined, by using an adiabatic Floquet approach, the situation when the Rabi frequencies are comparable to the Bohr frequencies. Then the feasibility of adiabatic population transfer can be deduced by analyzing a plot of the eigenenergies of a Floquet Hamiltonian.

Yatsenko *et al.* (1998) have studied the case when the envelopes of the laser pulses are not smooth but are modulated periodically in time. In the adiabatic Floquet picture, a success or failure of adiabatic population transfer can be deduced, again, from a plot of the eigenenergies of a Floquet Hamiltonian. In such a plot, there occurs an infinite sequence of eigenenergy triplets. The distance between the triplets is proportional to the modulation frequency, while the splitting of the Floquet energies within each triplet is proportional to the peak Rabi frequency Ω_0. When the modulation frequency exceeds the peak Rabi frequency, high transfer efficiency can be achieved because the adjacent triplets are well separated and do not interfere with each other. When Ω_0 is comparable or larger than the modulation frequency, the success or failure of adiabatic population transfer is determined by an interplay between the splitting within each triplet and the separation of the triplets.

It may also occur that the two laser fields act on both the pump and Stokes transitions, e.g., when the two laser fields have the same polarization. If the two Bohr frequencies are sufficiently different, so that their difference is large compared to the Rabi frequencies of the pump and Stokes pulses ($|\omega_{12} - \omega_{32}| \gg \Omega_p, \Omega_s$), one can neglect the off-resonant channels, i.e., the action of the pump laser on the Stokes transition and the action of the Stokes laser on the pump transition. If the Rabi frequencies are comparable to or bigger than the difference of the Bohr

frequencies (Ω_p, $\Omega_s \gtrsim |\omega_{12} - \omega_{32}|$), the off-resonant channels have to be accounted for (Unanyan *et al.*, 2000c). Then efficient and robust population transfer can still be possible under certain conditions with the exchange of one or more (odd-number) photons between each laser field and the atom. With the multiple-photon scenario, however, the transient population of the intermediate level is no longer negligibly small, even when the evolution is adiabatic.

IV. Three-State STIRAP: Experiments

When continuous-wave lasers are used in combination with atomic or molecular beams, it is straightforward to expose the atoms or molecules to a delayed sequence of interactions by spatially displacing the axes of the laser beams (see Fig. 15). When pulsed lasers are used, the axes of the laser beams need to coincide but the pulses must be delayed in time.

A. Experimental Demonstrations with CW Lasers

1. Sodium Dimers

After preliminary, incomplete, results (Gaubatz *et al.*, 1988), the first convincing experimental demonstration of STIRAP was achieved by Bergmann and coworkers in studies of Na_2 (Gaubatz *et al.*, 1990). A beam of sodium molecules crossed two spatially displaced but partially overlapping CW laser beams. When

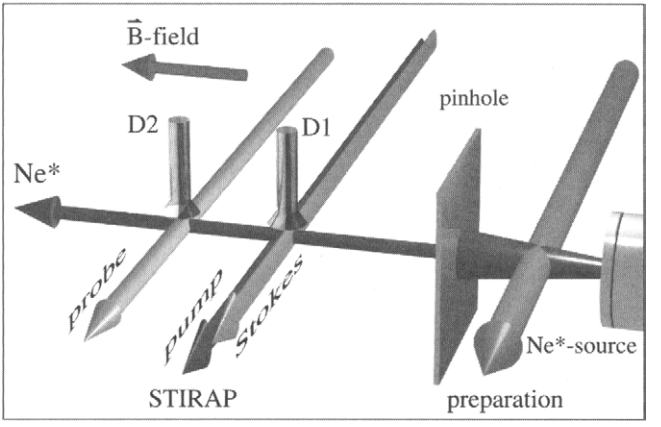

FIG. 15. Experimental setup for the Ne experiment. (From K. Bergmann, H. Theuer, and B. W. Shore. Coherent population transfer among quantum states of atoms and molecules. *Rev. Mod. Phys.* 1998;70:1003–1025.)

the molecules interacted first with the Stokes laser (counterintuitive ordering), complete population transfer was observed from the initial level ($v = 0$, $J = 5$) to the final level ($v = 5$, $J = 5$) of the molecules in their electronic ground state $X^1\Sigma_g^+$ via an intermediate level ($v = 7$, $J = 6$) of the excited electronic state $A^1\Sigma_u^-$. The time required for a molecule to traverse the two laser beams was about 200 ns. Although this interaction time was much longer than the excited-state lifetime ($\approx$15 ns), efficient population transfer was achieved because STIRAP does not populate the excited state appreciably. Because the interaction time was relatively long and because the sodium dimers have relatively strong transition moments, only moderate laser intensities were needed to induce large pulse areas. Typical intensities in the range of 100 W/cm^2 were sufficient to produce adiabatic passage. This radiation was provided by CW lasers having of the order of 100 mW power, with radiation mildly focused to a spot diameter of a few hundred micrometers into the molecular beam.

2. *Metastable Neon Atoms*

STIRAP has been studied in detail in metastable neon in a similar crossed-beam geometry (Rubahn *et al.*, 1991; Martin *et al.*, 1996; Lindinger *et al.*, 1997; Theuer and Bergmann, 1998). In the experiment by Theuer and Bergmann (1998), the population was transferred from state $2p^5 3s\,^3P_0$ to state $2p^5 3s\,^3P_2$ via the intermediate state $2p^5 3p\,^3P_1$. In the experiment, a beam of Ne* atoms emerged from a discharge source (see Fig. 15). A preparation laser depleted the population of the $^3P_2$ metastable level by optical pumping. Excitation of the $^3P_2$ level to the $^3D_2$ level resulted in spontaneous emission to the short-lived levels of the $2p^5 3s$ configuration, followed by decay to the ground state. After passing through a collimating slit, the atoms crossed the STIRAP zone, composed of the Stokes and pump lasers, with their axes suitably displaced. In the STIRAP region, the population of the $^3P_0$ state was transferred to the other metastable level $^3P_2$. If the population transfer was incomplete, some transient population would reside in the intermediate level and VUV fluorescence (photon energy 16.7 eV) would be observed at the channeltron detector D1. Downstream from the STIRAP zone a probe laser excited atoms in the $^3P_2$ level and the subsequent VUV radiation was monitored by a channeltron detector D2, with almost no background signal. The pump and Stokes intensities used in the experiment, typically a few W/cm^2, were provided by CW radiation, focused into the atomic beam by cylindrical lenses.

Figure 16 displays typical evidence for STIRAP. The upper frame shows laser-induced fluorescence from the final state $^3P_2$ (monitored by detector D2) as a function of the pump laser frequency, while the Stokes laser frequency is held fixed slightly off-resonance. The signal shows a broad feature, widened by strong saturation to exceed the natural linewidth by an order of magnitude. At a specific pump detuning, the two-photon resonance condition is met and coherent population

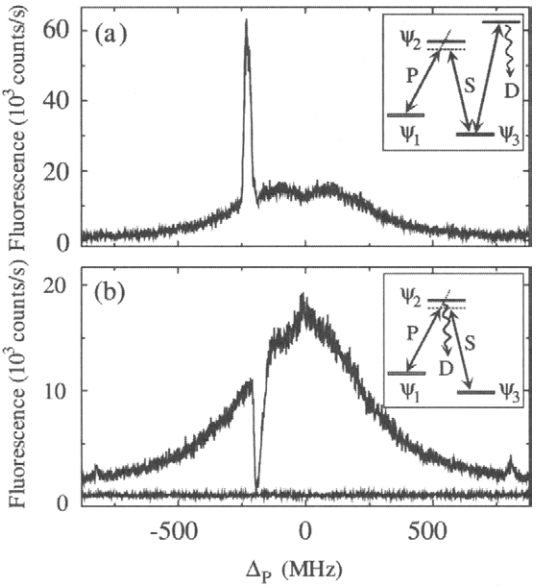

FIG. 16. Laser-induced fluorescence from the final state $^3P_2$ (upper frame) and fluorescence from the intermediate state $^3P_1$ in the Ne* experiment plotted against the pump laser frequency, while the Stokes laser frequency, tuned slightly off-resonance, remains unchanged. (From K. Bergmann, H. Theuer, and B. W. Shore. Coherent population transfer among quantum states of atoms and molecules. *Rev. Mod. Phys.* 1998;70:1003–1025.)

transfer occurs. Then very little (if any) transient population will reside in the intermediate state $^3P_1$ and the fluorescence from there (monitored by detector D1) will disappear, as shown in Fig. 16b. Thus, efficient population transfer is accompanied by a pronounced dark resonance. Indeed, although the typical time required for passage of atoms across the laser beams was more than 20 times longer than the radiative lifetime ($\approx$20 ns) of the intermediate state, no more than 0.5% of the population was detected in this state at the center of the dark resonance (i.e., at two-photon resonance).

Figure 17 displays another characteristic signature for STIRAP. This figure shows the transfer efficiency plotted versus the spatial displacement between the pump and Stokes laser beams, i.e., versus the pulse delay from the viewpoint of the Ne* atoms. Positive displacement (on the left-hand side) corresponds to counter-intuitive pulse ordering (Stokes before pump) and negative displacement (on the right-hand side) to intuitive ordering (pump before Stokes). When the Stokes beam was shifted too far upstream (far left in the figure), it was excluded from the interaction because there was no overlap with the pump pulse; in this case about 25% of the population was optically pumped into the target state because the pump laser excited the atoms to the intermediate state from which they decayed radiatively.

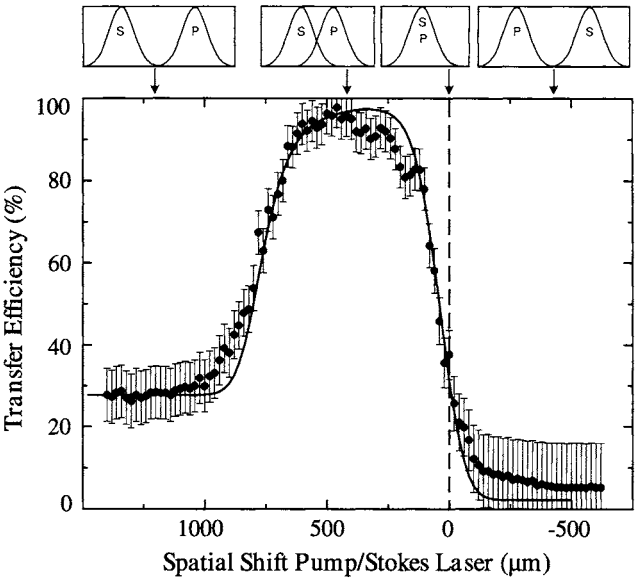

FIG. 17. Transfer efficiency versus displacement between pump and Stokes pulses in Ne* experiment. The broad plateau, showing nearly complete population transfer for counterintuitive pulse sequence, is a typical STIRAP signature, as contrasted with the low efficiency for intuitively ordered pulses. The dots are experimental data and the solid curve shows numeric simulation. (From K. Bergmann, H. Theuer, and B. W. Shore. Coherent population transfer among quantum states of atoms and molecules. *Rev. Mod. Phys.* 1998;70:1003–1025.)

As the Stokes beam was shifted toward the pump beam, while still preceding it, the transfer efficiency increased dramatically and reached almost unity. When the axes of the two lasers coincided, the transfer efficiency dropped to about 25%. Virtually no transfer was observed when the Stokes beam was moved farther downstream so that the Ne* atoms encountered the pump laser first (intuitive pulse ordering). In this configuration the atoms were transferred to the intermediate state by the pump laser and reached the final state by spontaneous emission from there; toward the end of the interaction they were exposed to the Stokes laser only and were thus lost from state ψ_3 by optical pumping and subsequent spontaneous emission of VUV radiation in a two-step radiative-decay cascade to the neon ground state. The broad plateau for counterintuitive pulse ordering is a characteristic feature of STIRAP and indicates the robustness of the population transfer.

In the previously discussed setups the propagation direction of pump and Stokes fields was chosen parallel. This is not necessary, however, as was demonstrated experimentally again using Ne* atoms (Theuer *et al.*, 1999). Here circularly (σ) polarized Stokes radiation couples the $^3P_2 \leftrightarrow {}^3P_1$ transition and a linear (π) polarized pump laser the $^3P_1 \leftrightarrow {}^3P_0$ transition. As will be shown in Fig. 36, pump and Stokes are at 90° with respect to each other and both intersect the beam of

metastable Ne* at right angles to minimize the effect of Doppler shifts. They are properly displaced in order to guarantee a counterintuitive coupling in the frame of the moving atoms. After careful preparation of the initial state by depopulation optical pumping, a two-photon resonance width of 6 MHz (FWHM) was measured, which is clearly below the single-photon value. This type of coupling using σ–π polarizations and orthogonal propagation directions is of particular importance for the realization of a variable coherent atomic beam splitter, which will be discussed in Section VI.

B. Experimental Demonstrations with Pulsed Lasers

1. General Considerations for Pulsed Lasers

A very interesting and important application of STIRAP is the selective excitation of high-lying vibrational levels in molecules. In most molecules the first electronically excited states have energies more than 4 eV above the ground state. Therefore a Raman-type linkage from the vibrational ground level to a high vibrational level requires ultraviolet lasers. Strong ultraviolet radiation is most readily provided by frequency-conversion techniques involving high-intensity pulsed lasers. Furthermore, since the molecular transition dipole moments are usually considerably smaller than for atoms, the adiabaticity condition is difficult to satisfy with CW lasers. Sufficiently strong light intensity, and hence large enough couplings, can be delivered only by pulsed lasers. Pulsed lasers, however, often have inferior coherence properties, e.g., they suffer from phase fluctuations and frequency chirping; both of these effects increase the pulse bandwidth.

As follows from the adiabatic condition (59), the required laser energy increases quadratically with the pulse bandwidth. For conventional nanosecond lasers that are not specially designed to yield nearly transform-limited pulses, the ratio $\Delta\omega/\Delta\omega_{\mathrm{TL}}$ is typically bigger than 10. According to the above estimate, the intensity needed for STIRAP has to be increased by a factor of 100 with respect to transform-limited pulses. While in principle it is possible to obtain higher intensities by focusing the laser beam, this would be detrimental for most applications, where large volumes of the molecular jet have to be excited, e.g., in reactive scattering experiments. Therefore, it is very difficult to satisfy the adiabaticity criterion for laser pulses whose bandwidth clearly exceeds the transform-limited bandwidth.

In short-pulse implementations of STIRAP, one should also account for the rapidly increasing laser energy required to ensure adiabatic evolution, as prescribed by condition (58). Thus, if a pulse energy of 1 mJ were sufficient to ensure adiabatic evolution for a 1-ns laser pulse, then the same degree of adiabaticity would require energy of 1 J for a 1-ps laser pulse, even if the bandwidth of the latter is transform limited. Still, this does not mean that long-pulse or CW lasers offer the best possibilities to implement STIRAP. Indeed, the product $\Omega_0 T$, which is proportional to the square root of the pulse energy times the pulse duration T,

is typically largest for tunable laser sources of intermediate pulse duration, i.e., nanosecond lasers. Conventional tunable picosecond and femtosecond lasers typically cannot compensate for the shorter pulse duration by an adequate increase in pulse energy. High peak intensity leads to detrimental multiphoton couplings and ionization. On the other hand, CW lasers may provide longer interaction times, but suffer for the weak intensities available.

2. *Nitrous Oxide Molecules*

STIRAP has been successfully demonstrated with nanosecond pulses in NO molecules (Schiemann *et al.*, 1993; Kuhn *et al.*, 1998), where highly efficient and selective population transfer has been achieved in the electronic ground state from the $X\ ^2\Pi_{1/2}(v = 0, J = \frac{1}{2})$ rovibrational state to the $X\ ^2\Pi_{1/2}(v = 6, J = \frac{1}{2})$ state via the intermediate state $A\ ^2\Sigma(v = 0, J = \frac{1}{2})$. The NO molecule provides an example of complications that may arise due to hyperfine structure. What seems to be a three-level system is actually a system of 18 sublevels (see Fig. 18). Because $^{14}N^{16}O$ has a nuclear spin of $I = 1$, each of the three levels is split into a pair of sublevels with $F = \frac{1}{2}$ and $F = \frac{3}{2}$, which in turn possess magnetic sublevels. For linearly polarized light, and when the pump and Stokes polarizations are parallel, the 18-state system decomposes into two independent three-state systems (one with $F = \frac{3}{2}, m_F = \frac{3}{2}$ and another with $F = \frac{3}{2}, m_F = -\frac{3}{2}$) and two six-state systems for $m_F = \frac{1}{2}$ and $m_F = -\frac{1}{2}$. Because the hyperfine splittings of the initial and final levels (214 MHz) is large enough to be resolved experimentally, the complexity of the system can be further reduced. Thus, despite the complications, a nearly complete transfer has been achieved, as shown in Fig. 19.

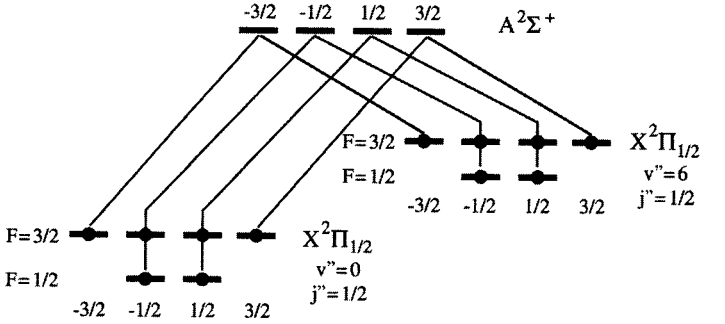

FIG. 18. Linkage scheme in the NO experiment. With hyperfine levels included, the seemingly three-level system becomes an 18-level system, because each of the three levels is split into two hyperfine levels with $F = \frac{1}{2}$ and $F = \frac{3}{2}$, which in turn have magnetic sublevels. The splitting of the excited hyperfine components of 15 MHz is too small to be resolved with pulsed lasers of a few nanoseconds duration and is not shown.

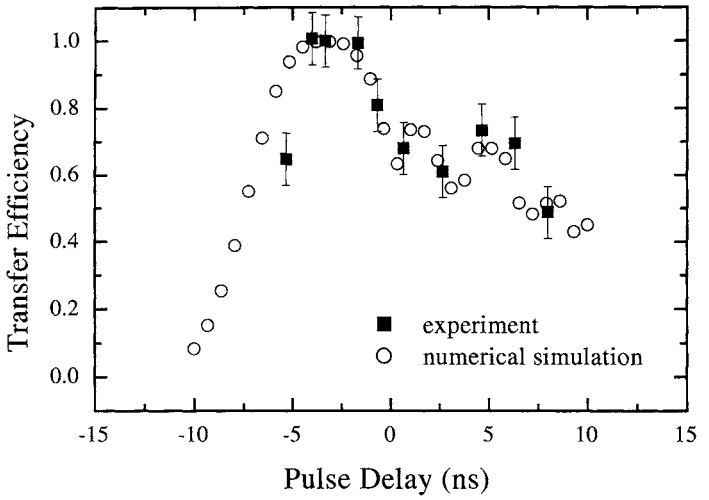

FIG. 19. Experimental demonstration of STIRAP in NO molecules versus the pulse delay. (From S. Schiemann, A. Kuhn, S. Steuerwald, and K. Bergmann. Efficient coherent population transfer in NO molecules using pulsed lasers. *Phys. Rev. Lett.* 1993;71:3637–3640.)

3. Sulfur Dioxide Molecules

The population transfer achieved in SO_2 molecules (Halfmann and Bergmann, 1996) is an example of STIRAP in a polyatomic molecule. The enormously increased density of levels, as compared to atoms or diatomic molecules, results in much smaller transition dipole moments. Nevertheless, efficient population transfer becomes possible with adequate laser power, when the level density in the final state is not too high. Figures 20 and 21 show examples of population transfer from the rotational state 3_{03} of the vibrational ground state (0,0,0) to the same rotational level of the (9,1,0) overtone in the electronic ground state $X\ ^1A_1$ via the vibrational level (1,1,0) of the excited electronic state C^1B_2. The wavelengths were 227 nm for the pump and 300 nm for the Stokes lasers (Halfmann and Bergmann, 1996), with pulse durations of 2.7 ns for the pump and 3.1 ns for the Stokes pulse. Typical laser intensities were 10 MW/cm^2, yielding Rabi frequencies of about 10^{10} s^{-1}. The population in the target state was probed by laser-induced fluorescence. The lower trace in Fig. 20 displays a signal of the probe laser-induced fluorescence from the final state (magnified 10 times) in the case when only the pump pulse was present; then the final state was populated by spontaneous emission from the intermediate state. When the Stokes pulse was turned on and applied before the pump pulse (with an appropriate overlap between them) the final-state population increased by more than two orders of magnitude. When the delay between the pump and Stokes pulses was varied, the typical plateau region of complete population transfer for

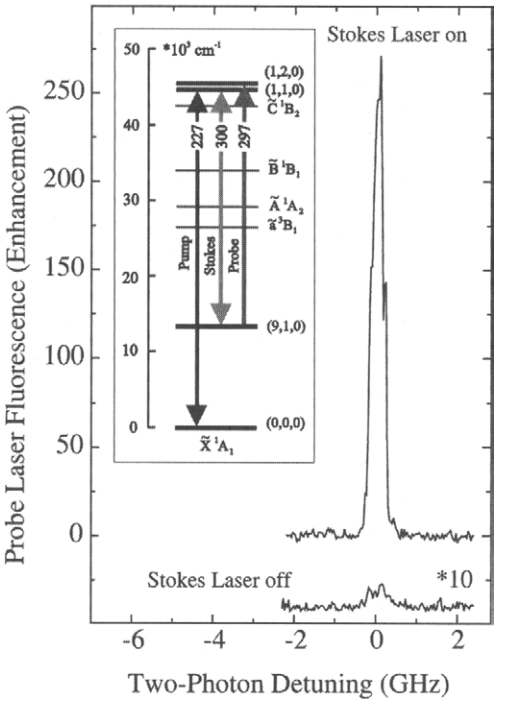

FIG. 20. Experimental demonstration of STIRAP in SO_2 molecules: fluorescence versus two-photon detuning. The inset shows the level linkage. (From T. Halfmann and K. Bergmann. Coherent population transfer and dark resonances in SO_2. *J. Chem. Phys.* 1996;104:7068–7072.)

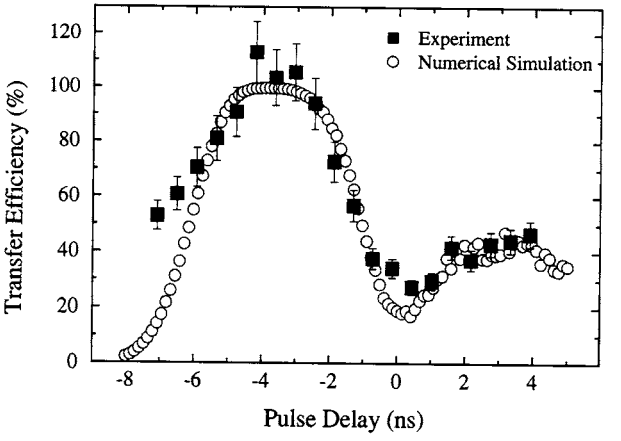

FIG. 21. Experimental demonstration of STIRAP in SO_2 molecules: efficiency versus pulse delay (right plot). (From T. Halfmann and K. Bergmann. Coherent population transfer and dark resonances in SO_2. *J. Chem. Phys.* 1996;104:7068–7072.)

negative pulse delay was observed, as shown in Fig. 21. For positive pulse delay (pump before Stokes), i.e., the case of SEP, a transfer efficiency of about 25% was observed, as one expects from rate equation calculations.

4. STIRAP in a Ladder System: Rubidium Atoms

STIRAP has been successfully implemented to produce samples of ultracold highly excited rubidium atoms by using the ladder transition $5S_{1/2} \rightarrow 5P_{3/2} \rightarrow 5D_{5/2}$ (Süptitz *et al.,* 1997). The Rb atoms in their ground state $5S_{1/2}$ were initially laser cooled to less than 500 μK and trapped in a magnetooptical trap with a diameter of 7 mm. Then the excitation was performed by illuminating the trapped sample with laser pulses from two injection-locked high-power (100-mW) diode lasers tuned near resonance with the $5S_{1/2}(F = 3) \rightarrow 5P_{3/2}(F' = 4)$ and $5P_{3/2}(F' = 4) \rightarrow 5D_{5/2}(F' = 5)$ transitions at 780 nm and 776 nm, respectively. The pulses were generated by acustooptic modulators and the delay was controlled electronically. The pulses had nearly Gaussian shapes and were linearly polarized in the same direction. The laser pulse durations of 33 ns (FWHM) were short compared to the lifetime of the target $5D_{5/2}$ state (241 ns), but longer than the lifetime of the intermediate state $5P_{3/2}$ (27 ns). Transfer efficiencies exceeding 90% have been achieved for counterintuitively ordered pulses (the $5P_{3/2} \rightarrow 5D_{5/2}$ transition driven first) with peak laser intensities about 10 W/cm^2 (corresponding to peak Rabi frequencies about 2×10^8 s^{-1}). There are no principal limitations to use STIRAP for efficient excitation of even higher-lying (Rydberg) states in this and other atoms.

C. STIRAP WITH DEGENERATE OR NEARLY DEGENERATE STATES

A problem that often arises when implementing STIRAP in real atoms and molecules is the existence of multiple intermediate and final states. These states may be present due to fine and/or hyperfine structure, Zeeman sublevels, or closely spaced rovibrational levels in polyatomic molecules. A multistate system has multiple eigenenergies, which may present a very complicated picture when plotted in time. For example, narrow avoided crossings between the eigenenergies may appear; if such avoided crossings involve the eigenstate that provides the adiabatic linkage for population transfer, then the adiabatic path will be blocked and STIRAP may fail.

A detailed numerical, analytical, and experimental investigation of this problem has been presented in a series of papers on STIRAP in metastable neon atoms (Shore *et al.,* 1995; Martin *et al.,* 1995, 1996). It has been concluded and demonstrated that the presence of closely spaced levels near the intermediate and final state may pose a problem and even be detrimental for STIRAP.

The level scheme in the neon experiment (Martin *et al.,* 1996), shown in Fig. 22, involves states with $J = 0$, 1, and 2, and thus there are $1 + 3 + 5 = 9$ magnetic

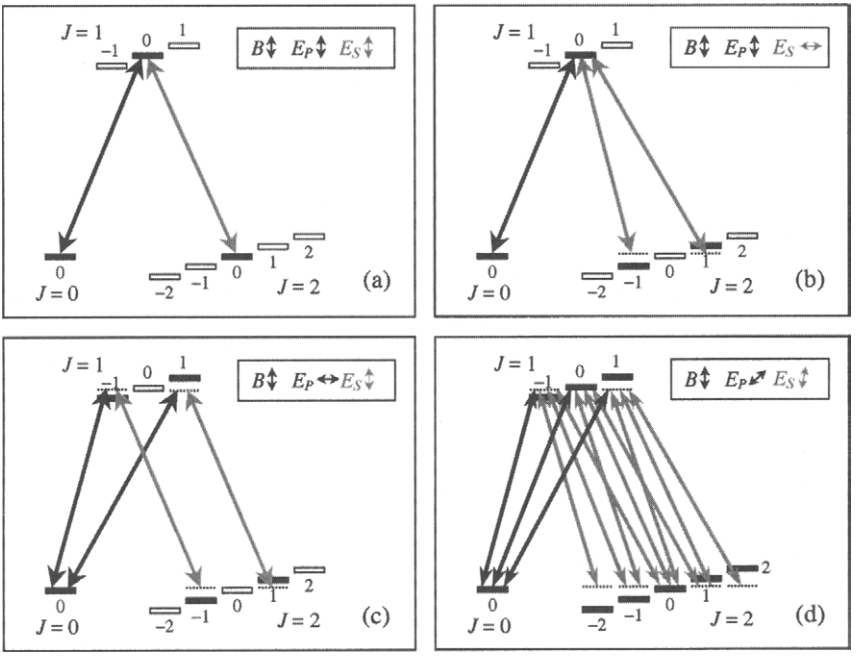

FIG. 22. Linkage patterns in Ne* for various choices of pump and Stokes polarizations with respect to the direction of the magnetic field B.

sublevels that may be coupled by the pump and Stokes lasers. A uniform magnetic field **B** can be used to remove the Zeeman degeneracy in the intermediate and final levels. On the other hand, the optical selection rules allow control of the number of levels participating in the process by an appropriate choice of the laser polarizations with respect to the direction of the uniform magnetic field, which sets the quantization axis. Four particular cases are shown in Fig. 22. When the pump and Stokes fields are linearly polarized along the direction of **B**, the selection rule $\Delta M = 0$ applies. Then only the three $M = 0$ sublevels (one in each of the initial, intermediate and final level) are coupled by the laser fields, as shown in Fig. 22a. When only the pump polarization is parallel to **B**, while the Stokes polarization is perpendicular to **B**, four states are coupled, as seen in Fig. 22b. By contrast, when the Stokes polarization is parallel to **B** and the pump polarization is perpendicular to **B**, five states are coupled, as illustrated in Fig. 22c. Finally, in the most general case when the pump and the Stokes are polarized in arbitrary directions, all nine magnetic sublevels are coupled by the laser fields, as seen in Fig. 22d.

Figure 23 shows the behavior of the final-state population for a set of incrementally increasing values of the magnetic field **B**. The pump laser polarization

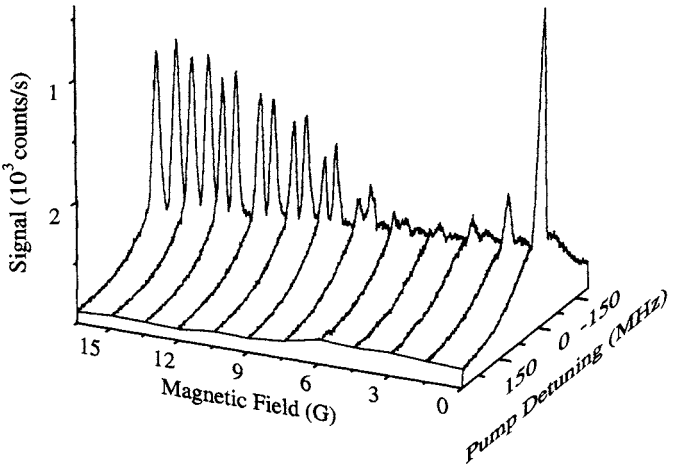

FIG. 23. Population transfer in Ne* versus magnetic field strength for the polarization choice in Fig. 22c. The Stokes laser frequency is held fixed on resonance, while the pump frequency is varied. (From J. Martin, B. W. Shore, and K. Bergmann. Coherent population transfer in multilevel systems with magnetic sublevels. III. Algebraic analysis. *Phys. Rev. A* 1996;54:1556–1569.)

is perpendicular to the magnetic field, while the Stokes polarization is parallel (Martin *et al.,* 1996); the ensuing linkage pattern is that in Fig. 24c and involves five states. The Stokes frequency is tuned to resonance with the Bohr frequency of the degenerate ($B = 0$) $^3P_2 \leftrightarrow {}^3P_1$ transition, while the pump laser frequency is scanned across the resonance. For small magnetic field, a single peak in the target-state population is observed near resonance ($\Delta_p = 0$), because the $M = +1$ and $M = -1$ sublevels are too close to be resolved. For large magnetic field, the Zeeman splitting increases and a symmetric two-peaked structure emerges, indicating populations of the $M = +1$ and $M = -1$ sublevels (depending in which sublevel is on two-photon resonance). A significant drop in the transfer efficiency is observed at intermediate magnetic field strengths. This drop was identified (Martin *et al.,* 1996) as due to lack of adiabatic connectivity between the initial and final states, i.e., the adiabatic path between them was blocked because of coupling to neighboring adiabatic states. Figure 23 also demonstrates the possibility of orienting the atomic angular momentum simply by tuning a laser frequency to the respective two-photon resonance.

The success of STIRAP at zero and large magnetic field and its failure at some intermediate values can be understood by examining the evolution of the energies of the adiabatic states, shown in Fig. 24. With five coupled states we also have five dressed eigenstates and five adiabatic energies. For $\mathbf{B} = 0$, the pattern looks similar to the one for three states. Because the pump and Stokes laser frequencies are tuned to the respective one-photon resonances, the five eigenenergies are degenerate at

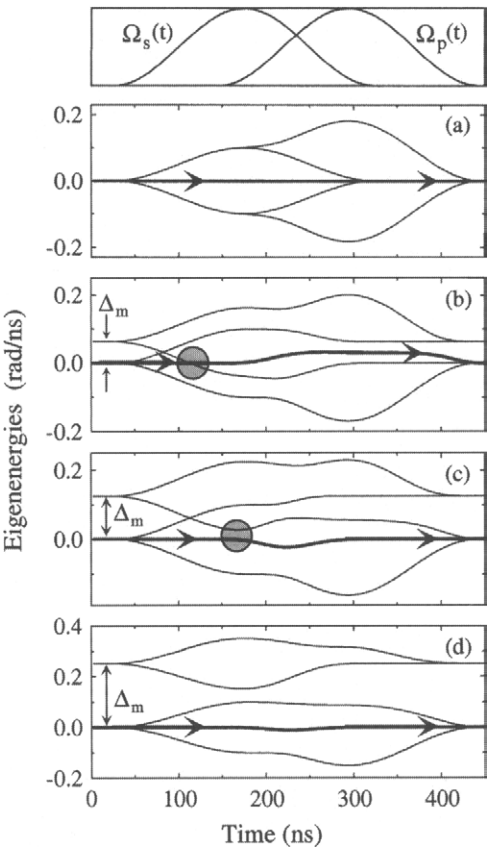

FIG. 24. Time evolution of the eigenenergies in Ne* for different magnetic fields. The circles mark avoided crossings of the eigenenergies, which block the adiabatic path (thick curves) and impede population transfer. (From J. Martin, B. W. Shore, and K. Bergmann. Coherent population transfer in multilevel systems with magnetic sublevels. III. Algebraic analysis. *Phys. Rev. A* 1996;54:1556–1569.)

early and late times, as seen in Fig. 24a. As in the case of three states, we have a zero adiabatic energy at all times, which is the adiabatic path linking state ψ_1 to state ψ_3. Thus STIRAP is possible, as verified in Fig. 23.

When the magnetic field is nonzero, the Zeemen splittings remove the M degeneracy. Two-photon resonance can be established between the initial state ψ_1 and only one of the final states. As a consequence, the eigenenergies are no longer degenerate at early and late times. Therefore, at early times we have a triple degeneracy, which is lifted as soon as the Stokes pulse arrives, and a double degeneracy of states, separated from the former ones by the detuning from the two-photon resonance, i.e., by the Zeeman splitting. The triplet is associated with the three bare states that are resonantly coupled by the laser field, while the doublet

is associated with the other two bare states. These latter states also show an Autlor-Townes splitting, and, since at early times their energy is separated from that of the other three states, a crossing of the states occur, provided the Rabi frequency exceeds the Zeeman detuning.

One can show that a coupling between states, related to the crossing energy levels, is induced by the pump laser. When the Zeeman splitting is small, this crossing occurs while the pump laser is still weak and the system, while following the zero-energy path, passes (diabatically) through this crossing (Fig. 24b). At intermediate times, the pump laser induces interaction between the states and forces the energy of the transfer path to deviate from zero. At later times, the transfer path does not connect to the state with zero energy when the Stokes laser is turned off, as is needed for successful completion of the transfer. Therefore the adiabatic transfer path is blocked and coherent population transfer is not possible.

With increasing magnetic field strength, leading to larger Zeeman splitting, the curve crossing with the zero-energy path occurs later, when the pump Rabi frequency is already large (Fig. 24c). Then the avoided crossing is sufficiently broad and does not impede the population transfer. Although a transient deviation from zero energy is observed (meaning that some population will transiently reside in the intermediate states and may be lost by radiative decay), the transfer path connects to the zero-energy eigenvalue as the Stokes laser is turned off; population transfer is again possible. At even larger Zeeman splitting, the avoided crossing is barely noticeable and a (nearly) zero-energy transfer path is again established (Fig. 24d). Moreover, when the Zeeman splitting is larger than the Rabi

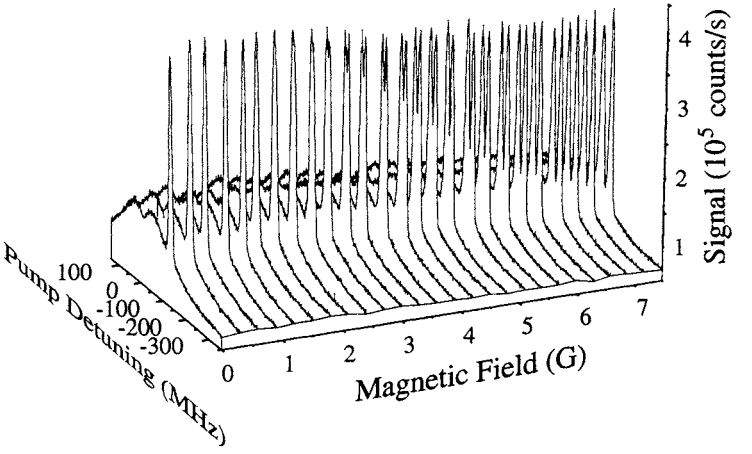

FIG. 25. Population transfer in Ne* versus magnetic field strength for the polarization choice in Fig. 22c. Unlike Fig. 23, here the Stokes laser frequency is held fixed off resonance ($\Delta_s = 200$ MHz), while the pump frequency is varied. (From J. Martin, B. W. Shore, and K. Bergmann. Coherent population transfer in multilevel systems with magnetic sublevels. III. Algebraic analysis. *Phys. Rev. A* 1996;54:1556–1569.)

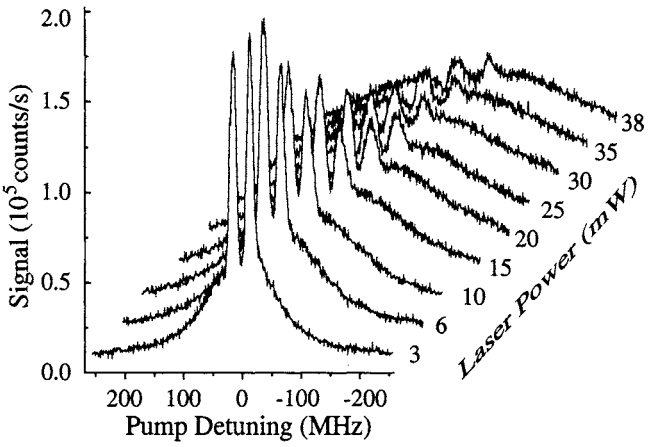

FIG. 26. Top: linkage patterns in Ne* for various choices of pump and Stokes polarizations with respect to the direction of the magnetic field B. Bottom: population transfer in Ne* versus magnetic field strength. (From J. Martin, B. W. Shore, and K. Bergmann. Coherent population transfer in multilevel systems with magnetic sublevels. III. Algebraic analysis. *Phys. Rev. A* 1996;54:1556–1569.)

frequencies, the relevant bare states can again be considered a (nearly) isolated three-state system.

Detuning of the Stokes laser from the one-photon resonance may eliminate the connectivity problem recognized in Fig. 24b. Figure 25 shows the fluorescence signal from the $^3P_2$ state for the same polarizations as in Fig. 23. Again, the figure shows traces for incrementally increasing magnetic field as the pump laser frequency is scanned across resonance. However, unlike Fig. 23, the Stokes laser frequency is held fixed off resonance by 200 Mhz. This detuning prevents the crossing at early times (Fig. 24b) from appearing and ensures high transfer efficiency for all magnetic field values.

Finally, Fig. 26 shows an example from Martin *et al.* (1996) in which population transfer is possible for small Rabi frequencies but fails at higher laser power. The reason is again the blocking of the adiabatic path and can be cured, again, by detuning the lasers off their single-photon resonances. Thus, while in three-state systems STIRAP gets more robust and efficient as the Rabi frequency increases, in multistate systems this is not garanteed in general.

In conclusion, coherent population transfer in multilevel systems depends on the availability of an adiabatic path that connects the initial and final states with only a small deviation from the zero eigenvalue at intermediate times when both laser fields are nonzero. Whether this is possible or not depends on the level structure and coupling scheme. In most cases, an analysis like the one shown in Fig. 24 is needed in order to understand the details of the transfer process and to make an appropriate choice of Rabi frequencies and detunings in order to control the crossing of dressed-state eigenvalues. In many cases, the connectivity problems can be avoided

if the laser frequencies are tuned sufficiently far from any one-photon resonance with an intermediate state. Moreover, for efficient population transfer the two-photon linewidth should not exceed the intermediate level separation, if the laser frequencies are close to one-photon resonance. An important conclusion, predicted theoretically and confirmed experimentally, is that one-photon resonances should be avoided (while the two-photon resonance is still essential) when more than three states are involved. Although the laser–atom coupling is strongest for one-photon resonance, this resonance may lead to blocking of the adiabatic connection and at least to non-negligible transient population in the decaying intermediate states.

Finally, we point out that some other aspects of the influence of multiple nearly degenerate final states in STIRAP have been explored theoretically (Band and Magnes, 1994; Kobrak and Rice, 1998b).

V. STIRAP-Like Population Transfer in Multistate Chains

The simplest extensions of the three-state coherent excitation chain are those dealing with multistate chainwise excitation, i.e., linkages of the type

$$\psi_1 \leftrightarrow \psi_2 \leftrightarrow \psi_3 \leftrightarrow \ldots \leftrightarrow \psi_N$$

in which each state is connected to at most two other states (see Fig. 27). For steady-amplitude fields, analytic solutions to the Schrödinger equation are available in a variety of cases (cf. Shore, 1990, chap. 15). The ordering of the energy levels is not important: the linkage pattern may appear as a simple ladder, or as some bent chain such as has the appearance of the letter N for four states or, for five states, the letter M or W. Chainwise ladder excitation is of considerable interest particularly for producing dissociation or ionization, whereas bent chains have interesting applications described in this section and in Section VI.

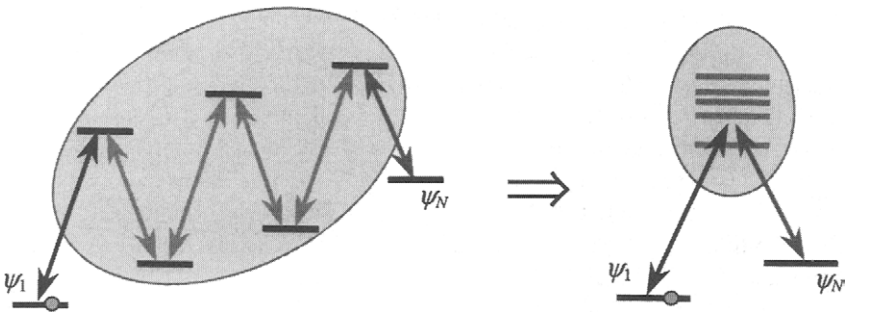

FIG. 27. Linkage pattern for chain-STIRAP (serial multi-Λ system) and equivalent parallel multi-Λ system, obtained by diagonalization of the subsystem comprising the intermediate states in the original chainwise system.

The extension of STIRAP to multistate chains has drawn considerable attention (Shore *et al.*, 1991; Marte *et al.*, 1991; Smith, 1992; Oreg *et al.*, 1992; Pillet *et al.*, 1993; Valentin *et al.*, 1994; Goldner *et al.*, 1994a,b; Malinovsky and Tannor, 1997; Theuer and Bergmann, 1998; Vitanov, 1998a, Vitanov *et al.*, 1998; Nakajima 1999). Chain-STIRAP has proved to be a viable technique of great potential, particularly for momentum transfer in atom optics (Section VI). In this section we will describe the basic features and problems of chain STIRAP and will provide a few illustrations.

The RWA Hamiltonian of a multistate chain is a tridiagonal matrix which has the diabatic energies (the detunings) on its diagonal, and the laser-induced couplings as off-diagonal elements,

$$\mathsf{H} = \frac{\hbar}{2}\begin{bmatrix} 0 & \Omega_{1,2} & 0 & \cdots & 0 & 0 \\ \Omega_{1,2} & 2\Delta_2 & \Omega_{2,3} & \cdots & 0 & 0 \\ 0 & \Omega_{2,3} & 2\Delta_3 & \cdots & 0 & 0 \\ \vdots & \vdots & \vdots & \ddots & \vdots & \vdots \\ 0 & 0 & 0 & \cdots & 2\Delta_{N-1} & \Omega_{N-1,N} \\ 0 & 0 & 0 & \cdots & \Omega_{N-1,N} & 0 \end{bmatrix}. \tag{69}$$

The zeros in the first and last diagonal elements indicate that the initial state and the final state of the chain are on $(N-1)$-photon resonance, a condition that generalizes the two-photon resonance in three-state STIRAP, whereas the intermediate states may be off-resonance in general. It has been discovered that such multistate chains behave differently when they involve odd and even numbers of states.

A. Resonantly Driven Chains with Odd Number of States

The key for STIRAP-like population transfer in multistate chainwise connected systems is the existence of a multilevel dark state, which generalizes the usual dark state (44b) of three-state Λ systems and links adiabatically the initial state ψ_1 to the final state ψ_N of the chain. Such a multilevel dark state exists only when the multistate chain comprises an odd number of states ($N = 2n + 1$). It also requires that all lasers are on resonance with the corresponding transitions or only the even states in the chain are detuned from resonance (Shore *et al.*, 1991; Marte *et al.*, 1991; Smith, 1992). Such a chain can be viewed as a sequence of serially connected Λ systems, each of which is on two-photon resonance.

The Hamiltonian describing such a multistate chain has a zero eigenvalue. The multilevel dark state $\Phi_0(t)$ is the corresponding zero-eigenvalue eigenstate and it is a time-dependent coherent superposition of the odd states in the chain

$\psi_1, \psi_3, \ldots, \psi_{2n+1}$. For example, the Hamiltonian of a five-state chain is given by

$$\mathsf{H} = \frac{\hbar}{2}\begin{bmatrix} 0 & \Omega_{1,2} & 0 & 0 & 0 \\ \Omega_{1,2} & 2\Delta & \Omega_{2,3} & 0 & 0 \\ 0 & \Omega_{2,3} & 0 & \Omega_{3,4} & 0 \\ 0 & 0 & \Omega_{3,4} & 2\Delta & \Omega_{4,5} \\ 0 & 0 & 0 & \Omega_{4,5} & 0 \end{bmatrix}. \tag{70}$$

States ψ_1 and ψ_3 are on two-photon resonance, and so are states ψ_3 and ψ_5. The even states in the chain ψ_2 and ψ_4 may be off the respective single-photon resonances by the same detuning Δ. The multilevel dark state of this system reads (Morris and Shore, 1983; Hioe and Carroll, 1988; Shore *et al.*, 1991; Marte *et al.*, 1991; Smith, 1992; Milner and Prior, 1998)

$$\Phi_0(t) = \frac{1}{\mathcal{N}(t)}[\Omega_{2,3}(t)\Omega_{4,5}(t)\psi_1 - \Omega_{1,2}(t)\Omega_{4,5}(t)\psi_3 + \Omega_{1,2}(t)\Omega_{3,4}(t)\psi_5], \tag{71}$$

where $\mathcal{N}(t)$ is a normalization factor.

A particularly suitable system for multistate STIRAP is the chainwise transition formed by the magnetic sublevels of a degenerate two-level system with excited-level angular momentum $J_e = J_g$ or $J_g - 1$, driven by two sequential pulses with opposite circular polarizations. For example, if the system is prepared initially in the $M_g = -J_g$ ground-state sublevel (e.g., by optical pumping), then a STIRAP-like transfer to the $M_g = J_g$ sublevel can be achieved by applying a pulse of σ^- polarization (the Stokes) before a pulse of σ^+ polarization (the pump), i.e., in the counterintuitive ordering.

In the five-state example, the Rabi frequencies $\Omega_{1,2}(t)$ and $\Omega_{3,4}(t)$ will follow the time dependence $f_+(t)$ of the σ^+ pulse [and the difference in their peak values is determined by the respective Clebsch–Gordan coefficients (cf. Shore, 1990, chap. 19.1)], while the Rabi frequencies $\Omega_{2,3}(t)$ and $\Omega_{4,5}(t)$ will follow the time dependence $f_-(t)$ of the σ^- pulse. Then the dark state (71) takes the form

$$\Phi_0(t) = \frac{1}{\mathcal{N}(t)}\left[\Omega_{2,3}^0\Omega_{4,5}^0 f_-^2(t)\psi_1 - \Omega_{1,2}^0\Omega_{4,5}^0 f_-(t)f_+(t)\psi_3 + \Omega_{1,2}^0\Omega_{3,4}^0 f_+^2(t)\psi_5\right]. \tag{72}$$

Hence, if the σ^- pulse precedes the σ^+ pulse (counterintuitive pulse ordering), state $\Phi_0(t)$ is equal to ψ_1 ($M = -J_g$) at early times and to ψ_5 ($M = +J_g$) at late times, i.e., it provides an adiabatic connection between the initial state ψ_1 and the last state ψ_5 of the chain. As in STIRAP, the sublevels of the excited level (ψ_2 and ψ_4 in this example) remain unpopulated throughout the transfer if the interaction is adiabatic; however, the intermediate odd states in the chain

(ψ_3 here)—the sublevels of the ground state—do acquire some transient populations. In this particular system these transient intermediate-state populations do not pose a problem because these sublevels do not decay and there are no population losses. Indeed, multistate STIRAP in such chainwise systems has been demonstrated experimentally by several groups (Pillet *et al.*, 1993; Valentin *et al.*, 1994; Goldner *et al.*, 1994a; Goldner *et al.*, 1994b; Theuer and Bergmann 1998). Sections VI and XI discuss some applications of STIRAP in multistate chains.

B. Resonantly Driven Chains with Even Number of States

The chains with an even number of states ($N=2n$) behave very differently in the resonant case (when all intermediate-state detunings vanish, $\Delta_2=\Delta_3=\ldots=\Delta_{N-1}=0$) compared with the chains with an odd number of states. For even-N systems we have $\det \mathsf{H} = (-)^{N/2}\Omega_{1,2}^2\Omega_{3,4}^2\ldots\Omega_{N-1,N}^2 \neq 0$, which means that the Hamiltonian does not have a zero eigenvalue, in contrast to the case of odd N. More important, $\mathsf{H}(t)$ does not possess any adiabatic state that provides an adiabatic connection between the initial state ψ_1 and the final state ψ_N of the chain. Consequently, even when such a system is driven adiabatically by counterintuitively ordered resonant pulses, a STIRAP-like population transfer between the initial and final states of the chain cannot occur. Instead, the final-state population exhibits Rabi-like oscillations as the pulse intensities increase (Oreg *et al.*, 1992; Vitanov, 1998a; Band and Julienne, 1991b). These oscillations occur because at early times the initial state is equal to a superposition of adiabatic states (rather than to a single adiabatic state as in STIRAP) and so is the final state at late times; hence interference between the different paths from the initial state to the final state takes place.

For example, in a resonantly driven four-state chain the four eigenvalues are $\pm\varepsilon_+$ and $\pm\varepsilon_-$, where

$$\varepsilon_\pm = \frac{1}{2}\sqrt{\frac{1}{2}\left(\Omega^2 \pm \sqrt{\Omega^4 - 4\Omega_p^2\Omega_s^2}\right)} \tag{73}$$

and $\Omega^2 = \Omega_p^2 + \Omega_i^2 + \Omega_s^2$, where Ω_i is the coupling between the two intermediate states. The initial state ψ_1 cannot be identified with a single adiabatic state at $-\infty$, but is rather given by a superposition of the two adiabatic states corresponding to the smallest eigenenergies $-\varepsilon_-$ and ε_-. The same applies to the final state ψ_4 at $+\infty$:

$$\psi_1 = \tfrac{1}{\sqrt{2}}[\Phi_{-\varepsilon_-}(-\infty) + \Phi_{\varepsilon_-}(-\infty)], \tag{74a}$$

$$\psi_4 = \tfrac{1}{\sqrt{2}}[\Phi_{-\varepsilon_-}(+\infty) + \Phi_{\varepsilon_-}(+\infty)]. \tag{74b}$$

If the system starts its evolution in state ψ_1 initially, then the adiabatic solution for the final populations of the bare states is (Vitanov 1998a)

$$P_1(\infty) \approx \cos^2 \vartheta \cos^2 \Theta, \tag{75a}$$

$$P_2(\infty) \approx 0, \tag{75b}$$

$$P_3(\infty) \approx \sin^2 \vartheta \cos^2 \Theta, \tag{75c}$$

$$P_4(\infty) \approx \sin^2 \Theta. \tag{75d}$$

Here $\tan \vartheta = \lim_{t \to +\infty} [\Omega_p(t)/\Omega_i(t)]$ and $\Theta = \int_{-\infty}^{\infty} \varepsilon_-(t)\, dt$. Hence, as we approach the adiabatic limit, $P_4(t)$ oscillates rather than tend to unity. Note that $P_3(\infty) = 0$ if the pump pulse $\Omega_p(t)$ vanishes before $\Omega_i(t)$ $[\Omega_p(t)/\Omega_i(t) \overset{t \to +\infty}{\longrightarrow} 0]$, while $P_1(\infty) = 0$ if the pump pulse $\Omega_p(t)$ vanishes after $\Omega_i(t)[\Omega_p(t)/\Omega_i(t) \overset{t \to +\infty}{\longrightarrow} +\infty]$.

We also point out that if the pulse $\Omega_i(t)$, coupling the intermediate states, is much stronger than the pump and Stokes pulses at all times, then $\vartheta \approx 0$. Hence, although not being of STIRAP-type, the excitation process in an on-resonance four-state system involving a strong intermediate pulse (Malinovsky and Tannor, 1997), is quite interesting by itself because it demonstrates how the population can flip between states ψ_1 and ψ_4, bypassing the intermediate states ψ_2 and ψ_3 despite the fact that the latter states are on resonance with the corresponding lasers.

C. The Off-Resonance Case

When the intermediate states are off resonance while the initial state and the final state of the chain are still on $(N-1)$-photon resonance, chains with odd and even number of states behave quite similarly. In both cases a STIRAP-like transfer is only possible if there exists an adiabatic path—adiabatic transfer state $\Phi_T(t)$—linking the initial and final states of the chain. This depends on the laser parameters, particularly on the intermediate detunings.

Let us consider the case when all intermediate detunings are nonzero, $\Delta_k \neq 0$ $(k = 2, 3, \ldots, N-1)$, and all couplings are pulse shaped. Let us also assume that the Stokes pulse $\Omega_{N,N-1} \equiv \Omega_s$, coupling the last transition, precedes the pump pulse $\Omega_{1,2} \equiv \Omega_p$, coupling the first transition. By setting $\Omega_p = 0$ and $\Omega_s = 0$ in Eq. (69), we find that there are two eigenvalues of $\mathsf{H}(t)$ which vanish as $t \to \pm\infty$ [although they are nonzero at finite times because $\det \mathsf{H}(t) \neq 0$ in general]. The other eigenvalues tend to the (nonzero) detunings Δ_k and the corresponding adiabatic states tend to the respective bare intermediate states ψ_k. At $\pm\infty$, each of the two adiabatic states, corresponding to the vanishing eigenvalues, is equal to either state ψ_1, or state ψ_N, or a superposition of ψ_1 and ψ_N. Obviously, if an AT state exists, its eigenvalue should be one of these two eigenvalues. Hence,

of particular interest are the asymptotic behaviors of the two vanishing eigenvalues and the corresponding adiabatic states at early and late times. We note here that only one eigenvalue vanishes when $\Omega_p \to 0$ and $\Omega_s \neq 0$, which happens at early times, or when $\Omega_p \to 0$ and $\Omega_s \neq 0$, which happens at late times. Hence, at early times ($t \to -\infty$) as soon as the Stokes pulse Ω_s arrives, one of the initially degenerate eigenvalues, ε_l^- (the "large" one), departs from zero, while the other, ε_s^- (the "small" one), remains zero until the pump pulse Ω_p arrives later.

A similar scenario takes place at late times when first one eigenvalue vanishes with the disappearance of the Stokes pulse, and then the other eigenvalue vanishes with the pump pulse. It can be shown that at early times ($t \to -\infty$), the two vanishing adiabatic energies behave as (Vitanov 1998a)

$$\varepsilon_s^- \approx -\frac{\mathcal{D}^{(3,N-2)}}{4\mathcal{D}^{(2,N-2)}}\Omega_p^2, \qquad \varepsilon_l^- \approx -\frac{\mathcal{D}^{(2,N-2)}}{4\mathcal{D}^{(2,N-1)}}\Omega_s^2, \tag{76}$$

and at late times ($t \to +\infty$) the two vanishing adiabatic energies behave as

$$\varepsilon_s^+ \approx -\frac{\mathcal{D}^{(3,N-2)}}{4\mathcal{D}^{(3,N-1)}}\Omega_s^2, \qquad \varepsilon_l^+ \approx -\frac{\mathcal{D}^{(3,N-1)}}{4\mathcal{D}^{(2,N-1)}}\Omega_p^2. \tag{77}$$

Here $\mathcal{D}^{(j,k)}$ denotes the determinant of the matrix obtained from H by keeping its columns from jth to kth and its rows from jth to kth,

$$\mathcal{D}^{(j,k)} = \begin{vmatrix} \Delta_j & \frac{1}{2}\Omega_{j,j+1} & 0 & \cdots & 0 \\ \frac{1}{2}\Omega_{j,j+1} & \Delta_{j+1} & \frac{1}{2}\Omega_{j+1,j+2} & \cdots & 0 \\ 0 & \frac{1}{2}\Omega_{j+1,j+2} & \Delta_{j+2} & \cdots & 0 \\ \vdots & \vdots & \vdots & \ddots & \vdots \\ 0 & 0 & 0 & \cdots & \Delta_k \end{vmatrix}. \tag{78}$$

It is easy to verify that the adiabatic eigenstates corresponding to ε_s^- and ε_l^+ tend to state ψ_1, while those corresponding to ε_l^- and ε_s^+ tend to state ψ_N. Hence, the AT state Φ_T, if it exists, must have an eigenvalue that coincides with ε_s^- as $t \to -\infty$ and with ε_s^+ as $t \to +\infty$. The energies ε_s^- and ε_s^+ do not necessarily correspond to the same eigenvalue and it may happen that ε_s^- is linked to ε_l^+ rather than ε_s^+; then an AT state does not exist. In any case, since the eigenvalues do not cross, the upper (the lower) of the two eigenvalues at $-\infty$ is connected to the upper (the lower) of the two eigenvalues at $+\infty$. Because $|\varepsilon_l^-| \gg |\varepsilon_s^-|$ and $|\varepsilon_l^+| \gg |\varepsilon_s^+|$, the linkage is determined by the signs of the "large" eigenvalues ε_l^- and ε_l^+. If they have the same signs, they will be both above (or below) ε_s^- and ε_s^+ and hence, the desired linkages $\varepsilon_l^- \leftrightarrow \varepsilon_l^+$ and $\varepsilon_s^- \leftrightarrow \varepsilon_s^+$ will take place. If ε_l^- and ε_l^+ have opposite signs, they cannot be connected because such an eigenvalue would cross the one linking

ε_s^- and ε_s^+. Thus, from this analysis and Eqs. (76) and (77), we conclude that the condition for existence of an AT state is

$$\mathcal{D}^{(2,N-2)}\mathcal{D}^{(3,N-1)} > 0. \tag{79}$$

The signs of the $\mathcal{D}$'s have to be determined at the early (or late) times when the Rabi frequencies are much smaller than the detunings (note that each of the $\mathcal{D}$'s has the same sign at early and late times). The above condition (79) remains valid also when one or more intermediate detunings are equal to zero (Vitanov, 1998a).

If all intermediate couplings are pulse shaped (i.e., vanish as $t \to \pm\infty$), we have $\mathcal{D}^{(2,N-2)} \to \Delta_2\Delta_3 \ldots \Delta_{N-2}$, $\mathcal{D}^{(3,N-1)} \to \Delta_3\Delta_4 \ldots \Delta_{N-1}$, and condition (79) reduces to

$$\Delta_2\Delta_{N-1} > 0. \tag{80}$$

Below we provide examples for existence and nonexistence of an AT state (and hence, of STIRAP-like transfer) in the cases of $N=4$ and 5 states.

- In a four-state chain, an AT state exists when the cumulative detunings of the two intermediate states have the same sign, $\Delta_2\Delta_3 > 0$, whereas it does not exist if $\Delta_2\Delta_3 \leqq 0$.
- In the five-state case, condition (79) reads $(\Delta_2\Delta_3 - \Omega_{2,3}^2)(\Delta_3\Delta_4 - \Omega_{3,4}^2) > 0$. Thus if all intermediate detunings are nonzero, an AT state exists only if $\Delta_2\Delta_4 > 0$. If $\Delta_2 = 0$, AT state exists only for $\Delta_3\Delta_4 < 0$. If $\Delta_4 = 0$, AT state exists for $\Delta_2\Delta_3 < 0$. If $\Delta_3 = 0$, an AT state always exists regardless of Δ_2 and Δ_4, which agrees with the result in Section V.A. If $\Delta_2 = \Delta_4 = 0$, an AT state also exists regardless of Δ_3.

Figure 28 displays examples of successful and unsuccessful adiabatic population transfer in four-state (top frames) and five-state (bottom frames) chains. In the on-resonant case (left frames), the final-state population approaches unity for $N=5$, while it oscillates for $N=4$. The middle frames show examples for which the AT condition (80) is satisfied; consequently, the transfer efficiency approaches unity for both $N=4$ and $N=5$. The right frames show examples when the AT condition (80) is not satisfied; then population transfer fails for both $N=4$ and $N=5$.

We point out that while condition (79) provides adiabatic connection between the two end states of the multistate chain, the AT state has in general nonzero components from all states involved, including from the decaying excited states. The even-state components (which correspond to the decaying excited states in the linkage pattern in Fig. 27) vanish only when the odd detunings are zero; then the AT state is a dark state (Section V.A). In the general case, beyond the particular case of chainwise transitions between magnetic sublevels of degenerate two-level systems,

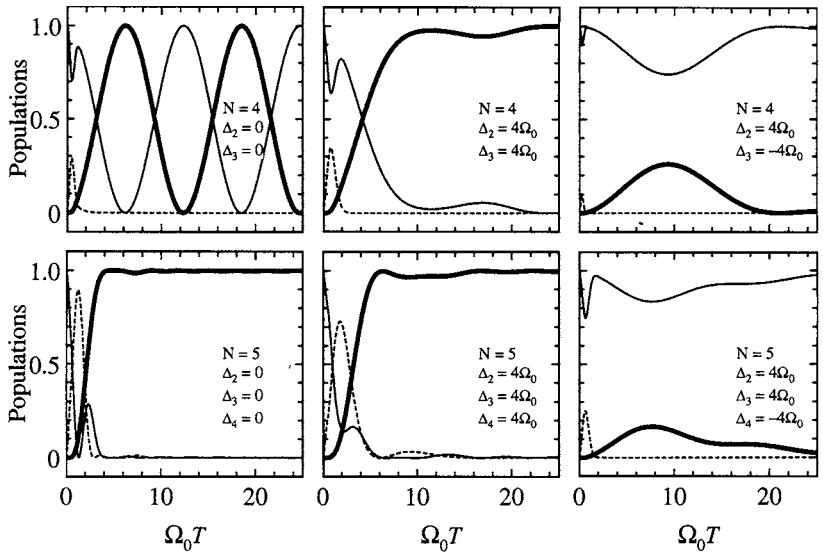

FIG. 28. Examples of success and failure of adiabatic population transfer in four-state (top frames) and five-state (bottom frames) chains. In each frame, we show the numerically calculated final-state population (thick solid curve), the initial-state population (thin solid curve), and the total population in the intermediate states (dashed curve). The dimensionless product $\Omega_0 T$ is proportional to the pulse area and as it increases, adiabaticity improves. The pump and Stokes Rabi frequencies are given by $\Omega_p = \Omega_0 \exp[-(t-\tau)^2/T^2]$, $\Omega_s = \Omega_0 \exp[-(t+\tau)^2/T^2]$, with $\tau = 0.5T$, and all intermediate-pulse Rabi frequencies are equal to $\Omega_0 \exp[-(t/2T)^2]$. The two left frames are for the on-resonance case, when excitation leads to STIRAP-like transfer for $N=5$ states but to Rabi-like oscillations for $N=4$. The middle frames show examples of successful multistate STIRAP for both $N=4$ and $N=5$, whereas the right frames show examples of failure of multistate STIRAP.

the transiently populated intermediate states can decay radiatively during the transfer; then it is important to reduce their populations. (Malinovsky and Tannor, 1997) suggested that these transient populations can be suppressed when the pulses coupling the intermediate transitions are much stronger than the pulses driving the first (pump) and the last (Stokes) transitions. They proposed a pulse sequence, named *straddle STIRAP,* in which all intermediate pulses arrive simultaneously with the Stokes pulse and vanish with the pump pulse, being much stronger than the pump and the Stokes at all times (Malinovsky and Tannor, 1997; Sola *et al.,* 1999).

D. Optimization of Multistate STIRAP: Dressed-State Picture

A dressed-state approach (Vitanov *et al.,* 1998) provides a particularly clear picture of multistate STIRAP, valid for both odd and even number of states. It is most useful when the pulses (or the pulse) driving the intermediate transitions arrive before

and vanish after the pulses that drive the first (the pump) and the last (the Stokes) transitions, as in Malinovsky and Tannor (1997), and are nearly constant during the time when the pump and the Stokes lasers are present. Then, before the arrival of the pump and Stokes pulses, the $N-2$ intermediate states are coupled into a dressed subsystem, as shown in Fig. 27. By changing the parameters of the dressing pulses (intensities and frequencies), one can manipulate the properties of this dressed subsystem and thus control the population transfer. By tuning the pump and Stokes lasers to one of the dressed eigenstates, Φ_k, the multistate dynamics is essentially reduced to a system of three strongly coupled states: $\psi_1 \leftrightarrow \Phi_k \leftrightarrow \psi_N$; this paves the road for an efficient STIRAP-like population transfer from state ψ_1 to state ψ_N. Furthermore, if the dressing pulses are constant, at least during the time when the pump and Stokes pulses are present, then the couplings between the dressed states vanish. Also, if the dressing pulses are strong, the splittings between the dressed energies are large. This makes the multi-Λ system resemble the single-Λ system in STIRAP and therefore place little population in the intermediate states.

The dressed picture also displays the difference between odd and even number of states in the on-resonance case (all detunings in the original chain equal to zero), when, as we noted above, odd-N chains have a zero eigenvalue and a corresponding trapped state, while even-N chains do not have such an eigenvalue, nor a trapped state. For odd-N chains, one of the dressed states is always on resonance with the pump and Stokes lasers. In contrast, for even-N chains, the pump and Stokes lasers are tuned in the middle between two adjacent dressed eigenvalues and the ensuing interference between different adiabatic paths leads to Rabi-like oscillations. Thus, while the on-resonance choice provides the best results for odd-N chains, the only possibility to achieve STIRAP-like population transfer in an even-N chain is to choose nonzero intermediate-state detunings and ensure that their values fall within an AT region.

Figure 29 shows the final-state population in four- and five-state systems against the cumulative detunings from the intermediate states. In the four-state case, high transfer efficiency (the white zones) is achieved for sufficiently adiabatic evolution only if $\Delta_2\Delta_3 > 0$, as discussed above. Near the dressed-state resonances (shown by hyperbolas) the transfer efficiency is high even when the evolution is not very adiabatic elsewhere (top left frame). As the pulse areas increase (top right frame), the two regions where $\Delta_2\Delta_3 > 0$ (first and third quadrants) get filled with white (unity transfer efficiency), while no high transfer is possible in the $\Delta_2\Delta_3 < 0$ regions (second and fourth quadrants). In the five-state case there are three AT regions in the $\Delta_2\Delta_4$ plane ($\Delta_2 = \Delta_3$ is assumed in order to display a two-dimensional plot), defined by the AT condition $(\Delta_2^2 - \Omega_{2,3}^2)(\Delta_2\Delta_4 - \Omega_{3,4}^2) > 0$. In each AT region, there is an intermediate-dressed-state resonance, shown by a thick curve. As in the four-state case, only the AT regions get filled with white as the adiabaticity improves (bottom right frame). Again near the dressed-state resonances the transfer efficiency is high even for poor adiabaticity elsewhere (bottom left frame).

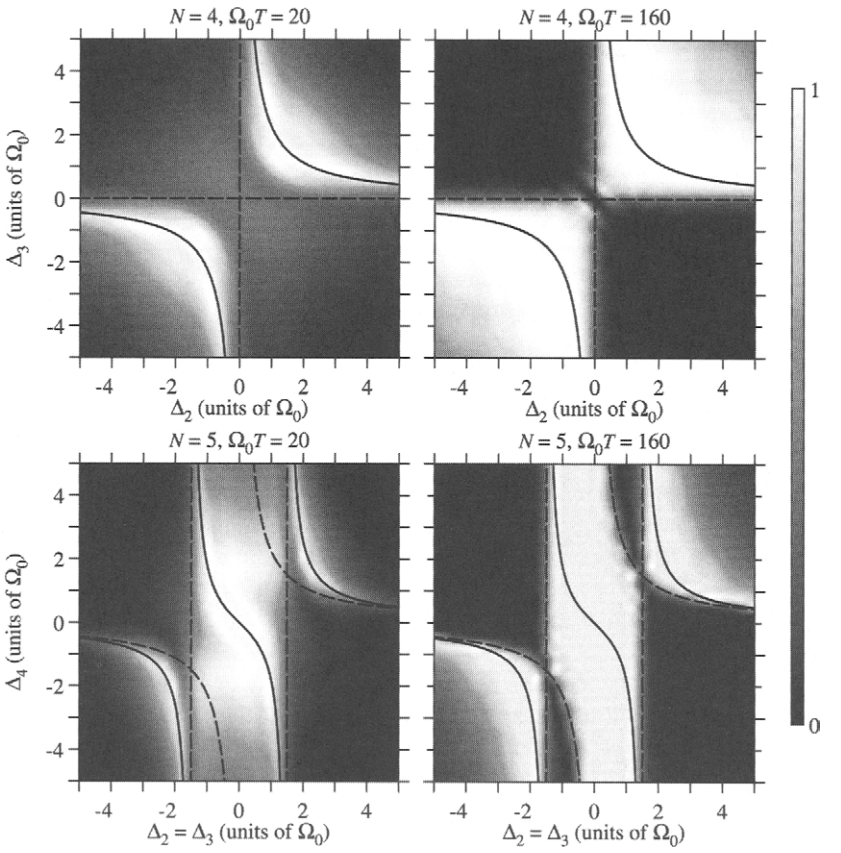

FIG. 29. Numerically calculated transfer efficiency for chain STIRAP. Upper frames: four-state system versus the two intermediate-state detunings Δ_2 and Δ_3. Lower frames: five-state system versus the three intermediate-state detunings $\Delta_2 = \Delta_3$ and Δ_4. In all frames, we have taken $\Omega_p = \Omega_0 \exp[-(t-\tau)^2/T^2]$, $\Omega_s = \Omega_0 \exp[-(t+\tau)^2/T^2]$, with $\tau = 0.5T$, and all intermediate Rabi frequencies constant and equal to $3\Omega_0$. In the left frames, $\Omega_0 T = 20$, while in the right frames, $\Omega_0 T = 160$. The solid curves show the dressed-state resonances and the dashed curves separate the regions where adiabatic transfer state does or does not exist. (From Vitanov, 1998.)

VI. Adiabatic Momentum Transfer

Coherent population transfer between atomic states is always accompanied by transfer of photon momenta to the atoms. Momentum transfer is the basis of atom optics, particularly in the design of its key elements—atom mirrors and beam splitters. An atomic beam splitter separates the single-atom wavefunction into a macroscopic superposition state corresponding to two center-of-mass wave packets

propagating in different spatial directions. An atomic mirror, on the other hand, deflects these wave packets so that the matter waves traveling along two paths of an interferometer can be brought together to interfere. This interference will be observed only if these scattering processes are coherent. Because STIRAP enables efficient, robust, and dissipation-free coherent population and momentum transfer, it has been quickly recognized that it is a perfect tool for building practically "ideal" atomic mirrors and beam splitters (Marte *et al.*, 1991).

A. Coherent Matter-Wave Manipulation

1. Atomic Mirrors

A particularly suitable system for coherent momentum transfer is the chainwise transition formed between the magnetic sublevels of two degenerate levels with total angular momentum J_g of the ground level and $J_e = J_g$ or $J_g - 1$ of the excited level. An example for such a chain in the case when $J_g = J_e = 2$ is shown in Fig. 30. When such a system is prepared initially in one of the chain-end ground sublevels, e.g., in $M = -J_g$, and is driven adiabatically by two counterintuitively ordered sequential laser pulses with opposite circular polarizations, then, as discussed in Section V, complete population transfer occurs between the two ends of the chain, i.e., from sublevel $M = -J_g$ to sublevel $M = J_g$. In the general case, the chain couples $J_g + 1$ ground sublevels and J_g excited sublevels. Thus, for $J_g = 1 \leftrightarrow J_e = 0$ and $J_g = 1 \leftrightarrow J_e = 1$ transitions, the σ^+ and σ^- laser fields couple three sublevels: two ground sublevels $M = -1$ and $M = +1$ and one excited sublevel $M = 0$. If the two laser beams propagate in opposite directions, each atom will receive, during its journey from the $M = -1$ sublevel to the $M = 1$ sublevel, a total momentum of $2\hbar k$ in the direction of the σ^+ beam: a momentum of $\hbar k$ from absorbing a photon from the σ^+ beam, and another $\hbar k$ in the *same* direction due to

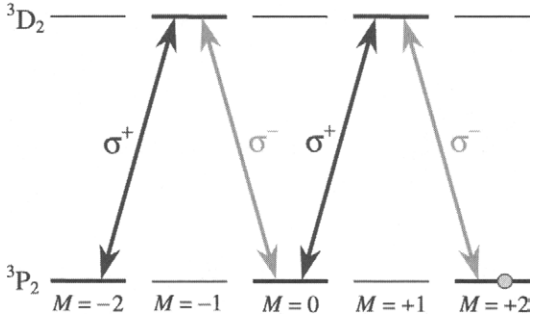

FIG. 30. Linkage pattern between the Zeeman sublevels in the $^3P_2 - {}^3D_2$ transition in Ne* driven by a pair of counterpropagating and displaced σ^+ and σ^- laser beams.

recoil from the stimulated emission of a photon into the σ^- beam. As a result, the atom is deflected in a single well-defined direction, determined by two σ^+ photon momenta.

An example in the case when $J_g = J_e = 2$, demonstrated in a recent experiment (Theuer and Bergmann, 1998), is shown in Fig. 31. A beam of metastable neon atoms, prepared by optical pumping in the $M = 2$ magnetic sublevel of the $^3P_2$ metastable level, crosses two slightly displaced circularly polarized CW laser beams. The two beams are ordered counterintuitively, so the atoms encounter the σ^+ beam (the Stokes) first and then the σ^- beam (the pump). In the adiabatic limit, the population is completely transferred to the $M = -2$ sublevel of the $^3P_2$ level, without residing at any time in the $M = -1$ and $M = 1$ sublevels of the decaying excited level $^3D_2$. Because the two laser beams propagated in opposite directions, each atom received a total momentum of $4\hbar k$ in the direction of the σ^- beam during its journey from the $M = 2$ sublevel to the $M = -2$ sublevel: $2\hbar k$ momentum due

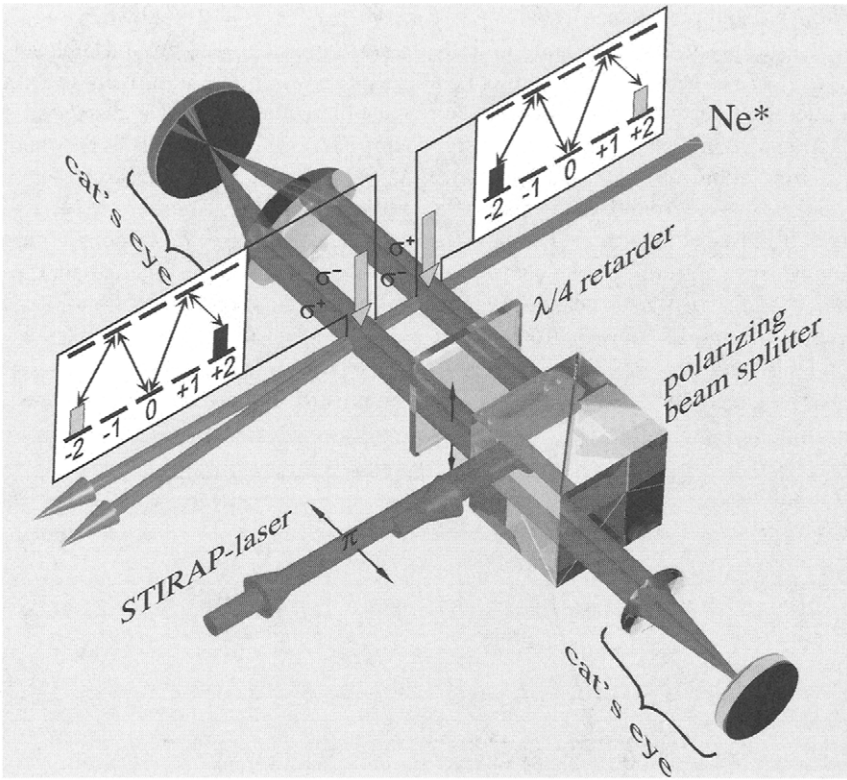

FIG. 31. Experimental setup for the Ne* atomic mirror. (From K. Bergmann, H. Theuer, and B. W. Shore. Coherent population transfer among quantum states of atoms and molecules. *Rev. Mod. Phys.* 1998;70:1003–1025.)

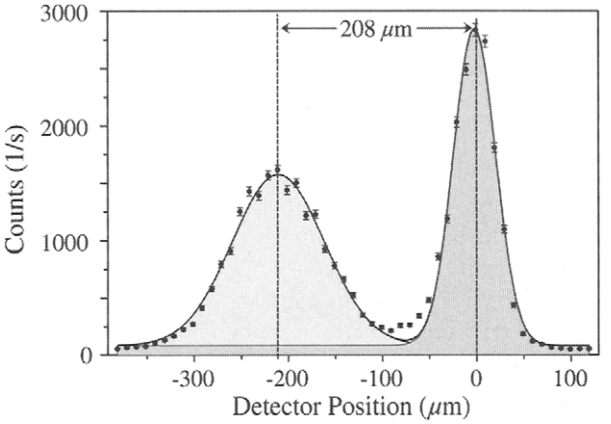

FIG. 32. Experimental results showing deflection of a beam of $^{20}Ne^*$ atoms due to transfer of eight photon momenta after double adiabatic passage from the $M=2$ sublevel to $M=-2$ and then back to $M=2$. The narrower, undeflected original distribution is observed due to the presence of ^{22}Ne isotope atoms which are insensitive to the light. (From H. Theuer and K. Bergmann. Atomic beam deflection by coherent momentum transfer and the dependence on weak magnetic fields. *Eur. Phys. J. D* 1998;2:279–289.)

to absorption of two photons from the σ^- beam (which transfer their momenta to the atom), and another momentum $2\hbar k$ in the same direction due to recoil from the stimulated emission of two photons into the σ^+ beam. The experimental results in Fig. 32 correspond to a double passage from the $M=2$ sublevel to the $M=-2$ sublevel and then back to the $M=2$ sublevel (by using a second interaction zone with a reversed ordering of the σ^+ and σ^- beams), resulting in the transfer of eight photon momenta.

The attraction of using STIRAP for atomic interferometry is based on several features. First, it provides nearly 100% population transfer to a single final state, corresponding to transferring a fixed momentum $2\hbar k$. Thus there is no splitting of the incident wave packet into a superposition corresponding to many momentum peaks $\pm\hbar k$, $\pm 2\hbar k$, $\pm 3\hbar k$, etc., as occurs for deflection of a beam of two-state atoms by a standing light wave. Second, since the process is adiabatic, it is insensitive to changes in the laser properties (intensity and frequency) and the interaction time (i.e., atomic velocity for crossed-beam experiments, or pulse width for pulsed experiments); this is in contrast to transfer by π pulses, which is very sensitive to pulse area and resonance tuning (and, hence, to the laser parameters and the interaction time). Moreover, although the interaction is resonant, the deflection process is unaffected by spontaneous decay, because the excited state is never populated during the transfer. One can therefore avoid the common approach of eliminating spontaneous decay by detuning the laser far off resonance to reduce the excited-state population, at the expense of reducing the effective laser–atom

coupling. Finally, using chainwise transitions between degenerate sublevels has the advantage that it requires only a single laser, because the σ^- wave can be derived by reflecting the σ^+ laser light. Having the two laser fields derived from the same laser is very convenient because the two-photon resonance condition, which is crucial for STIRAP, is automatically fulfilled (provided, of course, that there are no residual magnetic fields) and it is immune to laser frequency fluctuations.

STIRAP-based atomic mirrors are superior also to those based on the spontaneous emission force. In the latter, an atom absorbs a photon from a traveling-wave laser beam and then emits it spontaneously. Because the momenta from the absorbed photons are in the direction of the laser beam, while the momenta of the spontaneously emitted photons are distributed randomly (thus averaging to zero), the absorption-emission of N photons will result in a net momentum of $N\hbar k$ in the laser-beam direction. However, the dissipative nature of the emission process leads to a wide distribution of deflection angles. Moreover, it does not preserve any coherence, which is essential in an atom interferometer. STIRAP-based atom mirrors and beam splitters cure these drawbacks.

Coherent momentum transfer by adiabatic passage in similar chains of Zeeman sublevels has been demonstrated in a number of other experiments. Pillet *et al.* (Pillet *et al.*, 1993; Valentin *et al.*, 1994) and Goldner *et al.* (1994a,b) have reported momentum transfer of $8\hbar k$, with about 50% efficiency, resulting from the single-pass adiabatic passage between the $M_F = -4$ and $M_F = 4$ Zeeman sublevels in the hyperfine transition $F_g = 4 \leftrightarrow F_e = 4$ of the cesium D_2 line. Lawall and Prentiss (1994) have demonstrated momentum transfer of $4\hbar k$ with 90% efficiency in the $2^3S_1 \leftrightarrow 2^3P_0$ transition of He* with circularly polarized lasers, after double adiabatic passage ($M = -1 \rightarrow M = 1 \rightarrow M = -1$) between the ground-state sublevels. They demonstrated momentum transfer of $6\hbar k$ with 60% efficiency after a triple pass with linearly polarized lasers.

2. *Atomic Beam Splitters*

STIRAP can be used not only to transfer population and momentum completely from one state to another in a robust fashion, free of loss or incoherence, but also to create coherent superpositions of atomic states. In momentum space, this corresponds to splitting of the initial momentum distribution into two or more momenta distributions. The most obvious approach to achieve this objective is, starting with population in state ψ_1, to interrupt abruptly the time evolution of the dark state (44b) at a certain intermediate time, when it is the desired superposition of the initial state ψ_1 and the final state ψ_3 (Marte *et al.*, 1991; Weitz *et al.*, 1994a,b), before it has evolved into state ψ_3 as in STIRAP. Then only a fraction of the total population is transferred to ψ_3 and the composition of the superposition depends on the ratio between the pump and Stokes Rabi frequencies at the turn-off time. This fractional STIRAP scheme has been demonstrated experimentally (Weitz *et al.*, 1994a).

A smooth-pulse realization of this scheme that avoids sudden interruption of the pulses has been proposed for chains between degenerate sublevels (Vitanov *et al.*, 1999). In this scheme, starting from the $M = -1$ sublevel, a coherent superposition between states $M = -1$ and $M = 1$ is created by applying first a σ^- polarized pulse (Stokes), followed by a slightly delayed pulse which is elliptically polarized in the same plane as the σ^- pulse. Since elliptical polarization can be represented as a sum of σ^- and σ^+ polarizations, the elliptically polarized pulse couples both the pump and Stokes transitions. As a result, the pulses create a superposition of the $M = -1$ and $M = 1$ sublevels whose composition is controlled by the ellipticity of the latter pulse.

Another possible realization of an atomic beam splitter (Lawall and Prentiss, 1994), suitable for $J_g = 1 \leftrightarrow J_e = 0$ transitions, starts with a coherent superposition of the $M = -1$ and $M = 0$ sublevels. A pair of counterpropagating σ^- and σ^+ pulses transfers the population from $M = -1$ to the $M = 1$ state, which results in $2\hbar k$ momentum deflection with respect to the momentum of the $M = 0$ sublevel, which is unaffected by the laser fields.

3. *Atomic Interferometers*

Weitz *et al.* (1994a, 1994b) have built the first atomic interferometer based on STIRAP, by using the transition between the two cesium hyperfine ground states ($6S_{1/2}$, $F = 3$, $M_F = 0$) and ($6S_{1/2}$, $F = 4$, $M_F = 0$) via the excited state ($6P_{1/2}$, $F = 3$ or 4, $M_F = 1$). This atom interferometer had the Bordé four-$\pi/2$ geometry (Bordé, 1989; Riehle *et al.*, 1991) and involved four successive atomic beam splitters. Each of the beam splitters used two σ^+-polarized counterpropagating laser pulses and was based on interrupted STIRAP. Two 40-MHz accoustooptic modulators generated the pulse shapes for adiabatic following. A coherent superposition of two states of different momenta was created by turning the intensities of both pulses to zero in the middle of the transfer. The experiment achieved multiple-pass coherent transfer of more than 140 photon momenta with 95% efficiency per exchanged photon pair.

The transition used in the interferometer is insensitive to any magnetic field, which is essential for precision interferometry. Moreover, the σ^+–σ^+ configuration (the same helicity for the two pulses) increased the interferometer contrast because atoms that were not transfered adiabatically were optically pumped into the $F = 4$, $M_F = 4$ and $F = 3$, $M_F = 3$ states. Furthermore, using the cesium D_1 line (involving the $6P_{1/2}$ state) increased the transfer efficiency in comparison with using the cesium D_2 line (involving the $6P_{3/2}$ state) (Goldner *et al.*, 1994a,b), because the excited-state hyperfine splitting of the $6P_{1/2}$ state is 5.8 times larger and thus off-resonant excitation is significantly lower.

In the experiment (Weitz *et al.*, 1994a,b), a cesium atomic beam, slowed by a chirped laser beam, loaded a magnetooptic trap. Then the trapping magnetic field was shut off and the atoms were further cooled to 4 μK in polarization-gradient

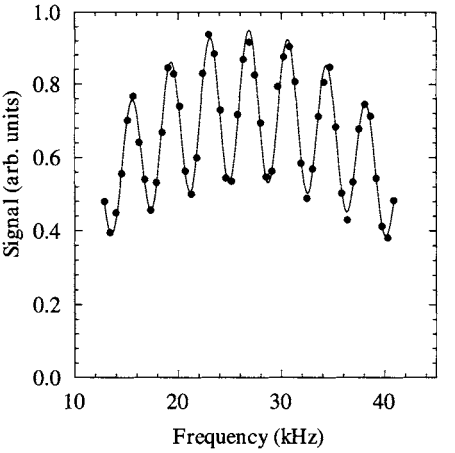

FIG. 33. Interference fringes for an atomic interferometer based on adiabatic passage. The dots are experimental data and the curve is a fit by a cosine function with a Gaussian envelope. (Reprinted with permission from M. Weitz, B. C. Young, and S. Chu. Atomic interferometer based on adiabatic population transfer. *Phys. Rev. Lett.* 1994;73:2563–2566.)

optical molasses. The atoms were then launched in a vertical ballistic trajectory at 2.3 m/s in a moving molasses. The molasses then was shut off. On their way up, the atoms were optically pumped into the $F=4, M=0$ sublevel and entered a magnetically shielded region with a homogeneous 100-mG magnetic bias field oriented parallel to the Raman beams. While the atoms were in the shielded region, a series of adiabatic pulses of the Raman beams were applied, which constituted the interferometer. The pulse sequence was designed to leave the coherently transferred atoms in the $F=3, M=0$ sublevel. As the atoms dropped back, a laser beam first removed the residual $F=4$ population and then the $F=3, M=0$ population was transferred to $F=4$, $M=0$ by a microwave π pulse and measured by recording the fluorescence induced by a probe laser. Figure 33 shows the observed interference fringes.

Burnett and co-workers (Featonby *et al.*, 1996, 1998; Morigi *et al.*, 1996, Godun *et al.*, 1999; Webb *et al.*, 1999) have also demonstrated coherent momentum transfer in trapped and laser-cooled cesium atoms, both with laser beams having circular/circular ($\sigma^+\sigma^-$) and with others having circular/linear ($\sigma^+\pi$) polarizations. They have built a separated-path Ramsey atom interferometer (Featonby *et al.*, 1998) in which the closed loop constituting the Mach–Zehnder-type interferometer was produced by manipulating the atomic internal and external states separately, which provided greater flexibility. This interferometer used a sequence of ground-state microwave interactions and optical adiabatic transfer pulses. The microwaves were used to create a superposition of the ground hyperfine levels, and the adiabatic transfer then selectively manipulated the momentum of the $F=4$ component of

this superposition. The scheme started with the application of a $\pi/2$ microwave pulse to create, starting from the $F=3$, $M=0$ sublevel, an equal superposition of the $F=3$, $M=0$ and $F=4$, $M=0$ sublevels. At the end, a second $\pi/2$ pulse was applied in order to induce Ramsey fringes (which were observed by scanning the phase of the latter $\pi/2$ pulse). Between the microwave pulses, the momentum of the $F=4$ component was manipulated by multistate STIRAP, using orthogonally propagating light pulses of linear (π) and right circular (σ^+) polarization. The laser fields were resonant with the D_1 $6S_{1/2}$, $F=4 \leftrightarrow 6P_{1/2}$, $F'=4$ transition in cesium, and thus only the atoms in the $F=4$, $M=0$ sublevel were subjected to adiabatic transfer. Since the $M=0 \leftrightarrow M'=0$ transition is forbidden, a sequence of partly overlapping π and σ^+ laser pulses transferred the population from $F=4$, $M=0$ to $F=4$, $M=4$ in an eight-photon transition. Because of the orthogonal $\sigma^+\pi$ geometry, the net momentum transferred to the atom was $4\sqrt{2}\hbar k$, rather than $8\hbar k$ as with $\sigma^+\sigma^-$ geometry. Once the $M=4$ was reached, the STIRAP was reversed in time and the population returned to $M=0$. Thus the first STIRAP was used to split the paths and the second reestablished the spatial overlap between the components of the superposition, $F=3$, $M=0$ and $F=4$, $M=0$. Although the net momentum transfer of such a process is zero, a small displacement was produced because of the finite momentum of the atom during the interaction. This atom interferometer was used to develop a method for measuring the temperature of an atomic ensemble (Featonby *et al.,* 1998) and a method for measuring the Berry phase (Webb *et al.,* 1999).

Incidentally, an interesting multiple-beam atomic interferometer not using adiabatic transfer has been demonstrated: a beam of cesium atoms has been split into five spatially distinct beams (separated by two-photon momenta), corresponding to the magnetic sublevels $M=-4, -2, 0, 2, 4$, and then recombined (Weitz *et al.,* 1996).

B. Coherent Manipulation of Laser-Cooled and Trapped Atoms

The STIRAP technique has been successfully applied in laser cooling experiments to coherently manipulate the atomic wave packets resulting from subrecoil laser cooling by velocity-selective coherent population trapping (VSCPT) (Aspect *et al.,* 1988, 1989; Kasevich and Chu, 1991; 1992; Kasevich *et al.,* 1991; Lawall *et al.,* 1994, 1995, 1996; Chu, 1998; Cohen-Tannoudji, 1998; Phillips, 1998). The momentum distribution of atoms cooled by VSCPT has two peaks, at $+\hbar k$ and $-\hbar k$, both with widths smaller than the photon recoil momentum $\hbar k$. Esslinger *et al.* (1996) have used adiabatic passage to coherently transfer rubidium atoms cooled by VSCPT into a single momentum state, still with a subrecoil momentum spread. Kulin *et al.* (1997) have demonstrated adiabatic transfer of metastable helium atoms into a single wave packet or into two coherent wave packets, while retaining the subrecoil momentum dispersion of the initial wave packets. They have

achieved nearly 100% transfer efficiency in one and two dimensions, and 75% in three dimensions, while being able to choose at will the momentum direction and the internal state of the atoms. The three-dimensional manipulation is particularly important because it can be used to produce an ultraslow, spin-polarized atomic beam with subrecoil momentum spread in all directions.

The wave packet manipulation uses the fact that the atomic state after VSCPT—the dark state—has the same structure as the laser field. Hence a slow, adiabatic change in the laser field induces a corresponding change of the trapping state. If the evolution is adiabatic, the atoms remain decoupled from the laser fields during the transfer process and hence are immune to spontaneous emission. The final state may be chosen at will, and in particular, if at the end of such a change a single laser beam remains, the ensuing atomic state will consist of a single wave packet. Hence, this manipulation can be seen as inverted fractional STIRAP (Section VI.A.2).

It is obvious that for such a wave packet manipulation, the coherence of both the two components of the initial momentum distribution and the adiabatic transfer are crucial. Hence, this operation can be also used as a proof of the coherence of the two momentum peaks at $+\hbar k$ and $-\hbar k$ (Esslinger *et al.*, 1996).

C. Measurement of Weak Magnetic Fields with Larmor Velocity Filter

The potential of STIRAP for inducing atomic beam deflection by coherent momentum transfer has been used to create a technique (called a *Larmor velocity filter*) for measuring very small magnetic fields along the axis of the atomic beam (Theuer and Bergmann, 1998). The scheme, which was demonstrated with metastable neon

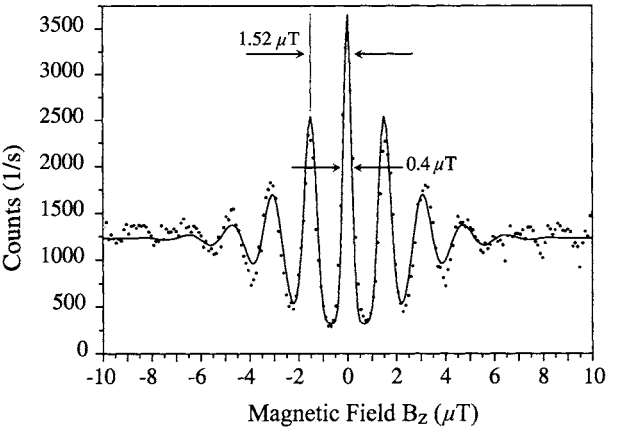

FIG. 34. Variation of the flux of deflected Ne* atoms in the Larmor velocity filter with the magnetic field strength. (From H. Theuer and K. Bergmann. Atomic beam deflection by coherent momentum transfer and the dependence on weak magnetic fields. *Eur. Phys. J. D* 1998;2:279–289.)

atoms, consisted of two STIRAP zones. In the first zone, atoms were prepared in the $M=2$ sublevel of the $^3P_2$ metastable state and transferred to the $M=-2$ sublevel. They were transferred back to the initial $M=2$ sublevel in the second zone provided they remained in the $M=-2$ state along the path between the two zones (cf. Fig. 31). The magnetic field in the region between the two transfer zones caused Larmor precession, thereby mixing the magnetic sublevels and affecting the momentum transfer. The resulting narrow-peaked pattern, an example of which is shown in Fig. 34, permitted measurement of weak magnetic fields.

VII. Branched-Chain Excitation

A. Branched Linkage Patterns

Just as the admission of a third energy state offers a wealth of new options for excitation in comparison to a two-state system, so too does the presence of a fourth (or fifth) state. The simplest cases are those in which the additional state merely links onto the end of the three-state chain, thereby forming a four-state chain, as discussed in Section V.

The four-state atom also offers interesting opportunities for competing and interfering paths. If the terminal level of the chain is the initial level, then the four states form a closed loop. The relative phases of the four Rabi frequencies then have special significance: they determine whether there is constructive or destructive interference and whether there are population nodes on some of the states.

Another possibility is that three of the states are linked, by as many as three separate pulsed fields, to a single state. The relative energies may be such that the linkage pattern appears as the letter Y (i.e., two of the levels are highly excited, perhaps dissociating or photoionizing) or as a tripod (i.e., a single state, connected to all the others, lies highest).

The variety of linkage patterns admits a variety of uses for pulsed coherent excitation. In either the Y or the tripod configuration, one might wish to consider a three-state main chain, to which the fourth state provides a branch. The effects of branches, weak or strong, on a main chain have been discussed not only for steady fields (Shore, 1990, chap. 21) but also for pulsed excitation (Kobrak and Rice, 1998a,b,c).

As with three-state excitation, mathematical analysis of four-state behavior is greatly facilitated by the use of dressed states (adiabatic states, if the fields are pulsed). These have been presented and utilized by several groups (Unanyan *et al.*, 1998a, 1999; Kobrak and Rice, 1998a,b,c). Notably, these configurations have two null-eigenvalue states instead of the single one obtained with the three-state system. The occurrence of this degeneracy has some interesting consequences, as will be noted below.

In the remainder of this section we consider the tripod configuration explicitly.

B. The Tripod Linkage

1. Concept

In the tripod version of STIRAP, proposed by Unanyan *et al.* (1998a, 1999) and demonstrated by Theuer *et al.* (1999), the usual three-state STIRAP system is supplied with an additional state ψ_4, coupled to the intermediate state ψ_2 by a third, control laser with Rabi frequency $\Omega_c(t)$. Such a *tripod STIRAP* scheme has two, rather than one, zero-energy dark states. Because they are degenerate, transitions between them take place even in the adiabatic limit. Time evolution will therefore eventually lead to the creation of a coherent superposition of states, rather to a population transfer to a single state. The composition of this superposition depends on, and therefore can be controlled by, the ordering of the pulses, by the time delay between the pump and Stokes pulses, and by the strength of the control pulse.

2. The Tripod Linkage

The RWA Hamiltonian describing an on-resonance tripod system has the form

$$\mathsf{H}(t) = \frac{\hbar}{2}\begin{bmatrix} 0 & \Omega_p(t) & 0 & 0 \\ \Omega_p(t) & 0 & \Omega_s(t) & \Omega_c(t) \\ 0 & \Omega_s(t) & 0 & 0 \\ 0 & \Omega_c(t) & 0 & 0 \end{bmatrix}, \tag{81}$$

where the real-valued functions of time $\Omega_p(t)$, $\Omega_s(t)$, and $\Omega_c(t)$ are the Rabi frequencies of the pump, Stokes, and control pulses, respectively. It is easy to verify that the Hamiltonian (81) has the following eigenvalues, two of which are degenerate,

$$\varepsilon_1(t) = \varepsilon_2(t) = 0, \qquad \varepsilon_3(t) = -\varepsilon_4(t) = \tfrac{1}{2}\hbar\Omega(t), \tag{82}$$

where $\Omega \equiv \sqrt{\Omega_p^2 + \Omega_s^2 + \Omega_c^2}$. The corresponding eigenvectors (the adiabatic states) are expressible in terms of two time-dependent angles $\vartheta(t)$ and $\varphi(t)$, defined as

$$\tan\vartheta(t) = \frac{\Omega_p(t)}{\sqrt{\Omega_s^2(t) + \Omega_c^2(t)}}, \qquad \tan\varphi(t) = \frac{\Omega_c(t)}{\Omega_s(t)}. \tag{83}$$

The angle $\vartheta(t)$ is the mixing angle used in standard STIRAP (where $\Omega_c \equiv 0$), and $\varphi(t)$ is an additional mixing angle related to the additional pulse. The adiabatic

states corresponding to the two null-valued eigenenergies are (Unanyan *et al.*, 1998a)

$$\Phi_1(t) = \psi_1 \cos\vartheta(t) - \psi_3 \sin\vartheta(t)\cos\varphi(t) - \psi_4 \sin\vartheta(t)\sin\varphi(t), \quad (84a)$$

$$\Phi_2(t) = \psi_3 \sin\varphi(t) - \psi_4 \cos\varphi(t), \quad (84b)$$

while the remaining adiabatic states are

$$\Phi_3(t) = \tfrac{1}{\sqrt{2}}[\psi_1 \sin\vartheta(t) + \psi_2 + \psi_3 \cos\vartheta(t)\cos\varphi(t) + \psi_4 \cos\vartheta(t)\sin\varphi(t)], \quad (84c)$$

$$\Phi_4(t) = \tfrac{1}{\sqrt{2}}[\psi_1 \sin\vartheta(t) - \psi_2 + \psi_3 \cos\vartheta(t)\cos\varphi(t) + \psi_4 \cos\vartheta(t)\sin\varphi(t)]. \quad (84d)$$

When the $\Omega_c(t)$ pulse is absent, one has the usual three-state atomic system and the adiabatic states turn into the adiabatic states (44) for STIRAP. However, the occurrence of two degenerate null-eigenvalue states here adds complications, and flexibility, that is not present with three-state STIRAP.

The systems of interest for the present discussion are those for which the atomic states ψ_1, ψ_3, and ψ_4 are stable states. Spontaneous emission occurs, if at all, only from state ψ_2. The two degenerate adiabatic states $\Phi_1(t)$ and $\Phi_2(t)$ receive no contribution from state ψ_2. They are therefore immune to loss of coherence and population that may occur due to spontaneous emission from ψ_2—these are dark or trapped states—and hence there is no difficulty in considering long pulses, as needed to ensure adiabatic evolution.

We note that because the zero-eigenvalue adiabatic states $\Phi_1(t)$ and $\Phi_2(t)$ are degenerate, any linear superposition of them will also be a zero-eigenvalue eigenstate of the Hamiltonian (81), and the choice of the two orthogonal zero-eigenvalue eigenstates of (81) is merely a matter of convenience. Furthermore, we point out that there is an obvious symmetry in the linkage of the three states ψ_1, ψ_3, and ψ_4. Our choice of the definitions of the angles $\vartheta(t)$ and $\varphi(t)$ and the dark states $\Phi_1(t)$ and $\Phi_2(t)$ is determined by the special role of state ψ_1 as the initial state.

3. Adiabatic Evolution

Nonadiabatic transitions between any pair of adiabatic states Φ_m and Φ_n are suppressed if the nonadiabatic coupling between these states is small compared to the difference between their energies (Messiah, 1962; Crisp, 1973; Shore, 1990); i.e.,

$$|\langle\dot{\Phi}_m(t)|\Phi_n(t)\rangle| \ll |\varepsilon_m - \varepsilon_n| .$$

If the adiabatic energies ε_m and ε_n are nondegenerate, this condition can always be satisfied for sufficiently large pulse areas, because the nonadiabatic couplings $|\langle\dot{\Phi}_m|\Phi_n\rangle|$ are proportional to $\dot{\vartheta}$ or $\dot{\varphi}$, which are in turn proportional to the inverse pulse width $1/T$, while the eigenenergy splittings $|\varepsilon_m - \varepsilon_n|$ are proportional to the maximum Rabi frequencies. Therefore, for large pulse areas the adiabatic states Φ_3 and Φ_4 are decoupled from the two dark states Φ_1 and Φ_2 and from each other. Then, unless states Φ_3 and Φ_4 are populated initially, the population dynamics is confined within the Hilbert subspace of the two nondecaying dark states, which allows us to realize coherent processes on time scales exceeding the lifetime of the excited state ψ_2.

Because the two dark states Φ_1 and Φ_2 are degenerate ($\varepsilon_1 = \varepsilon_2 = 0$), the adiabatic condition cannot be satisfied for the $\Phi_1 \leftrightarrow \Phi_2$ transition and hence transitions between Φ_1 and Φ_2 always occur, unless the nonadiabatic coupling between them vanishes identically (e.g., for constant fields). It is these transitions that lead to the controlled creation of a coherent superposition of states. The nonadiabatic coupling between the two trapped states is

$$\langle\dot{\Phi}_1(t)|\Phi_2(t)\rangle = \dot{\varphi}(t)\sin\vartheta(t).$$

If initially $\Omega_p = 0$ but one (or both) of the couplings Ω_s and Ω_c is nonzero, we have $\vartheta = 0$, meaning that $\psi_1 = \Phi_1$. Thus the system starts initially in state Φ_1, and if the laser pulses have large enough pulse areas to prevent transitions to the other adiabatic states Φ_3 and Φ_4, the system will end in a superposition of states Φ_1 and Φ_2,

$$\Phi_1(-\infty) \xleftarrow{-\infty} \Psi(t) \xrightarrow{+\infty} \Phi_1(+\infty)\cos\alpha - \Phi_2(+\infty)\sin\alpha. \tag{85}$$

Here the mixing angle α is the "area" of the nonadiabatic coupling,

$$\alpha = \int_{-\infty}^{\infty} \dot{\varphi}(t)\sin\vartheta(t)\,dt. \tag{86}$$

Because $\vartheta(t)$ and $\varphi(t)$ depend on the relative strengths of the pulses and their relative delays [see Eqs. (83)], the mixing angle α of the created superposition (85) of the dark states Φ_1 and Φ_2 also depends on, and therefore can be controlled by, these laser parameters.

According to Eqs. (84a), (84b), and (83), the asymptotic correspondence between the adiabatic states and the bare states at $\pm\infty$, and hence the bare-state composition of the created superposition (85), can be controlled by suitably choosing the pulse ordering. We provide four particular examples below.

- If the pulses are ordered so that the Stokes pulse starts before and ends after the pump pulse, while the control pulse is delayed with respect to both of

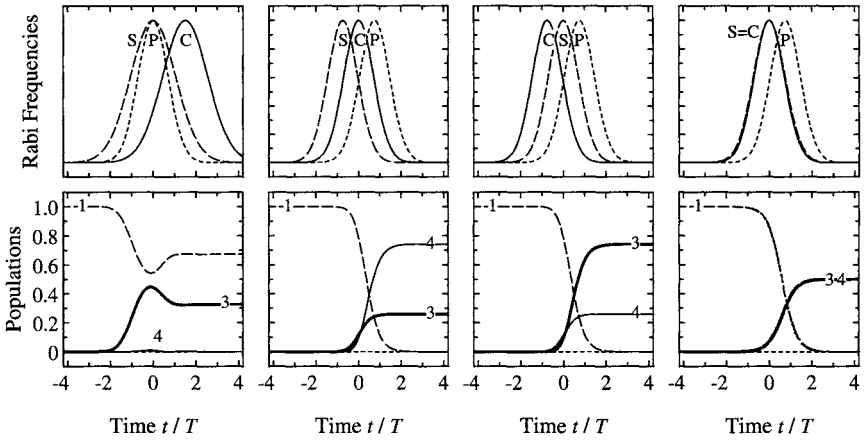

FIG. 35. Various possible orderings for the pump (P), Stokes (S), and control (C) laser pulses in tripod-STIRAP (top), and the corresponding population evolutions (bottom), where the numbers on the curves label the respective states.

them (Fig. 35, col. 1) (Unanyan *et al.*, 1998a), the following asymptotic relations apply: $\vartheta(-\infty) = \vartheta(+\infty) = 0, \varphi(-\infty) = 0, \varphi(+\infty) = \pi/2$. Then

$$\psi_1 \xleftarrow{-\infty} \Phi_1(t) \xrightarrow{+\infty} \psi_1,$$
$$-\psi_4 \xleftarrow{-\infty} \Phi_2(t) \xrightarrow{+\infty} \psi_3.$$

Hence, as follows from Eq. (85), the system, which by assumption starts in the bare state ψ_1, will end in a superposition of states ψ_1 and ψ_3,

$$\Psi(+\infty) = \psi_1 \cos\alpha - \psi_3 \sin\alpha. \tag{87}$$

- Alternatively, one can arrange the three pulses to arrive in the ordering Stokes–control–pump (Fig. 35, col. 2) (Theuer *et al.*, 1999). In this case, the following asymptotic relations apply: $\vartheta(-\infty) = 0, \vartheta(+\infty) = \pi/2$, $\varphi(-\infty) = 0, \varphi(+\infty) = \pi/2$. Therefore

$$\psi_1 \xleftarrow{-\infty} \Phi_1(t) \xrightarrow{+\infty} -\psi_4,$$
$$-\psi_4 \xleftarrow{-\infty} \Phi_2(t) \xrightarrow{+\infty} \psi_3.$$

Hence the system, starting from the bare state ψ_1, will end in a superposition

of states ψ_3 and ψ_4,

$$\Psi(+\infty) = -\psi_3 \sin\alpha - \psi_4 \cos\alpha. \tag{88}$$

- A third possibility is to arrange the three pulses in the ordering control–Stokes–pump (Fig. 35, col. 3) (Theuer *et al.*, 1999). Then the following asymptotic relations apply: $\vartheta(-\infty) = 0$, $\vartheta(+\infty) = \pi/2$, $\varphi(-\infty) = \pi/2$, $\varphi(+\infty) = 0$. Therefore

$$\psi_1 \xleftarrow{-\infty} \Phi_1(t) \xrightarrow{+\infty} -\psi_3,$$
$$\psi_3 \xleftarrow{-\infty} \Phi_2(t) \xrightarrow{+\infty} -\psi_4.$$

Hence the system, starting from the bare state ψ_1, will end in a superposition of states ψ_3 and ψ_4, but with reversed populations compared to the previous case (88),

$$\Psi(+\infty) = -\psi_3 \cos\alpha + \psi_4 \sin\alpha. \tag{89}$$

- Finally, if the pulses are ordered so that the Stokes and control pulses coincide in time and precede the pump pulse (Fig. 35, col. 4) (Unanyan *et al.*, 1998a), the following asymptotic relations apply: $\vartheta(-\infty) = 0$, $\vartheta(+\infty) = \pi/2$, $\varphi(-\infty) = \varphi(+\infty) = \pi/4$. Then

$$\psi_1 \xleftarrow{-\infty} \Phi_1(t) \xrightarrow{+\infty} -\tfrac{1}{\sqrt{2}}(\psi_3 + \psi_4),$$
$$\tfrac{1}{\sqrt{2}}(\psi_3 - \psi_4) \xleftarrow{-\infty} \Phi_2(t) \xrightarrow{+\infty} \tfrac{1}{\sqrt{2}}(\psi_3 - \psi_4).$$

Because in this case $\varphi(t)$ is constant (equal to $\pi/4$), we have $\dot{\varphi}(t) = 0$ and thus the diabatic mixing angle is zero, $\alpha = 0$. Hence the system, starting in state ψ_1, will remain at all times in the dark state $\Phi_1(t)$ and will end in an equal superposition of states ψ_3 and ψ_4,

$$\Psi(+\infty) = -\tfrac{1}{\sqrt{2}}(\psi_3 + \psi_4). \tag{90}$$

It is important to note that the analysis above will also apply when there is one-photon detuning Δ from state ψ_2, as long as any pair of states ψ_1, ψ_3, and ψ_4 are on two-photon resonance. For nonzero Δ, the two dark states Φ_1 and Φ_2 remain eigenstates of the Hamiltonian, but the other eigenstates Φ_3 and Φ_4 are different. This change has no effect on the results, which rely on adiabatic evolution to maintain the state vector as a combination of the dark states Φ_1 and Φ_2.

The relative phase in each of the created superpositions can be altered by changing the relative phases of the laser fields. On the other hand, once a superposition is created, its parameters can be measured independently by the Newton–Young method using Stern–Gerlach analyzers (Newton and Young, 1968) or by coupling the superposition states to a third, excited state and measuring the subsequent fluorescence for different ratios of laser intensities and different relative laser phases (Vitanov *et al.*, 2000; Vitanov, 2000).

In conclusion, branched-chain excitation, such as the tripod scheme described in this section, provides more freedom in manipulating the internal quantum state of atoms and molecules. In more complex systems, one can use the decomposition method of Morris and Shore (1983) to identify possible trapped (dark) states and devise excitation schemes that confine the dynamics within the trapped subspace.

C. Experimental Demonstration

The first experimental implementation of the tripod scheme was achieved in a beam of metastable neon atoms crossing three suitably arranged laser beams at right angles. The level scheme for this experiment is shown in Fig. 36a. The initially populated state $2p^5 3s\ ^3P_0 (M = 0)$ (state ψ_1) is coupled by a π-polarized pump laser field (Rabi frequency Ω_p) to an intermediate state $2p^5 3p\ ^3P_1 (M = 0)$ (state ψ_2), which in turn is coupled via σ^+ (Ω_s) and σ^- (Ω_c) laser fields to two final magnetic sublevels of level $2p^5 3s\ ^3P_2$, $M = -1$ (state ψ_3) and $M = +1$ (state ψ_4). The sequence of interaction with the three laser beams is controlled by the spatial displacement of their axes. The σ^+ and σ^- beams propagate in opposite directions, while the axis of the π polarized beam is at right angles to the others (see Fig. 36b).

In the experiment, the beam of metastable neon atoms emerged from a liquid-nitrogen-cooled cold cathode discharge. The mean longitudinal velocity was 600 m/s with FWHM of 200 m/s. The metastable states $2p^5 3s\ ^3P_0$ and $2p^5 3s\ ^3P_2$ were populated with an efficiency of the order of 10^{-4}. The on-axis beam intensity was increased by a factor of 27 by two-dimensional transverse polarization gradient

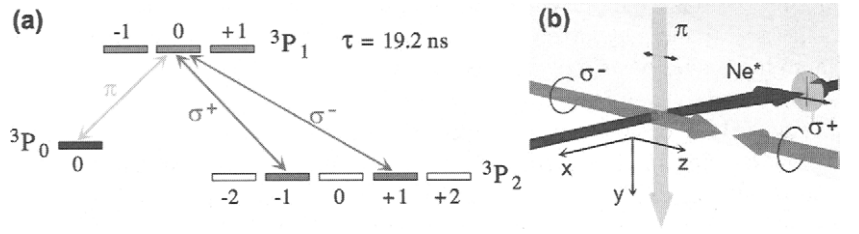

FIG. 36. Linkage pattern in tripod STIRAP (left) and laser beam geometry (right). (From H. Theuer, R. G. Unanyan, C. Habscheid, K. Klein, and K. Bergmann. Novel laser controlled variable matter wave beamsplitter. *Opt. Express* 1999;4:77–83.)

laser cooling. Next, the atoms in state $^3P_2$ were transferred to state $^3P_0$ by optical pumping. An excitation laser at 588 nm drove the transition to the excited level $^3P_1$, which has a lifetime of 18 ns. The atomic beam was highly collimated (1:47000) by two collimation slits, which is equivalent to a transverse velocity component of $\pm$ 1.3 cm/s (0.4 recoil velocities). The magnetic field was reduced to less than 1 μT in the relevant region using the Larmor velocity filter setup (Section VI.C). The transverse atomic beam profile was monitored farther downstream with a channeltron behind a 25-μm slit driven perpendicularly to the atomic beam axis by a stepper motor.

Three independent continuous single-mode dye lasers (Coherent 699) were used in this experiment. The cooling laser operated at 640 nm. The optical pumping laser and the Stokes beams were provided by the same dye laser (588 nm). The third laser generated the 616-nm radiation needed for the pump $^3P_0 \leftrightarrow {}^3P_1$ transition. The Stokes laser passed through a $\lambda/4$ waveplate, interacted with the atomic beam and was back-reflected by a cats-eye retroreflector with an integrated $\lambda/4$ retarder plate (Theuer *et al.*, 1999). The translation of the cats-eye parallel to the atomic beam axis allowed precise adjustment of the spatial displacement of the two Stokes lasers.

The laser beams were arranged in such a way that the atoms encountered the pump laser last, while the timing of the Stokes and control laser beams was varied by displacing their axes. Hence, it was possible to create with this setup various superpositions of the magnetic sublevels $M = -1$ (state ψ_3) and $M = +1$ (state ψ_4) of state $2p^5 3s^3 P_2$, as described by Eqs. (88)–(90). Furthermore, since the σ^+ and σ^- beams propagated in opposite directions, the momentum transfer to the $M = +1$ and $M = -1$ states had opposite signs, resulting in coherent beam splitting.

Figure 37 shows examples of atomic beam profiles recorded for different displacements of the Stokes and control laser beams. Two maxima separated by (122 $\pm$ 2) μm are observable. This separation corresponds to a difference in transverse momentum in the direction of Stokes propagation of $2\hbar k_s$. The momentum which was accumulated by an atom during the transfer process was $\hbar(\vec{k}_p \pm \vec{k}_s)$. Since the beam was collimated by slits and was detected behind a narrow slit, which was parallel to the π-polarized beam, only the component of the momentum parallel to the Stokes beam axis was observed. The data in Fig. 37 demonstrate that the splitting ratio could be smoothly controlled by the displacement of the Stokes and control laser beams. When the axes of the two beams coincided, a 50:50 beam splitting was observed, as predicted by Eq. (90). When the σ^+ (Stokes) beam precedes the σ^- (control) beam, the population was transferred predominantly to the $M = +1$ sublevel (state ψ_4), in agreement with Eq. (88). When the σ^- beam preceded the σ^+ beam, the population was transferred predominantly to the $M = -1$ sublevel (state ψ_3), in agreement with Eq. (89).

We note in conclusion that the robustness and relative simplicity of the tripod scheme can be beneficial for various fields in atomic and molecular physics utilizing

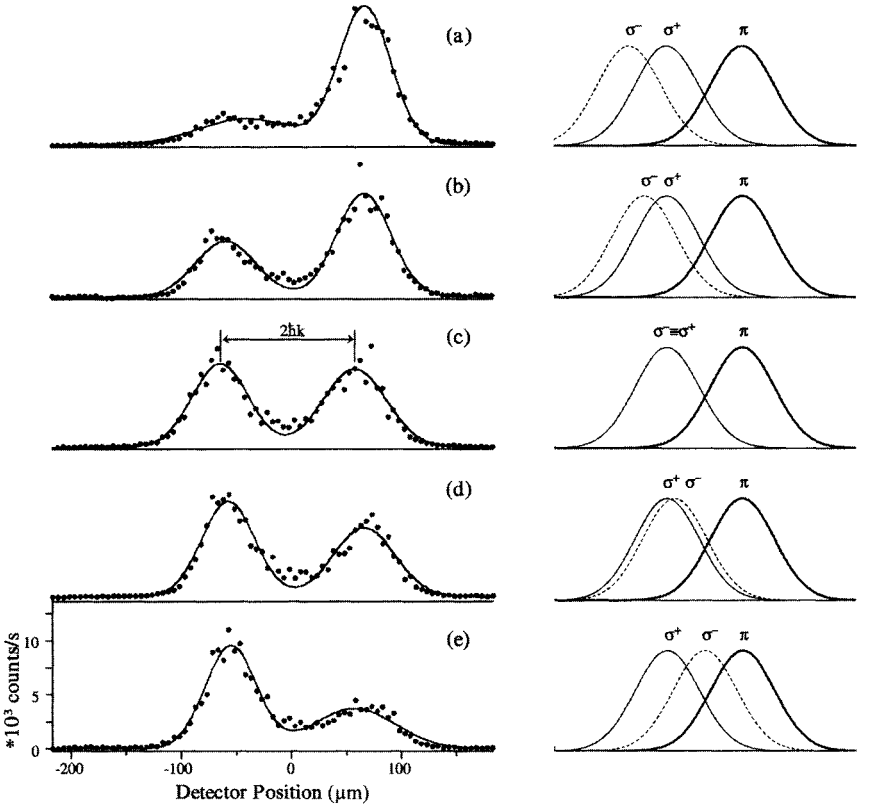

FIG. 37. Momentum distribution in the experiment of Theuer *et al.* (1999).

coherent superpositions of states, for instance, in quantum information [see, e.g., Williams and Clearwater (1997) and Steane (1998)].

VIII. Population Transfer via a Continuum of Intermediate States

Until the widespread use of lasers in atomic and molecular physics, the photoionization continuum was regarded as an incoherent terminus of probability flow, lacking any possibility for participating in a coherent process. Ionization was treated by means of rate equations, typically using the "Fermi golden rule" approximation (Messiah, 1962) to calculate ionization rates. Contemporary physics no longer views continuum as an irreversible drain of population. Laser interactions with a continuum have been found to exhibit coherent features, such as Rabi-like oscillations (Frishman and Shapiro, 1996), nearly complete population

transfer into a continuum (i.e., photoionization or photodissociation) (Vardi and Shapiro, 1996) or from a continuum (i.e., photorecombination or photoassociation) (Vardi *et al.*, 1997, 1999; Javanainen and Mackie, 1999; Mackie and Javanainen, 2000). Continuum coherence is essential in autoionization (Fano, 1961; Fano and Cooper, 1968), where it leads to a resonance in photoionization cross section plotted versus frequency; this is caused by destructive interference between two ionization channels, which can lead to complete suppression of photoionization at a specific wavelength. Laser-induced continuum structure (LICS) (Knight, 1984; Knight *et al.*, 1990; Halfmann *et al.*, 1998; Yatsenko *et al.*, 1999a) is another coherence phenomenon, closely related to autoionization, where a strong laser field embeds a discrete state in an otherwise flat, structureless photoionization continuum; this laser-induced resonance can be detected by a second, probe laser field.

A few years ago it was suggested (Carroll and Hioe, 1992, 1993) that a continuum can serve as an intermediary for population transfer between two discrete states in an atom or a molecule by using a sequence of two delayed partially overlapping laser pulses, ordered in the STIRAP fashion: with the Stokes pulse, coupling the initially unpopulated state ψ_2 to the continuum, preceding the pump pulse, coupling the initial state ψ_1 to the continuum. This intriguing scheme—which has yet to be demonstrated experimentally—can be seen as a variant of STIRAP in which the discrete intermediate state is replaced by a continuum of states. The advantage of this scheme for population transfer would be its flexibility because a continuum offers a continuous range of possible combinations to match the pump and Stokes laser frequencies to the two-photon resonance between the initial state and the target state. The Carroll–Hioe analytic model (Carroll and Hioe, 1992, 1993), which involves an infinite quasicontinuum of equidistant discrete states, equally strongly coupled to the two bound states, suggests that complete population transfer is possible, the ionization being completely suppressed. The physical reason for this unexpected conclusion is closely related to LICS created in the continuum by the Stokes laser. Another reason supporting this scheme is that, as in a discrete three-state Λ system, there exists a trapped (dark) state—a coherent superposition of the two bound states—that is immune to ionization. Nakajima *et al.* (1994) later demonstrated, however, that the completeness of the population transfer in the Carroll–Hioe model derives from the very stringent restrictions of the model which cannot be met in a realistic physical system with a real continuum, in particular with a nonzero Fano parameter (Fano, 1961; Knight, 1990) and Stark shifts. It has subsequently been recognized that although complete population transfer is unrealistic, significant partial transfer may still be feasible (Carroll and Hioe, 1995, 1996; Yatsenko *et al.*, 1997; Paspalakis *et al.*, 1997, 1998; Vitanov and Stenholm, 1997c). It has also been suggested that STIRAP-like process can take place via an autoionizing state (Nakajima and Lambropoulos, 1996; Paspalakis and Knight, 1998).

Below, we describe the problems in transferring population via a continuum and point out a few possible solutions.

A. Laser-Induced Continuum Structure

1. LICS Equations

The problem of two bound states coupled by two laser fields via a common continuum has been studied by a number of authors in the context of laser-induced continuum structure (LICS) (Knight *et al.*, 1990, and references therein). The most general expression of the wave function of such a system must be written as a superposition of the two bound states and the continuum with time-dependent coefficients (Knight *et al.*, 1990). By substituting this expansion in the Schrödinger equation and taking the Fourier transforms of the resulting differential equations for the probability amplitudes, one can eliminate the continuum adiabatically by substituting the adiabatic solution for its amplitudes in the other two equations. The summation over continuum states leads to a real part and an imaginary part representing a decay (via a pole) into the continuum (ionization or dissociation) and a coupling between the two bound states (via the principal value part). As a result of this elimination the wave function can be written as $\Psi(t) = C_1(t)\psi_1 + C_2(t)\psi_2$, where the probability amplitudes $\mathbf{C} = [C_1, C_2]^T$ satisfy the coupled equations

$$i\hbar \frac{d}{dt}\mathbf{C} = \mathsf{H}\mathbf{C} \tag{91}$$

where

$$\mathsf{H} = \hbar \begin{bmatrix} S_1 - \frac{1}{2}i\Gamma_1 & -\frac{1}{2}\sqrt{\Gamma_1^p \Gamma_2^s}(q+i) \\ -\frac{1}{2}\sqrt{\Gamma_1^p \Gamma_2^s}(q+i) & S_2 - \frac{1}{2}i\Gamma_2 + \delta \end{bmatrix}. \tag{92}$$

We shall assume that the system is initially in state ψ_1, $C_1(-\infty) = 1$, $C_2(-\infty) = 0$, and the quantities of interest are the populations of the discrete states $P_k(t) = |C_k(t)|^2 (k = 1, 2)$ and the ionization probability $P_i(t) = 1 - P_1(t) - P_2(t)$, particularly their values after the excitation ($t \to +\infty$).

The Hamiltonian matrix appearing here is that of two-photon excitation, but with a significant twist: the sum over intermediate states includes a continuum, and the consequent matrix elements therefore have both real and imaginary parts. On the diagonal, the elements appear as dynamic Stark shifts S_n and photoionization loss rates Γ_n. The off-diagonal elements are here parameterized by means of the Fano parameter q, the ratio of real to imaginary parts of the two-photon Rabi frequency (Fano, 1961; Knight *et al.*, 1990; Yatsenko *et al.*, 1997). As with auto ionization,

the Fano parameter governs the (asymmetric) shape of the curve of ionization versus frequency [as embodied in the static two-photon detuning $\delta = (E_2 - E_1)/\hbar + \omega_s - \omega_p$]. It also plays an important role in the context of population transfer (Nakajima *et al.*, 1994).

The Stark shifts and the ionization rates receive contributions from both of the fields,

$$\Gamma_n = \Gamma_n^p + \Gamma_n^s, \qquad S_n = S_n^p + S_n^s, \qquad (n = 1, 2).$$

The superscript labels p and s refer to the pump and Stokes lasers, respectively. The ionization widths and the Stark shifts are proportional to the laser fields intensities $I_p(t)$ and $I_s(t)$,

$$\Gamma_n^j(t) = G_n^j I_j(t), \qquad S_n^j(t) = S_n^j I_j(t),$$

with ($n = 1, 2$; $j = p, s$), where the parameters G_n^j and S_n^j depend on the particular atomic states and the laser frequencies.

With the exception of the Fano parameter, which is a dimensionless constant determined by the atomic structure, all variables involved in Eq. (91) can be controlled externally by the laser intensities and are generally time dependent.

2. *Coherent and Incoherent Channels*

The pump pulse applied on the ψ_1-continuum transition and the Stokes pulse applied on the ψ_2-continuum transition (the solid arrows in Fig. 38a) form a two-photon Raman transition which enables coherent population transfer between states ψ_1 and ψ_2. But the pulses also have other effects: the pump pulse applied on the ψ_2-continuum transition as well as the Stokes pulse applied on the ψ_1-continuum transition (the dashed arrows in Fig. 38a) cause irreversible ionization with rates $\Gamma_1^s(t)$ and $\Gamma_2^p(t)$. These two incoherent ionization channels turn out to be the main problem for population transfer. One of these channels may be eliminated by choosing a sufficiently small laser frequency, as for the Stokes laser in Fig. 38a, which cannot connect state ψ_1 to the continuum and hence $\Gamma_1^s = 0$. However, at least one of the incoherent channels is always present, as is $\Gamma_2^p(t)$ in Fig. 38a which prevents complete population transfer.

3. *Fano Profile*

The Fano profile emerges in a configuration similar to that in Fig. 38a, when the Stokes laser is strong (dressing laser) and its frequency is held fixed, while the pump laser is weak (probe laser) and its frequency is scanned across the two-photon resonance region. When plotted as a function of the probe-laser frequency ω,

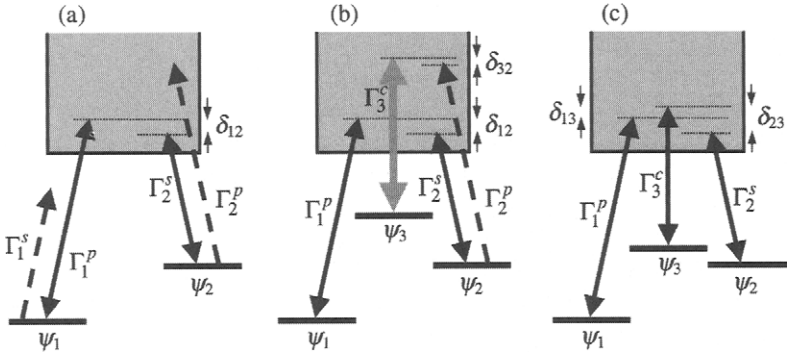

FIG. 38. Linkage patterns for bound states ψ_1 and ψ_2 coupled via a common continuum. (a) Two bound states coupled via a continuum. The solid arrow depict the ionization channels induced by the pump and Stokes lasers that form a Raman-type linkage. The dashed arrows show the irreversible (incoherent) ionization channels. (b) Same as (a) but with a third, compensatory laser (thick gray arrow), embedding a third auxiliary state ψ_3 and used to suppress incoherent ionization from state ψ_2 by a Fano-type resonance. (c) Three bound states coupled via a continuum (tripod-continuum scheme).

the photoionization probability $P_i(x)$ exhibits an asymmetric dependence—the famous Fano profile. It is described by (Fano, 1961; Fano and Cooper, 1968) as

$$P_i(x) = P_i^b + P_i^a \frac{(x+q)^2}{x^2+1} \tag{93}$$

where P_i^b is a background ionization, P_i^a is a scaling parameter for the resonance, and the dimensionless variable $x = (\omega - \omega_0)/\Gamma$ is the detuning from the resonance frequency ω_0 of the probe frequency ω in units of the ionization width Γ. As Eq. (93) shows, the Fano parameter q establishes the profile of the resonance. When $q = 0$, the photo ionization cross section is a symmetric, inverted-bell-shaped function of x and has a minimum at $x = 0$, i.e., at $\omega = \omega_0$, a frequency at which there is destructive interference between two photo ionization channels. For nonzero q, the Fano profile (93) is asymmetric, with a minimum $P_i^{\min} = P_i^b$ at $x = -q$, and maximum $P_i^{\max} = P_i^b + P_i^a(1+q^2)$ at $x = 1/q$. Far from resonance, we have $P_i^\infty = P_i^b + P_i^a$. The Fano parameter q can be determined from experimental data by measuring the values of the ionization cross section at its minimum, its maximum, and far from resonance and taking the ratio

$$\frac{P_i^{\max} - P_i^{\min}}{P_i^\infty - P_i^{\min}} = 1 + q^2.$$

Alternatively, one can measure the distance between the minimum and the maximum, which is $q + 1/q$.

At the trapping frequency $\omega_{\text{trap}} = \omega_0 - q\Gamma$, the ionization is suppressed. In the absence of background, $P_i^b = 0$, the ionization probability there is zero, $P_i = 0$, and the material will be completely transparent.

Equation (93) is derived using perturbation theory and assuming strong dressing (Stokes) laser and weak probe (pump) laser, and that both lasers have constant amplitudes. When the probe laser gets stronger, the distinction between dressing and probing becomes inaccurate because the probe field itself begins to affect the continuum. Also, when the two laser fields are pulse shaped, the Fano formula (93) becomes inaccurate. A detailed theoretical and experimental study of the behavior of LICS for pulsed lasers, both for coincident and delayed pulses, has been carried out by Halfmann *et al.* (1998), Yatsenko *et al.* (1999a) and Kylstra *et al.* (1998). Figure 39 shows a typical LICS profile, observed experimentally in metastable helium.

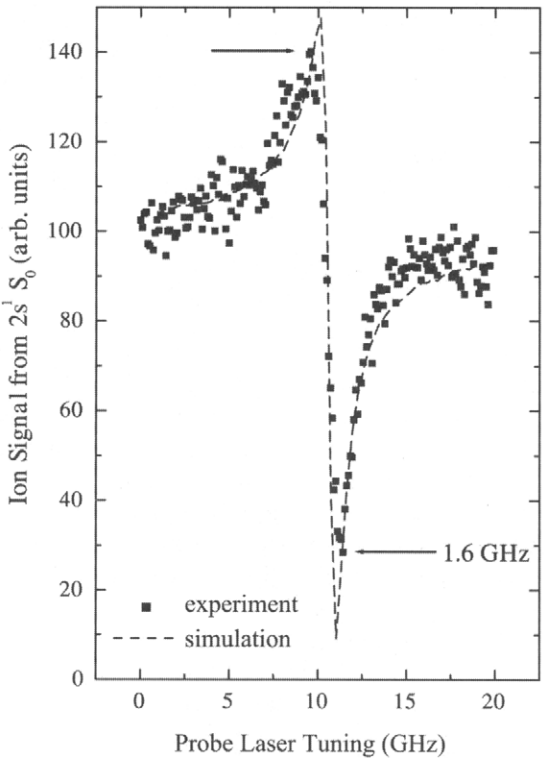

FIG. 39. Observation of laser-induced continuum structure in helium. The observed (almost 70%) reduction in the far-off-resonance ionization signal results from the coherence of the interaction. (From T. Halfmann, L. P. Yatsenko, M. Shapiro, B. W. Shore, and K. Bergmann. Population trapping and laser-induced continuum structure in helium: Experiment and theory. *Phys. Rev. A* 1998;58:R46–R49.)

4. Population Trapping: Dark and Bright States

Coherent excitation in a Raman configuration—with a continuum as well as with a discrete intermediate state—leads to the phenomenon of population trapping. Population trapping occurs when the imaginary part of one of the eigenvalues of the Hamiltonian vanishes; then the corresponding eigenstate is not coupled to the continuum—it is a nondecaying (trapped, dark) state. The trapping condition reads (Knight *et al.*, 1990)

$$\delta_0 = \tfrac{1}{2}q\left[\Gamma_1^p(t) - \Gamma_2^s(t)\right] + S_1(t) - S_2(t). \tag{94}$$

Population trapping is most easily revealed in the basis of the dark and bright states, which are defined as

$$\Phi_d(t) = \psi_1 \cos\vartheta(t) - \psi_2 \sin\vartheta(t), \tag{95a}$$

$$\Phi_b(t) = \psi_1 \sin\vartheta(t) + \psi_2 \cos\vartheta(t), \tag{95b}$$

with

$$\tan\vartheta(t) = \sqrt{\frac{\Gamma_1^p(t)}{\Gamma_2^s(t)}}. \tag{96}$$

The reason for the names "bright" and "dark" is that, as follows from Eq. (91), the total ionization rate is

$$\frac{d}{dt}P_i = \Gamma_1^s P_1 + \Gamma_2^p P_2 + \sqrt{\Gamma_1^p + \Gamma_2^s}\,P_b. \tag{97}$$

Hence, in the absence of incoherent ionization ($\Gamma_1^s = \Gamma_2^p = 0$), the rate of change of the ionized population is proportional to the population in the bright state $\Phi_b(t)$. Therefore only the population in the bright state is exposed to ionization, whereas the ionization cannot occur from the dark state. If transitions between the dark and bright states are negligible, the population residing initially in the dark state remains trapped there. For constant laser field amplitudes (then the coupling between the dark and bright states vanishes), with the system starting in state ψ_1, the trapped population is

$$P_1 + P_2 = P_d = \frac{\Gamma_2^s}{\Gamma_1^p + \Gamma_2^s}.$$

Hence, for $\Gamma_1^p \ll \Gamma_2^s$, i.e., strong Stokes (dressing) laser and weak pump (probe) laser, almost all population is trapped, provided the trapping condition (94) is

satisfied. For $\Gamma_1^p = \Gamma_2^s$, half of the population is trapped, and for $\Gamma_1^p \gg \Gamma_2^s$, the entire population can be ionized.

For pulsed lasers, there is some time-dependent nonzero coupling between the dark and bright states. However, if the evolution can be made adiabatic, this coupling can be reduced to negligible values. In this case, while the population of the dark state Φ_d remains nearly constant, its composition changes in time and the populations of the bare states ψ_1 and ψ_2 change accordingly; this ultimately enables population transfer between them.

When the trapping condition (94) is satisfied and when incoherent ionization is negligible, the dark and bright states are adiabatic states, i.e., eigenstates of the Hamiltonian in Eq. (91). When the trapping condition is not satisfied, the dark and bright states are no longer adiabatic states, i.e., adiabatic evolution does not guarantee staying in the dark state. Then the equations for the amplitudes of the dark and bright states $\mathbf{B} = [B_d, B_b]^T$ read

$$\hbar \frac{d}{dt}\mathbf{B} = -i\mathsf{H}_b\mathbf{B}$$

where

$$\mathsf{H}_b = \hbar \begin{bmatrix} D\sin^2\vartheta & -\frac{1}{2}D\sin 2\vartheta - i\dot{\vartheta} \\ -\frac{1}{2}D\sin 2\vartheta + i\dot{\vartheta} & D\cos^2\vartheta - \frac{1}{2}(q+i)\left(\Gamma_1^p + \Gamma_2^s\right) \end{bmatrix},$$

and

$$D(t) = \delta + S_2(t) - S_1(t) - \tfrac{1}{2}q\left[\Gamma_1^p(t) - \Gamma_2^s(t)\right]$$

is the deviation from the trapping condition. Here $\dot{\vartheta}$ is the usual nonadiabatic coupling, which can be overcome by making the evolution sufficiently adiabatic. However, the deviation D from the trapping condition introduces an additional coupling between the dark and bright states, which does not vanish in the adiabatic limit and which drives some population from the dark state into the bright state, where it is subjected to ionization.

B. Population Transfer via a Continuum

1. Population Transfer in the Ideal Case

Let us assume that the trapping condition (94) is satisfied exactly, i.e., $D = 0$, and that there is no incoherent ionization, $\Gamma_1^s = \Gamma_2^p = 0$. Then, if the evolution is made adiabatic, the transitions between the dark and bright states will be suppressed completely.

If, as in STIRAP, the Stokes pulse precedes the pump, then the mixing angle $\vartheta(t)$ will change from $\vartheta = 0$ initially to $\vartheta = \pi/2$ at the end; hence the dark state

$\Phi_d(t)$ will coincide with the initial state ψ_1 before the interaction and with state $-\psi_2$ after it, i.e., $\psi_1 \xleftarrow{-\infty} \Phi_d(t) \xrightarrow{+\infty} -\psi_2$. Therefore complete population transfer is possible (in principle) if the evolution is adiabatic, if the trapping condition (94) is maintained, and if there is no incoherent ionization; then no population is lost from the dark state.

In contrast, if the pump pulse precedes the Stokes, then $\vartheta = \pi/2$ initially and $\vartheta = 0$ at the end; hence now the bright state Φ_b coincides with the initial state ψ_1 before the interaction and with state ψ_2 after it, $\psi_1 \xleftarrow{-\infty} \Phi_b(t) \xrightarrow{+\infty} \psi_2$. In this case, adiabatic evolution leads to maximal ionization, rather than to population transfer to state ψ_2, because no population resides in the dark state and thus all population is exposed to ionization.

In reality, neither the trapping condition (94) can be satisfied exactly for pulsed excitation, nor can incoherent ionization be eliminated completely. As a result, complete population transfer is ruled out. Various authors have proposed, however, schemes that reduce the negative effects of the deviation from the trapping condition and the incoherent ionization; we summarize them below.

2. *Satisfying the Trapping Condition*

If $q = 0$ and there are no Stark shifts, the trapping condition (94) is satisfied on two-photon resonance, $\delta = 0$. For $q \neq 0$ and for nonzero Stark shifts, which is the case in real atoms, the trapping condition (94) becomes time dependent in the general case of time-dependent ionization rates, as for pulse-shaped laser fields. For delayed pump and Stokes pulses, the trapping condition can be satisfied exactly only if the detuning δ is made time dependent and matches exactly the time dependence of the RHS of Eq. (94). This can be achieved, at least in principle, by using chirped laser pulses with a carefully tailored time-dependent frequency (chirp) (Paspalakis *et al.,* 1997; Vitanov and Stenholm, 1997c). Another possibility to enforce the trapping condition on the effective detuning is to make use of controlled Stark shifts induced by a pair of auxiliary far-off-resonant laser pulses with suitable intensities (whose frequencies are small enough not to influence the system otherwise) (Carroll and Hioe, 1995; Yatsenko *et al.,* 1997), which show up as additional time-dependent terms in the two-photon detuning δ.

If the trapping condition (94) is not satisfied exactly, the nonzero D-coupling causes transitions from the dark state to the bright state with subsequent ionization losses. These losses can be reduced by suitably tuning the laser frequencies slightly off two-photon resonance (i.e., for nonzero detuning δ) to a value that minimizes D. We also point out that it is easier to fulfill the trapping condition (94) approximately when the Fano parameter q is small; then the Γ terms have a less detrimental effect.

3. Suppressing Incoherent Ionization

The main difficulty in achieving efficient population transfer is related to the incoherent ionization channels (Yatsenko *et al.*, 1997; Vitanov and Stenholm, 1997c), of which at least one is always present; these lead to inevitable irreversible population losses. It has been suggested (Carroll and Hioe, 1996; Yatsenko *et al.*, 1997) that these losses can be reduced (although not eliminated) by choosing an appropriate region in the continuum where the incoherent-ionization probability is minimal.

Unanyan *et al.* (1998b) have proposed another approach to suppress incoherent ionization from state ψ_2. It makes use of a Fano-type resonance induced by an additional, strong compensatory laser which embeds a third, highly lying bound state ψ_3 into the region in the continuum where the incoherent ionization takes place. This laser, depicted by a thick gray arrow in Fig. 38b, forms with the incoherent channel Γ_2^p a nearly resonant Raman transition between states ψ_2 and ψ_3. It is assumed that the compensatory laser does not affect the system otherwise and, particularly, that its frequency is small enough so that it cannot ionize states ψ_1 and ψ_2 directly, i.e., $\Gamma_1^c \approx \Gamma_2^c \approx 0$. Also, if state ψ_3 is close enough to the ionization threshold, ionization from ψ_3 by the pump and Stokes lasers can be ignored because these lasers point deeply into the continuum where the probability for ionization is small ($\Gamma_3^p \approx \Gamma_3^s \approx 0$). The Hamiltonian describing the interaction between the bound states reads

$$\mathsf{H} = \frac{\hbar}{2}\begin{bmatrix} 2\Delta_{12} - i\Gamma_1^p & -\sqrt{\Gamma_1^p\Gamma_2^s}(q_{12}+i) & 0 \\ -\sqrt{\Gamma_1^p\Gamma_2^s}(q_{12}+i) & -i\Gamma_2^s - i\Gamma_2^p & -\sqrt{\Gamma_2^p\Gamma_3^c}(q_{23}+i) \\ 0 & -\sqrt{\Gamma_2^p\Gamma_3^c}(q_{23}+i) & 2\Delta_{32} - i\Gamma_3^c \end{bmatrix},$$

where $\Delta_{12}(t) = \delta_{12} + S_1(t) - S_2(t)$ and $\Delta_{32}(t) = \delta_{32} + S_3(t) - S_2(t)$, with δ_{12} and δ_{32} being the static detunings for the $\psi_1 \leftrightarrow \psi_2$ and $\psi_2 \leftrightarrow \psi_3$ transitions, respectively. Here q_{jk} is the Fano parameter characterizing the two-photon transition between states ψ_j and ψ_k, while $\Gamma_k(t)$ and $S_k(t)$ are the total ionization rate and the total Stark shift for state ψ_k.

The additional laser creates a new structure in the continuum in the region where the incoherent ionization from state ψ_2 takes place. The idea is to suppress the incoherent ionization channel Γ_2^p by tuning the parameters of the compensatory laser pulse near a Fano-type minimum in the ionization probability. For this to occur, the ionization width Γ_3^c should be sufficiently larger than Γ_2^p. Then $|2\Delta_{32} - i\Gamma_3^c| \gg |\sqrt{\Gamma_2^p\Gamma_3^c}(q_{23}+i)|$ and, hence, state ψ_3 can be eliminated adiabatically. The effective two-state LICS system has a new modified two-photon detuning δ

and incoherent-ionization width γ of state ψ_2,

$$\delta = \Delta_{12} + S_2 - S_1 - \tfrac{1}{2}q_{12}\left(\Gamma_1^p - \Gamma_2^s\right) - \mathrm{Re}\frac{\frac{1}{4}\Gamma_3^c\Gamma_2^p(q_{23}+i)^2}{\delta_{32} + S_3 - \frac{1}{2}i\Gamma_3^c}, \tag{98a}$$

$$\gamma = \tfrac{1}{2}\Gamma_2^p + \mathrm{Im}\frac{\frac{1}{4}\Gamma_3^c\Gamma_2^p(q_{23}+i)^2}{\delta_{32} + S_3 - \frac{1}{2}i\Gamma_3^c}. \tag{98b}$$

By appropriately choosing the parameters of the compensatory laser, one can make both γ and δ vanish; this cancellation takes place when

$$\delta_{21} = S_1 - S_2 + \tfrac{1}{2}q_{12}\left(\Gamma_1^p - \Gamma_2^s\right) - \tfrac{1}{2}q_{23}\Gamma_2^p, \tag{99a}$$

$$\delta_{32} = -S_3 - \tfrac{1}{2}q_{23}\Gamma_3^c. \tag{99b}$$

Condition (99b) ensures that the incoherent ionization is suppressed, whereas Eq. (99a) is the new trapping condition. Then, as discussed above, the efficiency of the population transfer from state ψ_1 to ψ_2 can approach unity for the counter-intuitive pulse order in the adiabatic limit.

This idea for Fano-type suppression of incoherent ionization is illustrated in Fig. 40, where the populations of the two bound states ψ_1 and ψ_2 and the ionization

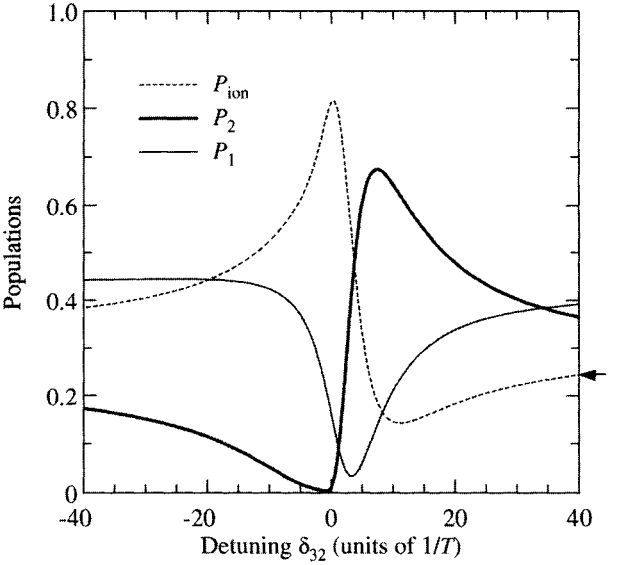

FIG. 40. Numerically calculated populations of the initial state ψ_1 and the final state ψ_2 and the ionization against the two-photon detuning δ_{32} between the target state ψ_2 and the auxiliary state ψ_3. The arrow on the RHS shows P_2 in the absence of compensatory laser. (From R. G. Unanyan, N. V. Vitanov, and S. Stenholm. Suppression of incoherent ionization in population transfer via continuum. *Phys. Rev. A* 1998;57:462–466.)

probability are plotted versus the detuning δ_{32}, i.e., versus the frequency of the compensatory laser. At a certain value of δ_{32} the population of the target state ψ_2 reaches 0.69, which is considerably higher than the value 0.26 in the absence of a compensatory laser. The P_2 curve, as well as the ionization curve, are reminiscent of the Fano profile of Fig. 39.

In Fig. 41, the target-state population P_2 is plotted versus the peak ionization rate Γ_0 of the three lasers in four cases. The transfer efficiency to state ψ_2 is lowest when there is no compensation of incoherent ionization and the trapping condition (94) is not fulfilled (curve 1). Satisfying the trapping condition alone, still without incoherent-ionization reduction, increases the transfer efficiency (curve 2). When the incoherent ionization is (partly) suppressed by a compensatory laser, without satisfying the trapping condition $\delta = 0$, the transfer efficiency increases further (curve 3). Finally, when the incoherent ionization is (partly) suppressed and the trapping condition $\delta = 0$ is satisfied, the transfer efficiency is highest and can exceed 0.8 in this example. If both the $\delta = 0$ and $\gamma = 0$ conditions were satisfied exactly, the transfer efficiency could approach unity.

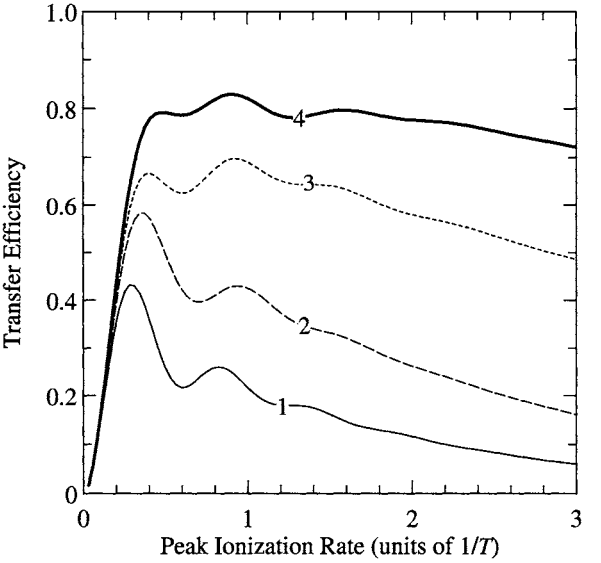

FIG. 41. Numerical calculated population of the target state ψ_2 against the peak ionization rate Γ_0 of the three lasers. The four curves correspond to the following cases: (1) no compensatory laser and $\delta_{12} = 0$; (2) the condition $\delta = 0$ is satisfied, but the condition $\gamma = 0$ is not; (3) the condition $\gamma = 0$ is satisfied approximately, but the condition $\delta = 0$ is not satisfied; (4) the condition $\delta = 0$ is satisfied exactly, and the condition $\gamma = 0$ is satisfied approximately. (From R. G. Unanyan, N. V. Vitanov, and S. Stenholm. Suppression of incoherent ionization in population transfer via continuum. *Phys. Rev. A* 1998;57:462–466.)

C. Tripod Coupling via a Continuum

Recently, the two-state LICS scheme has been extended to a tripod-continuum scheme involving three discrete states coupled to each other by two-photon processes via a common continuum (Unanyan *et al.*, 2000a). All three lasers are tuned approximately in the same region of the continuum, as shown in Fig. 38c. This scheme may also be seen as an extension of the discrete-state tripod scheme discussed in Section VII. The Hamiltonian describing the tripod-continuum system is given by

$$\mathsf{H} = \tfrac{1}{2}\begin{bmatrix} 2\Delta_{13} - i\Gamma_1 & -\sqrt{\Gamma_1\Gamma_2}(q_{12}+i) & -\sqrt{\Gamma_1\Gamma_3}(q_{13}+i) \\ -\sqrt{\Gamma_1\Gamma_2}(q_{12}+i) & 2\Delta_{23} - i\Gamma_2 & -\sqrt{\Gamma_2\Gamma_3}(q_{23}+i) \\ -\sqrt{\Gamma_1\Gamma_3}(q_{13}+i) & -\sqrt{\Gamma_2\Gamma_3}(q_{23}+i) & -i\Gamma_3 \end{bmatrix},$$

where $\Delta_{13}(t) = \delta_{13} + S_1(t) - S_3(t)$ and $\Delta_{23}(t) = \delta_{23} + S_2(t) - S_3(t)$, with δ_{13} and δ_{23} being the static detunings for the $\psi_1 \leftrightarrow \psi_3$ and $\psi_2 \leftrightarrow \psi_3$ transitions, respectively, q_{jk} are the Fano parameters, and $\Gamma_k(t)$ and $S_k(t)$ are the total ionization rate and the total Stark shift for state ψ_k.

Unlike the two-state Raman coupling via a continuum, there are two trapping conditions for the tripod-continuum system (Unanyan 2000a),

$$\Delta_{13}(t) = \tfrac{1}{2}q_{13}[\Gamma_3(t) - \Gamma_1(t)] + \tfrac{1}{2}(q_{12} - q_{23})\Gamma_2(t), \tag{100a}$$

$$\Delta_{23}(t) = \tfrac{1}{2}q_{23}[\Gamma_3(t) - \Gamma_2(t)] + \tfrac{1}{2}(q_{12} - q_{13})\Gamma_2(t). \tag{100b}$$

If these conditions are satisfied, there are two dark states, as for the discrete-state tripod system (Section VII). Likewise, the presence of two dark states provides greater flexibility in performing coherent population transfer between the bound states, compared to the two-state scheme. Moreover, for large and constant Γ_2, the trapping conditions (100) can be satisfied approximately at the (constant) detunings $\Delta_{13} = \frac{1}{2}(q_{12} - q_{23})\Gamma_2$ and $\Delta_{23} = \frac{1}{2}(q_{12} - q_{13})\Gamma_2$; hence, it may be easier to satisfy the two trapping conditions (100) for the tripod-continuum system than the single-trapping condition (94) in the two-state-via-continuum scheme.

In the case when one of the discrete states is strongly coupled to the continuum, for example ψ_3, it can be eliminated adiabatically. Then the population dynamics reduces to an effective two-state LICS problem, involving the other two states ψ_1 and ψ_2, described by Eqs. (91), but with modified parameters. In particular, the effective Fano parameter is (Unanyan, 2000a)

$$q = \frac{q_{12} - q_{13} - q_{23}}{q_{13}q_{23}}. \tag{101}$$

Thus, using an auxiliary third laser embedding a third state into the continuum provides the possibility to customize the parameters of a given two-state LICS system.

IX. Extensions and Applications of STIRAP

A. Control of Chemical Reactions

The remarkable properties of STIRAP have already had applications in many diverse areas. The first implementation of STIRAP has been in a crossed-beam reactive scattering experiment (Dittmann *et al.*, 1992). It allowed investigation of the effect of vibrational excitation on the cross section for the chemiluminescent channel in the process $Na_2(v) + Cl \rightarrow NaCl + Na^*$ in crossed particle beams. It was found that the cross sections increased by about 0.75% per vibrational level in the range $3 \simeq v \simeq 19$.

Another example is the detailed study of the reaction $Na_2(v'', j'') + H \rightarrow NaH(v', j') + Na$, where the angular distribution and the population distribution have been determined for the product molecule NaH for a range of selectively populated levels v'' of the reagent molecule Na_2 (Pesl, 1999). STIRAP has been used also to investigate the dependence of the dissociative attachment process $Na_2(v'', j'') + e^- \rightarrow Na + Na^-$ (with electron energies <1 eV) on the vibrational excitation by exciting efficiently and very selectively the Na_2 molecules to a specific vibrationally excited level (Külz *et al.*, 1993, 1995, 1996; Ekers *et al.*, 1999a,b; Keil *et al.*, 1999; Kaufmann *et al.*, 2001). The vibrational excitation to $v'' = 12$ has increased the state-dependent dissociative attachment rate by more than three orders of magnitude.

B. Hyper-Raman STIRAP (STIHRAP)

The application of standard STIRAP to molecules, using two single-photon transitions (pump and Stokes), is often impeded by the fact that most molecules require ultraviolet or even vacuum ultraviolet (VUV) pump photons to reach the first electronically excited states. For the Stokes pulse, which connects the excited electronic state to a high vibrational level of the ground electronic state, optical wavelengths are usually sufficient. It is difficult to provide VUV pulses with adequate power and coherence properties. It is natural to consider achieving the pump excitation (and possibly also the Stokes excitation) by a two-photon transition. The corresponding $(2 + 1)$ and $(2 + 2)$ versions of STIRAP have been named hyper-Raman STIRAP (Yatsenko *et al.*, 1998; Guérin and Jauslin, 1998; Guérin *et al.*, 1998, 1999). Although these extensions seem obvious, they turn out to be nontrivial.

The main obstacle in hyper-Raman STIRAP are the dynamic Stark shifts induced by the two-photon coupling. These Stark shifts, which are proportional to the

laser intensities, modify the Bohr frequencies of the pump and Stokes transitions and destroy the multiphoton resonance between the initial and final states, which is crucial for the existence of the dark state. It has been found, both numerically and analytically, that high transfer efficiency in such a scheme can still be achieved by a suitable choice of static detunings of the carrier frequencies of the two pulses, which suppress the detrimental effect of the Stark shifts; these detuning ranges have been estimated analytically (Guérin *et al.,* 1998). It is interesting to note that, unlike the purely adiabatic evolution in STIRAP, successful population transfer in hyper-Raman STIRAP occurs as a result of a combination of adiabatic and diabatic time evolution, as in SCRAP (see below). Moreover, unlike STIRAP, the intermediate state does acquire some transient population; again, it can be reduced by suitable static detunings.

It should be pointed out that the Stark shifts are also nonzero in traditional STIRAP, but they are usually negligible compared to the one-photon on-resonance couplings (given by the Autler–Townes splittings). In (2 + 1) STIRAP the fundamental field (ω_p) is very strong and the related Stark shift is usually not small compared to the two-photon coupling ($2\omega_p$).

C. Stark-Chirped Rapid Adiabatic Passage

An interesting alternative of STIHRAP for electronic excitation of molecules is the technique of Stark-chirped rapid adiabatic passage (SCRAP), introduced (Yatsenko *et al.,* 1999b) and demonstrated (Rickes *et al.,* 2000) recently for two-state systems. Like STIRAP, it makes use of two delayed and partially overlapping laser pulses, but unlike STIRAP, here one of the pulses is far off resonance and its objective is to induce dynamic Stark shifts in the coupled levels. This time-dependent Stark shift, combined with an appropriate detuning and a time delay of the pump laser, leads to an effective level crossing and adiabatic population transfer between the two states of the pump transition.

Using laser-induced Stark shifts to modify the transition frequency appears the easiest method to induce a level-crossing transition with laser pulses of nanosecond duration. Techniques for producing frequency-swept pulses are not well developed for nanosecond pulses. Nanosecond laser systems are used for many applications because they provide a very good combination of sufficiently high intensity (and hence large interaction strength) as well as long interaction time. The successful implementation of adiabatic evolution of laser–matter interaction relies on a combination of both parameters. Laser frequency chirping by active phase modulation, although possible in principle, is difficult for nanosecond laser pulses because it requires driving modulators at gigahertz frequencies. On the other hand, the spectral bandwidth of nanosecond pulses is too small for successful application of the techniques based on spatial dispersion that are well developed for femtosecond pulses.

1. Theory

Figure 42 illustrates the idea of SCRAP. One of the pulses—the pump pulse—is slightly detuned off resonance with the transition frequency and moderately strong; it serves to drive the population from the ground to the excited state. The other pulse—the Stark pulse—is far off resonant and strong; it is used merely to modify the atomic transition frequency by inducing Stark shifts in the energies of the two states. Because the Stark shifts $S_1(t)$ and $S_2(t)$ of the ground and excited states are generally different (usually $|S_2(t)| \gg |S_1(t)|$) and each of them is proportional to the intensity of the Stark pulse, the transition frequency will experience a net Stark shift $S(t) = S_2(t) - S_1(t)$.

By choosing an appropriate detuning for the pump pulse, it is always possible to create two diabatic level crossings in the wings of the Stark pulse: one crossing

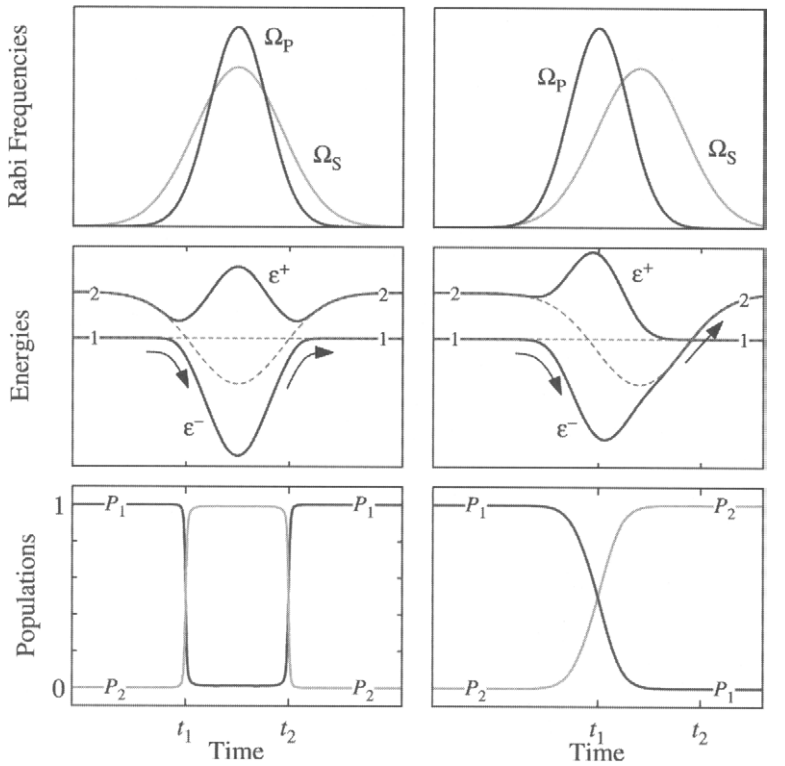

FIG. 42. Time evolution of the Rabi frequencies (top frames), the level energies (middle frames), and the populations (bottom frames) in a two-state system driven by a pump pulse Ω_p and a Stark-shifting pulse Ω_s. Left-hand frames: simultaneous pump and Stark pulses. Right-hand frames: pump pulse before Stark pulse (SCRAP method).

during the growth and another during the decline of the Stark pulse. For successful population transfer, the evolution must be adiabatic at one, and only one, of these crossings. This asymmetry can only occur if the pump and Stark pulses are not applied simultaneously. Rather, the pump pulse must be strong at one and only one of the crossings.

It proves appropriate to set the time delay between the two pulses so that the maximum of the pump pulse occurs at one of the crossings in order to optimize the adiabatic passage there. It is also appropriate that the pump pulse width be smaller than both the Stark pulse width and the delay between the pulses, in order to suppress adiabatic passage at the other crossing. In this adiabatic–diabatic scenario the system will follow the path shown in the middle right frame in Fig. 42: the state vector will adiabatically follow the lower adiabatic state through the first crossing, while during the second crossing it will follow the diabatic state ψ_2 (rather than an adiabatic state) and remain there till the end of the interaction. The net result is complete population transfer from state ψ_1 to state ψ_2. It should be appreciated that the adiabatic and diabatic intervals can occur in either ordering: the pump pulse may either precede or follow the Stark pulse.

The SCRAP technique resembles the early experiment by Loy (1974), who used adiabatic quasistatic pulses of about 5 ms duration to induce Stark shifts. However, he induced two sequential population transfers per pulse—excitation for the leading edge and deexcitation for the trailing edge of each pulse as in the left column of Fig. 42—resulting in no net population transfer. In contrast, the time delay between the pump and Stark pulses in SCRAP ensures that population transfer takes place at just one of the crossings, thus leading to overall population transfer.

It should be obvious from the above description that complete population transfer will only occur within finite ranges of values of the various interaction parameters. For example, in order that there be level crossings, the static detuning Δ_0 must be smaller than the maximum Stark shift S_0 and must have the same sign as S_0. Also, the pump pulse should be strong enough to ensure adiabatic passage at one of the crossings, but weak enough to prevent adiabatic passage at the other. For Gaussian pulse shapes, $\Omega(t) = \Omega_0 \exp(-t^2/T_p^2)$ and $S(t) = S_0 \exp[-(t-\tau)^2/T_s^2]$, the latter requirements lead to the conditions (Rickes *et al.*, 2000)

$$1 \ll \frac{(\Omega_0 T_s)^2}{\Delta_0 \tau} \ll \exp\left(\frac{8\tau^2}{T_p^2}\right). \tag{102}$$

These conditions set upper and lower limits on the peak pump Rabi frequency Ω_0 and the static detuning Δ_0.

The SCRAP technique benefits from the fact that strong fixed-frequency long-wavelength pulsed laser radiation, suitable for Stark-shifting the levels, is often available because it is used to generate (by frequency conversion) the visible or

ultraviolet radiation needed for the pump interaction. Moreover, its pulse width is longer than the pump pulse width, which is beneficial for SCRAP.

As with simple adiabatic passage, the SCRAP technique can produce population transfer in an ensemble of atoms having a distribution of Doppler shifts. The peak value of the Stark shift sets the maximum detuning that can be accessed; in turn, this sets the range of Doppler shifts for which population transfer can be produced.

2. *Experimental Demonstration*

The first experimental demonstration of SCRAP was achieved in metastable helium (Rickes *et al.*, 2000). The initial state $1s2s\,^3S_1$ was coupled to the target state $1s2s\,^3S_1$ by a two-photon transition induced by a 855-nm pump laser pulse with a pulse duration of 3 ns (half-width at 1/e of intensity), as shown in Fig. 43 (left). The Stark shift was induced by a 1064-nm laser pulse with a pulse duration of 4.6 ns, delayed by 7 ns with respect to the pump pulse. Both laser pulses were mildly focused into the atomic beam. Nearly complete population transfer was observed with typical intensities of 20–30 MW/cm^2 for the pump pulse and 200–500 MW/cm^2 for the Stark pulse.

As an example, Fig. 43 (right) displays the transfer efficiency plotted versus the static two-photon detuning $\Delta_0 = \omega_{12} - 2\omega_p$. Nearly complete population transfer was observed within a certain detuning range, as predicted by analytical estimates. For large positive detuning, the adiabatic condition at the first crossing is violated and the transfer efficiency decreases. For small positive detunings (near $\Delta_0 = 0$),

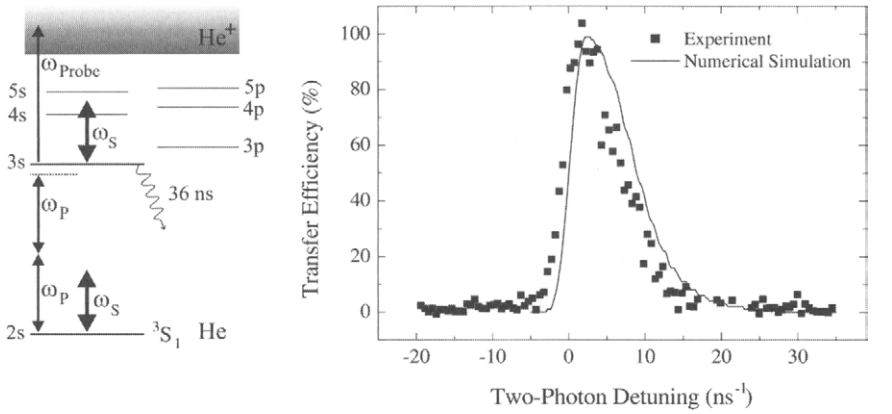

FIG. 43. Left-hand plot: simplified energy-level diagram of helium atom used in the demonstration of SCRAP. Right-hand plot: population transfer efficiency versus the static two-photon detuning Δ_0. (From T. Rickes, L. P. Yatsenko, S. Steuerwald, T. Halfmann, B. W. Shore, N. V. Vitanov, and K. Bergmann. Efficient adiabatic population transfer by two-photon excitation assisted by a laser-induced Stark shift. *J. Chem. Phys.* 2000;113:534–546.)

the diabatic condition at the second crossing is violated and the transfer efficiency decreases. For $\Delta_0 < 0$ and for very large positive Δ_0, there are no level crossings at all and little population is transferred to the excited state.

An interesting extension of SCRAP—potentially very important for molecules—is the application of two sequential SCRAP processes. For example, the first SCRAP can transfer the population from the electronic ground state to an electronically excited state via a two-photon excitation. The second SCRAP then transfers the population to a target state in the electronic ground state, e.g., a highly vibrationally excited state. The second step can take place via a one-photon process [(2 + 1) SCRAP] or by a two-photon process [(2 + 2) SCRAP]. It is easily seen that only one Stark-shifting laser is needed in the (2 + 1) SCRAP scheme. The (2 + 2) SCRAP can be realized even without a separate Stark pulse because the Stokes pulse can induce Stark shifts for the pump transition, and the pump pulse can induce the Stark shift for the Stokes transition (Rickes *et al.*, 2000).

D. Adiabatic Passage by Light-Induced Potentials (APLIP)

Recently, Garraway and Suominen (1998) (see also Kalush and Band, 2000, and Sola *et al.*, 2000) have suggested, on the basis of numerical calculations for sodium dimers, that the STIRAP ideas of counterintuitively ordered laser pulses and adiabatic evolution can be applied to the transfer of a wave packet from one molecular potential to the displaced ground vibrational state of another. This process—termed adiabatic passage by light-induced potentials (APLIP)—seemingly violates the Frank–Condon principle because the overlap between the initial and final wavefunctions is very small (the two wave packets were displaced at a distance seven times larger than their widths). There is, however, no such violation because the time scale of the process is close to, but longer than, the vibrational time scale. APLIP shares many features with STIRAP, such as high efficiency and insensitivity to pulse parameters. However, in contrast to STIRAP, the two-photon resonance condition in APLIP cannot be satisfied (except at a certain time), and the main mechanism for the transfer of the wave packet is through a "valley" which emerges in the time-dependence of the light-induced potential, as shown in Fig. 44 (left). Figure 44 (right) shows how the wave packet gradually disappears from the ground-state potential (lower plot) and appears in the excited-state one (upper plot). While the original proposal assumed transitions between the lowest vibrational states ($v = v' = v'' = 0$), recent calculations (Rodriguez *et al.*, 2000) extended APLIP to excited vibrational states.

E. Photoassociative STIRAP as a Source for Cold Molecules

With the experimental realization of Bose–Einstein condensation of weakly interacting atoms, the physics of cold gases has become a topic of increasing interest. While the formation of condensates of atomic gases is by now an established

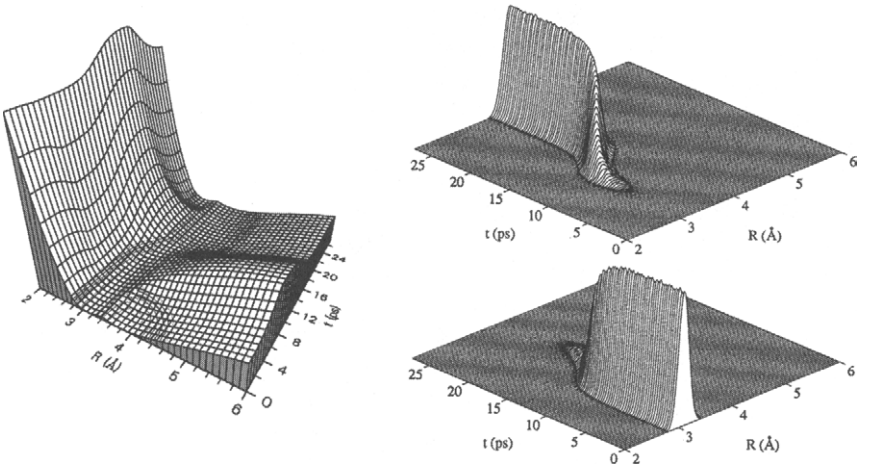

FIG. 44. Left: APLIP potential. The population flows through the "valley" in this potential. Right: time evolution of the ground-state (lower plot) and excited-state (upper plot) populations. (Reprinted with permission from B. M. Garraway and K.-A. Suominen. Adiabatic passage by light-induced potentials in molecules. *Phys. Rev. Lett.* 1998;80:932–935.)

technique in many laboratories, the generation of the molecular counterpart is still an open problem. Standard cooling techniques cannot be applied to molecules due to the lack of closed two-level transitions and the many rovibrational degrees of freedom. Instead, it has been suggested to produce molecular condensates by photoassociation of a condensate of atoms. An essential limitation of this process, however, is the fast stimulated dissociation of the molecular condensate into atoms in noncondensate states (Goral *et al.,* 2000). Due to their state selectivity and directionality, adiabatic transfer techniques such as STIRAP may be used to overcome this problem of "rogue dissociation." Numerical simulations based on a two-mode model, which does not include rogue dissociation, have shown that STIRAP can be used to induce coherent two-color photoassociation of an atomic Bose–Einstein condensate in free–bound–bound transitions and convert it to a molecular on short time scales (Javanainen and Mackie, 1998, 1999; Mackie and Javanainen 1999; Mackie *et al.,* 2000). It was predicted that Bose stimulation can enhance the atomic free–bound dipole matrix element to the extent enabling photoassociative STIRAP.

X. Propagation Phenomena

The preceding sections of this chapter all treated the dynamics of atoms exposed to prescribed fields, emphasizing the transfer of population. As noted in Section II.B, populations $P_n(t)$ can be regarded as the diagonal elements of a density matrix. The

off-diagonal elements describe another important property of coherent excitation, the induced dipole moments. The density of dipole moments, whether intrinsic or induced, provides the polarization field **P** for use in the Maxwell equations for the fields (cf. Shore, 1990; chap. 12). More specifically, the acceleration (second time derivative) of the dipole moments contributes to the radiation field. As a pulse of radiation passes by an atom, it induces a dipole moment that modifies the original field, and subsequent atoms along the propagation path will experience this modified field. In this section we discuss some aspects of a self-consistent treatment of atoms responding to a pulsed field, and traveling waves being modified by such atomic response.

The importance of the induced polarization field depends on the number density of atoms, $\mathcal{N}$, the length of the propagation path (measured as the product of the absorption coefficient and the physical distance), and on the strength of the induced dipole moment. For a two-state atom the quantity relevant for coherent propagation modification is the expectation value of instantaneous dipole moment $d_{12}C_1(t)C_2(t)^*$, where d_{ij} is the transition dipole moment. This same quantity alters the pump field in a Raman process; the Stokes field is affected by $d_{23}C_2(t)C_3(t)^*$. (These expressions provide slowly varying dipole moments, for use with the RWA and carrier frequency ω.)

When the atomic density is low and the path length is short, one can disregard any action of the atoms on the field. But Raman adiabatic passage has some very interesting effects for beam propagation. For example, STIRAP can be employed to make an otherwise optically thick ensemble of three-level atoms transparent to a pair of pump and Stokes pulses. This phenomenon, called *electromagnetically induced transparency* (EIT) (Boller *et al.,* 1991; Harris, 1997; Marangos, 1998), has a number of important applications ranging from communication to laser design and nonlinear optical processes (Harris *et al.,* 1990). EIT does not require careful control of pulse shapes or areas. Therefore it is qualitatively different from self-induced transparency and other soliton-like phenomena (cf. Allen and Eberly, 1975), which will not be discussed here.

A. Electromagnetically Induced Transparency (EIT)

1. Complete Decoupling of Light and Matter

As is customary when simplifying the description of propagation effects, we consider an infinite medium through which pass pulses of radiation that travel in the z direction and that are uniform in the transverse x, y plane. We assume that the atoms are distributed uniformly, and that their properties are described by a state vector $\Psi(z, t)$ and probability amplitudes $C_n(z, t)$. For further simplicity we assume that the atoms are stationary (i.e., no Doppler shifts) and that both the pump and the Stokes carriers are resonant with their respective Bohr frequencies. This assumption allows us to remove from each field a rapidly varying carrier exp $(ik_jz - \omega_jt)$

and to treat the probability amplitudes and the Rabi frequencies $\Omega_j(z, t)$ as slowly varying functions of the coordinates z and t (cf. Shore, 1990, sect. 12.4). The resonance assumption permits us to choose the Rabi frequencies to be real valued; in general, it is not possible to separate phase and amplitude so clearly.

The evolution of the atoms is described by the three-state Schrödinger equation for the amplitudes $C_n(z, t)$, $n = 1, 2, 3$. The needed RWA Hamiltonian is given by Eq. (40), with $\Delta_p = \Delta_s = 0$. Because the decay of the polarization plays an important role for the propagation of the fields, even if it is negligible for each individual atom, a decay out of the excited state ψ_2 with rate Γ is included. This can be done by adding in Eq. (40) an imaginary term $i\hbar\Gamma/2$ to the energy of the excited state. The propagation of the slowly varying Rabi-frequencies is described by one-dimensional first-order wave equations,

$$\left(\frac{\partial}{\partial z} + \frac{1}{c}\frac{\partial}{\partial t}\right)\Omega_p(z, t) = i\frac{\alpha_p}{2}\Gamma C_2(z, t)C_1^*(z, t), \tag{103}$$

$$\left(\frac{\partial}{\partial z} + \frac{1}{c}\frac{\partial}{\partial t}\right)\Omega_s(z, t) = i\frac{\alpha_s}{2}\Gamma C_2(z, t)C_3^*(z, t), \tag{104}$$

where the effect of the atoms on the fields is parameterized by the resonant absorption coefficients

$$\alpha_p = \frac{\omega_p \mathcal{N}|d_{12}|^2}{2\epsilon_0 c\hbar\Gamma}, \qquad \alpha_s = \frac{\omega_s \mathcal{N}|d_{32}|^2}{2\epsilon_0 c\hbar\Gamma}. \tag{105}$$

An important property of the adiabatic dark state of the atomic system is the absence of a dipole moment for either of the two transition $C_2C_1^* = C_2C_3^* = 0$. Atoms in that state therefore have no effect on the fields, i.e., light and matter are exactly decoupled. Typically, all atoms are initially in the ground state rather than in the dark state. The question is how to transfer atoms from the ground state into the dark state. This is best done by adiabatic passage. If all atoms start in the ground state ψ_1, approximate decoupling of the pulses requires (1) the instantaneous dark state be connected asymptotically to ψ_1, and (2) deviations from the dark state are small.

The first requirement can be fulfilled by a counterintuitive pulse ordering. The second condition is more involved. Satisfying the adiabaticity criterion of Section IV is not sufficient, because the fields interact with many atoms during propagation. The range of validity of the approximation can be estimated by considering the atomic eigenstates in lowest order of nonadiabatic corrections (cf. Section III.A.8).

$$|C_2| \sim \left|\frac{1}{\Omega T}\right|, \qquad |C_1| \sim \frac{\Omega_s}{\Omega}, \qquad |C_3| \sim \frac{\Omega_p}{\Omega}, \tag{106}$$

where $\Omega = \sqrt{\Omega_p^2 + \Omega_s^2}$. Although $\Omega T \gg 1$ is a sufficient condition to allow neglect of nonadiabatic corrections for individual atoms, one recognizes, by integrating the field equations (103) and (104) in steady state, that laser pulses propagate freely over a distance L only if

$$\frac{\Omega^2 T}{\Gamma} \gg \alpha_S L \tan\vartheta \qquad \text{and} \qquad \frac{\Omega^2 T}{\Gamma} \gg \alpha_P L \cot\vartheta, \tag{107}$$

where ϑ is the mixing angle defined in Eq. (45). If condition (107) is fulfilled, the interaction of the pulses with the otherwise optically thick medium ($\alpha L \gg 1$) is completely eliminated.

It is worth noting that the adiabaticity condition (107) implies that the spectral width $\Delta\omega \sim T^{-1}$ over which undisturbed propagation is possible is inversely proportional to the density-length product $\alpha_s L$ or $\alpha_p L$ (Lukin *et al.*, 1997).

2. *Elimination of Absorption; Slow Light*

It is possible to achieve transparency, i.e., an elimination of the absorptive part of the interaction, for even smaller intensities than those required by condition (107). However, the light-induced modification of the refractive effects remains. Since nonadiabatic corrections are relevant here, they need to be taken into account in an approximate way. For this it is convenient to work in the basis of dark Φ_d and bright states Φ_b,

$$\begin{bmatrix} \Phi_d(z,t) \\ \Phi_b(z,t) \end{bmatrix} = \begin{bmatrix} \cos\vartheta(z,t) & -\sin\vartheta(z,t) \\ \sin\vartheta(z,t) & \cos\vartheta(z,t) \end{bmatrix} \begin{bmatrix} \psi_1 \\ \psi_2 \end{bmatrix}. \tag{108}$$

The probability amplitudes in this basis, $\mathbf{C}(t) = [C_d, C_b, C_2]^T$, obey a Schrödinger equation with a Hamiltonian,

$$\tilde{\mathsf{H}} = \hbar \begin{bmatrix} 0 & i\dot{\vartheta} & 0 \\ -i\dot{\vartheta} & 0 & \frac{1}{2}\Omega \\ 0 & \frac{1}{2}\Omega & -\frac{i}{2}\Gamma \end{bmatrix},$$

that is equivalent to a three-state system driven by two pulsed "fields," of strength $\dot{\vartheta}$ and Ω. Under adiabatic conditions $\dot{\vartheta}$ is small and can be treated perturbatively. Solving the Schrödinger equation to leading order of $\eta = |\dot{\vartheta}/\Omega|$, one finds:

$$C_d = 1 + \mathcal{O}(\eta), \qquad C_b = \mathcal{O}(\eta), \qquad C_2 = \frac{2i}{\Omega}\dot{\vartheta} + \mathcal{O}(\eta^2),$$

or, after transformation back to the bare atomic basis,

$$C_1 = \cos\vartheta \qquad C_2 = \frac{2i}{\Omega}\dot{\vartheta} \qquad C_3 = -\sin\vartheta. \tag{109}$$

An important special case is that of a strong and approximately constant Stokes field, as shown in Fig. 45, i.e., $|\Omega_s| \gg |\Omega_p|$ and

$$\dot{\vartheta} = \frac{\dot{\Omega}_p\Omega_s - \Omega_p\dot{\Omega}_s}{\Omega^2} \approx \frac{\dot{\Omega}_p}{\Omega}. \tag{110}$$

Substitution of (109) and (110) into the propagation equations (103) and (104) yields, in lowest order of η,

$$\left(\frac{\partial}{\partial z} + \frac{1}{v_g}\frac{\partial}{\partial t}\right)\Omega_p(z,t) = 0, \tag{111}$$

$$\left(\frac{\partial}{\partial z} + \frac{1}{c}\frac{\partial}{\partial t}\right)\Omega_s(z,t) = 0, \tag{112}$$

with

$$v_g = \frac{c}{1+n_g} \qquad \text{and} \qquad n_g = \frac{\alpha_P\Gamma c}{\Omega^2}. \tag{113}$$

Thus the pump pulse propagates without changing form (form stable) at a reduced group velocity v_g, while the strong Stokes fields remains unaffected by the interaction (see Fig. 45). It is important to note that the only effect of the medium is a

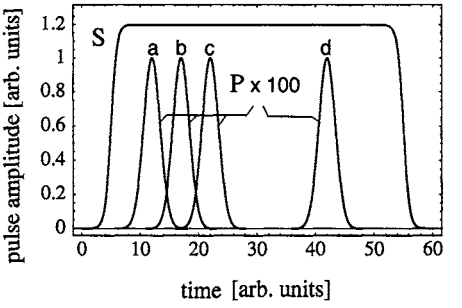

FIG. 45. Slow light propagation: Amplitudes of pump (×100) and Stokes fields as function of time in a co-moving frame for $n_g z/c = 0$ (a), 5 (b), 10 (c), and 30 (d). Weak pump field propagates with reduced group velocity. Arbitrary space and time units with $c = 1$.

temporal delay of the pump pulse. No energy is lost by absorption or spontaneous emission. At the leading edge of the pump pulse the atoms absorb photons from this pulse and transfer them into the Stokes field (which is much stronger and therefore effectively unchanged) by Raman adiabatic passage. The process is reversed at the tail of the pump pulse, i.e., all energy is returned to it.

In typical optical materials such as glass, the group index n_g is of the order of unity. In a dense medium (large α_p) with EIT the alteration of the propagation velocity can be quite substantial, however. Hau *et al.* (1999) observed a reduction of the group velocity to 17 m/s in a Bose condensate of Na atoms, corresponding to a group index of the order of 10^7. Similarly small values where obtained in a buffer-gas cell of hot Rb (Kash *et al.*, 1999) and Cs atoms (Budker *et al.*, 1999).

One easily verifies that the group-velocity reduction has little effect in the strong-field limit of Eq. (107). In this case the delay time $\tau_d = L/v_g - L/c = n_g L/c$, i.e., the time delay by which the Stokes pulse in the medium lags behind a corresponding pulse in vacuum, is much smaller than the pulse duration T.

The maximum group delay is limited by the finite lifetime of the dark state and higher-order nonadiabatic corrections. The latter lead to a maximum ratio of delay time to pulse length (Harris and Hau, 1999),

$$\left.\frac{\tau_d}{T}\right|_{\max} = \sqrt{\alpha_p L}. \tag{114}$$

The slowing down of light has a number of important applications. When a pulse enters a medium with a smaller group velocity, it becomes spatially compressed by the ratio of group velocity to the speed of light outside the medium. Thus, information contained in long pulses can be compressed to a small spatial volume. A reduction of the group velocity leads to an enhanced interaction time, important for efficient nonlinear optical processes (Harris and Hau, 1999; Hemmer *et al.*, 1995; Lukin and Imamoglu, 2000). When the light velocity matches the speed of sound, a new type of Brillouin scattering is possible (Matsko *et al.*, 2001). The enhancement of the field gradient, associated with the spatial pulse compression, can lead to very large pondermotive forces on atoms (Harris, 2000) with potential applications for atom optics and cooling.

B. ADIABATONS

It was shown by Grobe *et al.* (1994) that the equations of nonlinear propagation [(103), (104)] are adiabatically integrable for fields of comparable strength and—within the adiabatic approximation—of arbitrary shape. To see this, we adopt the method of Fleischhauer and Manka (1996) and transform the field equations for Ω_p and Ω_s in propagation equations for the total Rabi frequency Ω and the

nonadiabatic coupling $\dot{\vartheta}$ assuming equal coupling strength $\alpha_p = \alpha_s = \alpha$:

$$\left(\frac{\partial}{\partial z} + \frac{1}{c}\frac{\partial}{\partial t}\right)\Omega(z,t) = i\frac{\alpha}{2}\Gamma C_2 C_b^*, \tag{115}$$

$$\left(\frac{\partial}{\partial z} + \frac{1}{c}\frac{\partial}{\partial t}\right)\dot{\vartheta}(z,t) = i\frac{\alpha}{2}\Gamma\frac{\partial}{\partial t}\left(\frac{C_2 C_d^*}{\Omega}\right). \tag{116}$$

The transformation of both the atomic states and the fields leads to three dressed states coupled to two new "fields," characterized by Ω and $\dot{\vartheta}$. Under adiabatic conditions $|\dot{\vartheta}| \ll \Omega$, so a weak-field approximation is justified. Substituting the lowest-order adiabatic solutions (109) into these equations, one finds that the total Rabi frequency fulfills the free-space equation

$$\left(\frac{\partial}{\partial z} + \frac{1}{c}\frac{\partial}{\partial t}\right)\Omega(z,t) \approx 0.$$

No photons are lost by absorption and there is only a coherent transfer from one field into the other.

At the same time, $\dot{\vartheta}$ obeys the equation

$$\left(\frac{\partial}{\partial z} + \frac{1}{c}\frac{\partial}{\partial t}\right)\dot{\vartheta}(z,t) = -\alpha\Gamma\frac{\partial}{\partial t}\left(\frac{\dot{\vartheta}}{\Omega^2}\right).$$

This equation is exactly integrable (Grobe *et al.*, 1994). The corresponding solutions, called *adiabatons,* are particularly simple if Ω is approximately constant over the time interval of interest. In that case the pump and Stokes pulses have complementary envelopes and $\dot{\vartheta}$ propagates without changing form, at the group velocity v_g given in Eq. (113). The quasi-form-invariant propagation of an adiabaton is shown in Fig. 46. First experimental evidence of adiabaton propagation was reported by Kasapi *et al.* (1995) in Pb vapor. Adiabatons in more complicated configurations, such as double-lambda systems and double pairs of pulses, were studied by Cerboneschi and Arimondo (1995).

C. Matched Pulses

An interesting feature of the interaction of bichromatic fields with three-level systems was noted by Harris (1993): the dark state corresponding to a pair of pulses with identical envelope (*matched pulses*), i.e., $\Omega_p(z,t) = \Omega_p f(z,t)$ and $\Omega_s(z,t) = \Omega_s f(z,t)$, is time independent. After an appropriate preparation of the medium, matched pulses will remain exactly decoupled from the interaction for all times.

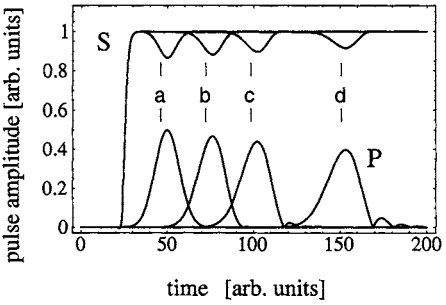

FIG. 46. Propagation of adiabatons. Shown are amplitudes of Pump and Stokes fields as function of time in a co-moving frame for $n_g z/c = 0$ (a), 25 (b), 50 (c), and 100 (d) from numerical solution of propagation equations (Fleischhauer and Manka, 1996). Arbitrary space and time units with $c = 1$.

If a pair of matched pulses is applied to an atomic ensemble in the ground state, they will prepare the atoms by a STIRAP process (Harris and Luo, 1995): during the first few single-photon absorption lengths, the front end of the pump pulse experiences a small loss. In this way a counterintuitive pulse ordering is established. This provides asymptotic connectivity of the dark state to the initial state of the atoms. The leading end of this slightly deformed pair of pulses will then prepare all atoms in the pathway via STIRAP and the pulses can propagate unaffected through the rest of the medium (Harris, 1994; Eberly *et al.*, 1994).

Apart from the preparation at the front end, matched pulses are stable solutions of the propagation problem. They should therefore be formed whenever pulses of arbitrary shape are applied to optically thick three-level media. In fact, it has been shown (Harris, 1993) that pairs of pulses with a strong CW carrier,

$$\Omega_p(z, t) = [1 + f(z, t)]\Omega_p e^{-i\omega_p(t-z/c)}, \tag{117a}$$

$$\Omega_s(z, t) = [1 + g(z, t)]\Omega_s e^{-i\omega_p(t-z/c)}, \tag{117b}$$

tend to adjust their amplitude modulations $f(z, t)$ and $g(z, t)$ in the course of propagation:

$$\left.\frac{f(z, t)}{g(z, t)}\right|_{z\to\infty} = 1.$$

Fast fluctuations of f and g lead to a nonadiabatic coupling of the dark state, established by the CW components, to other states and will be absorbed. Thus pulses of identical envelope are formed. This phenomenon of *pulse matching* also causes a correlation of quantum fluctuations in both fields (Fleischhauer, 1994; Jain, 1994; Agarwal, 1993).

The tendency to generate pulses with identical envelopes is not restricted to fields with a strong CW carrier. The adiabaton solutions are approximately stable over many single-photon absorption lengths. However, as shown by Fleischhauer and Manka (1996), they eventually decay to matched pulses after sufficiently long propagation distances.

D. Coherence Transfer between Matter and Light

It was shown in Section A that a strong and constant Stokes field leads to a slowing down of the propagation velocity of the pump pulse, while the shape and photon flux of the pump remained unaffected. The coherent information of the pump pulse is temporarily stored in the medium (in contrast to its energy, which is mostly transferred back and forth to the Stokes field). However, the maximum delay time is rather limited [see Eq. (114)]. It was shown recently (Fleischhauer *et al.*, 2000) that this limit can be overcome. In fact it is possible to control the propagation velocity of the pump pulse, to bring it to a full stop, and to reaccelerate it on demand. This behavior is associated with the existence of quasi-particles called *dark-state polaritons* that are a mixture of atomic and field components,

$$F(z,t) = \cos\theta(t)\,\Omega_p(z,t) - \sin\theta(t)\,\sqrt{\alpha c\Gamma}\,C_3(z,t)C_1^*(z,t).$$

The angle θ (not to be confused with the mixing angle ϑ used earlier) is defined by

$$\tan\theta(z,t) = \frac{\sqrt{\alpha c\Gamma}}{\Omega_s(z,t)}.$$

The dark-state polariton obeys the simple propagation equation

$$\left[\frac{\partial}{\partial t} + c\cos^2\theta(z,t)\frac{\partial}{\partial z}\right] F(z,t) = 0. \tag{118}$$

If Ω_s (and hence θ) is approximately uniform in z, Eq. (118) describes a form-invariant propagation of the quasi-particle with propagation velocity

$$v(t) = c\cos^2\theta(t).$$

When $\theta(t)$ is adiabatically rotated from 0 to $\pi/2$ by externally controlling the amplitude of the Stokes field Ω_s, an initially pure electromagnetic polariton ($F = \Omega_p$) is transformed into a pure atomic polarization ($F = \sqrt{\alpha c\Gamma}C_3C_1^*$). At the same

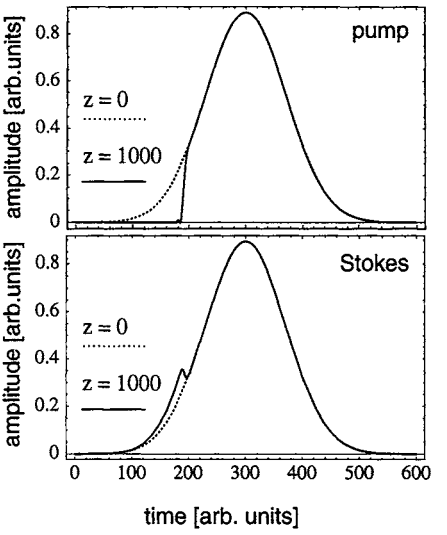

FIG. 47. Top: Amplitude of pump field as a function of time in arbitrary units at medium entrance $z = 0$ (dotted line) and for $z = 1000$ (full line). Bottom: The same for the Stokes field. Distance is measured in units of absorption length $\alpha_P^{-1} = \alpha_S^{-1}$ and peak values are $\Omega_s = \Omega_p = 10\Gamma$.

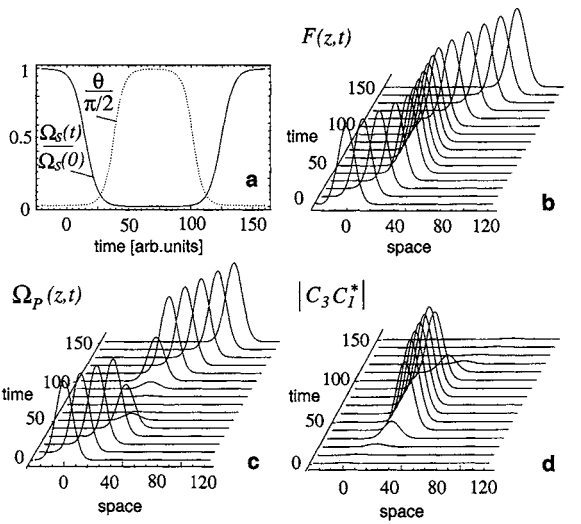

FIG. 48. Stopping and reaccelerating a dark-state polariton. Rabi frequency of control (Stokes) field and mixing angle are shown in (a). Coherent amplitude of dark-state polariton F is plotted in (b), and the amplitudes of pump field Ω_p and atomic coherence $|C_3 C_1^*|$ are shown in (c) and (d), respectively. Space and time have arbitrary units, with $c = 1$. (From M. Fleischhauer and M. D. Lukin. Dark-state polaritons in electromagnetically induced transparency. *Phys. Rev. Lett.* 2000;84:5094–5097.)

time, the propagation velocity is changed from the vacuum speed of light to zero. The pump pulse is thus "stopped," which means that its coherent information is transferred to collective atomic states. During the transfer process the spectrum of the electric field component is narrowed. As a consequence, the limitation (114) does not apply. The atomic polarization can be extracted by reversing the transfer process, i.e., rotating θ back from $\pi/2$ to 0 and re-creating the pump pulse. The deceleration, storage, and reacceleration of a polariton is illustrated in Fig. 48. First experimental demonstrations of light stopping have recently been reported (Phillips *et al.*, 2001; Liu *et al.*, 2001). Figure 49 shows the observed light pulse storage in Rb vapor from Phillips *et al.* (2001).

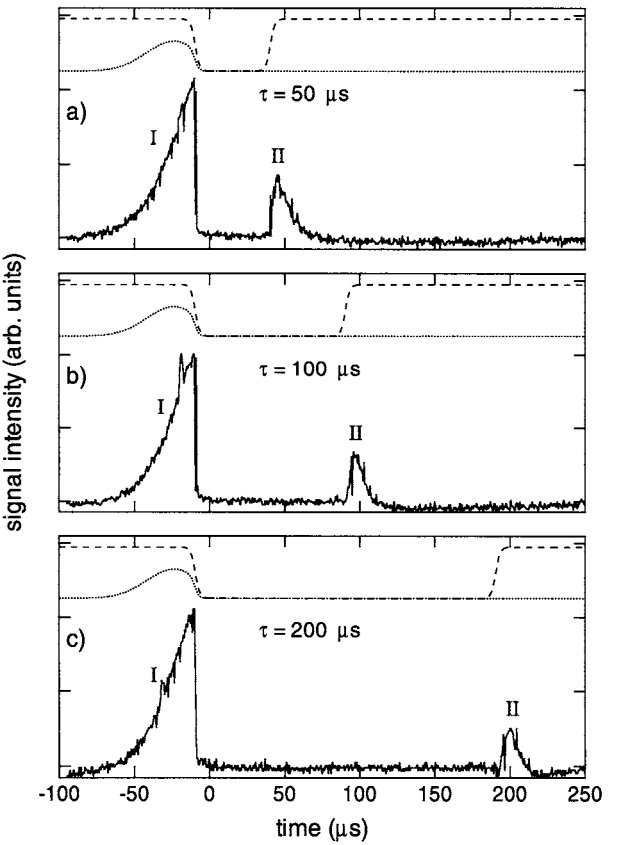

FIG. 49. Light pulse storage in ^{87}Rb cell. Shown above the data in each graph are calculated values of control field (dashed line) and input signal (dotted). (Reprinted with permission from D. F. Phillips, A. Fleischhauer, A. Mair, R. L. Walsworth, and M. D. Lukin. Storage of light in atomic vapor. *Phys. Rev. Lett.* 2001;86:783–786.)

XI. Applications of STIRAP in Quantum Optics and Quantum Information

The growing interest in quantum information science in recent years, and the resulting need for methods that allow controlled and coherent manipulation of quantum states, has led to another field of applications of STIRAP. An important new aspect here is the possibility for coherent control not only of quantum states of atomic and molecular systems, but also of quantum states of the radiation field.

In all aspects of quantum information, *decoherence* (e.g., the loss of coherence through uncontrolled random variations of state vector phases) must be avoided. Here STIRAP, by utilizing radiatively dark states, has definite advantages.

A. Single-Atom Cavity Quantum Electrodynamics

The potential usefulness of STIRAP in studies of cavity quantum electrodynamics (QED) was first pointed out by Parkins *et al.* (1993, 1995, 1999). They proposed to use STIRAP to create coherent superpositions of photon-number states by strongly coupling an atom to the field within a cavity of volume V. The quantized field of the single-mode resonator provided the Stokes field. Within the RWA, the interaction coupled only triplets of bare eigenstates of the combined atom–field system, viz., $\psi_1^{n+1} \equiv |\psi_1, n+1\rangle$, $\psi_2^n \equiv |\psi_2, n\rangle$, and $\psi_3^n \equiv |\psi_3, n\rangle$, where n denotes the number of photons in the mode. The appropriate Hamiltonian is that given in Eq. (40) with the Rabi frequency of the pump field replaced by the *vacuum Rabi frequency* (in cavity volume V),

$$\Omega_{\text{vac}} = d_{12}/\hbar\sqrt{\hbar\omega_{12}/2\varepsilon_0 V}, \tag{119}$$

the coupling strength between the atom and the resonator mode. The system has an infinite set of adiabatic dark states,

$$\Phi_0^n \equiv \psi_1^{n+1}\cos\theta_n(t) - \psi_3^n \sin\theta_n(t), \qquad n = 0, 1, 2, \ldots,$$

where the mixing angles θ_n are defined as

$$\tan\theta_n(t) = \frac{\Omega_{\text{vac}}\sqrt{n}}{\Omega_p(t)}.$$

Of particular interest is the case $n = 1$. Adiabatic rotation of the dark state maps an atomic excitation ($|\psi_3, n = 0\rangle$) onto an excitation of the resonator mode ($|\psi_1, n = 1\rangle$), and vice versa, in a decoherence-free fashion. Because the RMS Rabi frequency $\Omega = \sqrt{\Omega_{\text{vac}}^2 n + \Omega_s^2}$ is equal to $\Omega_{\text{vac}}\sqrt{n}$ in the asymptotic

limit $\theta_n \to \pi/2$, the adiabatic condition in the presence of decay takes the form (Fleischhauer and Manka 1996)

$$\frac{\Omega_{\text{vac}}^2 n}{\Gamma} T \gg 1,$$

where Γ is the decay rate of the excited state ψ_2.

The transfer time T is usually limited by the finite decoherence time of the field state, e.g., due to cavity losses. If κ denotes the photon loss rate of the resonator mode, the decoherence time of a photon number state $|n\rangle$ is of the order $1/(n\kappa)$. Thus adiabaticity requires a strong-coupling regime of the cavity

$$\Omega_{\text{vac}}^2 \gg \kappa\Gamma, \tag{120}$$

a condition which is technically very challenging to satisfy.

Despite these difficulties in the practical realization, adiabatic transfer between atomic and resonator excitations is interesting because of a number of potential applications. For example, successive interactions of atoms with the cavity system can be used to create arbitrary coherent superpositions of photon number states (Parkins *et al.*, 1993). This idea can be extended to two degenerate cavity modes of orthogonal polarizations (Lange and Kimble, 2000).

Furthermore, as first suggested by Law and Eberly (1996, 1998) and Law and Kimble (1997), it is possible to generate a single-photon wave packet, with an envelope determined by $\theta_1(t)$, in the output of the resonator. Single-photon wave packets on demand are important for quantum information processing utilizing photons as information carriers. A first step toward an experimental realization of such a "photon pistol" was recently reported by Hennrich *et al.* (2000). Here individual atoms prepared in state ψ_3 were dropped from a magneto-optical trap (MOT) and fell through a resonator setup as shown in Fig. 50. Raman adiabatic passage induced by a counterintuitive coupling to the resonator field and a subsequent pump laser beam led to stimulated emission into the resonator mode.

The process of transferring excitation from atoms to a field mode is reversible and allows the opposite process of mapping cavity-mode fields onto atomic ground-state coherences. This mapping provides a possibility for measuring cavity fields (Parkins *et al.*, 1995). The atomic angular momentum state can be measured by the Newton–Young method (Newton and Young, 1968) with a finite number of magnetic dipole measurements using Stern–Gerlach analyzers. Alternatively, the parameters of the atomic superposition can be measured by coupling this degenerate atomic state to an excited state by an elliptically polarized laser pulse and measuring the subsequent fluorescence (Vitanov *et al.*, 2000; Vitanov, 2000).

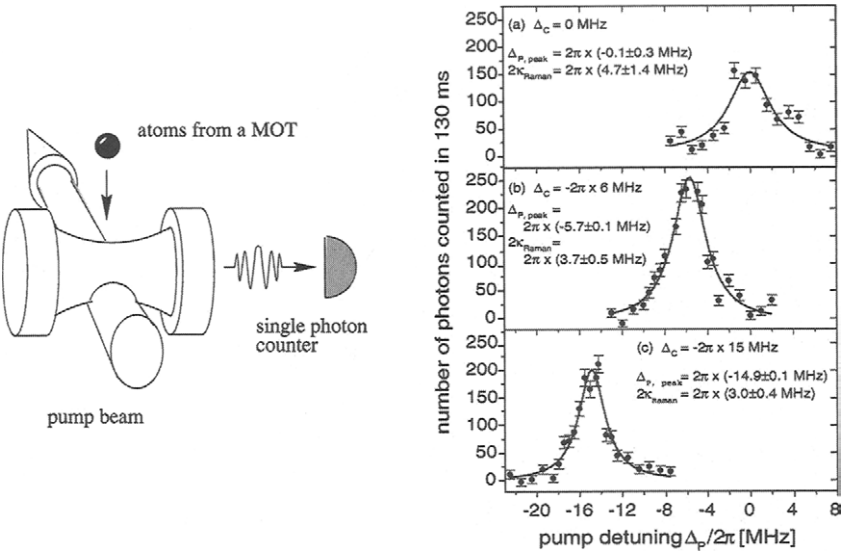

FIG. 50. First evidence of vacuum stimulated Raman scattering into cavity mode via STIRAP. Top: Experimental setup. Bottom: Number of counted photons as function of pump detuning for different probe detunings. Maximum at $\Delta_P = \Delta_C$ proves two-photon nature of the stimulated process. (Reprinted with permission from M. Hennrich, T. Legero, A. Kuhn, and G. Rempe. Vacuum-stimulated Raman scattering based on adiabatic passage in high-finesse optical cavity. *Phys. Rev. Lett.* 2000;85:4872–4875.)

B. Quantum Logic Gates Based on Cavity QED

Quantum information processing requires the coherent manipulation of elementary units, called *quantum bits* (*qubits*), which are equivalent to spin-$\frac{1}{2}$ systems. Besides performing arbitrary rotations within the two-dimensional Hilbert space of individual qubits, H_i, one must be able to perform operations, known as elementary quantum gates, between arbitrary pairs of them. It was shown by Pellizzari *et al.* (1995) that the required two-bit gate can be implemented in a cavity system by employing STIRAP to transfer quantum states between different atoms. The quantum states of two qubits i and j, stored in two different atoms, are first mapped to four different internal states of a single atom. The required gate operation in the 2×2-dimensional Hilbert space $H_i \otimes H_j$ of the ith and jth qubits can then be performed by simply applying the appropriate laser pulses to the second atom. Finally, the qubits are transferred back to the original atoms, where they will generally be in an *entangled* state, i.e., in a quantum state which cannot be factorized.

To illustrate the essence of the qubit transfer from one atom to another via the resonator field, we consider two three-level atoms A and B. The $2 \rightarrow 3$ transitions of both atoms are coupled to the same quantized mode of the resonator. Assume

that atom A is initially in a coherent superposition of states 1 and 3 with amplitudes α and β, i.e., $\psi^{\mathrm{A}} = \alpha\psi_1^{\mathrm{A}} + \beta\psi_3^{\mathrm{A}}$. Atom B is assumed to be in state 3, for simplicity, and there are no photons in the cavity. Under these conditions the dynamics of the total system involves only the state

$$\Phi_0^0 = \left|\psi_3^{\mathrm{A}}, \psi_3^{\mathrm{B}}, 0\right\rangle, \tag{121}$$

where $|\ldots, 0\rangle$ denotes the photon vacuum. Φ_0^0 is an exact eigenstate of the interaction with zero eigenvalue. In addition there is a resonant, chainwise-coupled system of five states:

$$\begin{aligned}\left|\psi_1^{\mathrm{A}}, \psi_3^{\mathrm{B}}, 0\right\rangle &\overset{\Omega_p^{\mathrm{A}}}{\longleftrightarrow} \left|\psi_2^{\mathrm{A}}, \psi_3^{\mathrm{B}}, 0\right\rangle \overset{\Omega_{\mathrm{vac}}}{\longleftrightarrow} \left|\psi_3^{\mathrm{A}}, \psi_3^{\mathrm{B}}, 1\right\rangle, \\ &\overset{\Omega_{\mathrm{vac}}}{\longleftrightarrow} \left|\psi_3^{\mathrm{A}}, \psi_2^{\mathrm{B}}, 0\right\rangle \overset{\Omega_p^{\mathrm{B}}}{\longleftrightarrow} \left|\psi_3^{\mathrm{A}}, \psi_1^{\mathrm{B}}, 0\right\rangle.\end{aligned} \tag{122}$$

The Hamiltonian of this system has the adiabatic dark state (i.e., a state without component of state ψ_2)

$$\begin{aligned}\Phi_0^1 = \frac{1}{\mathcal{M}}\big[&\Omega_p^{\mathrm{A}}(t)\Omega_{\mathrm{vac}}\left|\psi_3^{\mathrm{A}}, \psi_1^{\mathrm{B}}, 0\right\rangle \\ &-\Omega_p^{\mathrm{A}}(t)\Omega_p^{\mathrm{B}}(t)\left|\psi_3^{\mathrm{A}}, \psi_3^{\mathrm{B}}, 1\right\rangle + \Omega_p^{\mathrm{B}}(t)\psi_1\left|\psi_1^{\mathrm{A}}, \psi_3^{\mathrm{B}}, 0\right\rangle\big],\end{aligned} \tag{123}$$

with $\mathcal{M}$ being a normalization constant. Any superposition of the zero-eigenvalue states Φ_0^0 and Φ_0^1 is also a dark state. In particular, if at $t \to -\infty$, the pump field of atom A vanishes, i.e., $\Omega_p^{\mathrm{A}} = 0$, but that of atom B is nonzero, i.e., $\Omega_p^{\mathrm{B}} \neq 0$, then the initial statevector of the system is a superposition of dark states,

$$\begin{aligned}\Psi(t = -\infty) &= \left(\alpha\left|\psi_1^{\mathrm{A}}\right\rangle + \beta\left|\psi_3^{\mathrm{A}}\right\rangle\right)\left|\psi_3^{\mathrm{B}}\right\rangle\left|0\right\rangle \\ &= \alpha\left|\psi_1^{\mathrm{A}}, \psi_3^{\mathrm{B}}, 0\right\rangle + \beta\left|\psi_3^{\mathrm{A}}, \psi_3^{\mathrm{B}}, 0\right\rangle \\ &= \alpha\Phi_0^1(-\infty) + \beta\Phi_0^0.\end{aligned} \tag{124a}$$

Adiabatic reduction of Ω_p^{B} to zero while increasing Ω_p^{A} rotates the superposition of dark states to

$$\begin{aligned}\Psi(t = +\infty) &= \alpha\Phi_0^1(\infty) + \beta\Phi_0^0 \\ &= \alpha\left|\psi_3^{\mathrm{A}}, \psi_1^{\mathrm{B}}, 0\right\rangle + \beta\left|\psi_3^{\mathrm{A}}, \psi_3^{\mathrm{B}}, 0\right\rangle \\ &= \left|\psi_3^{\mathrm{A}}\right\rangle\left(\alpha\left|\psi_1^{\mathrm{B}}\right\rangle + \beta\left|\psi_3^{\mathrm{B}}\right\rangle\right).\end{aligned} \tag{124b}$$

As a result, the qubit state of atom A is mapped onto atom B—an example of *state swapping*. Implementation of an actual quantum gate requires a slightly more

complicated system, in which atom B has two degenerate states "$\pm$" in each energy level 1, 2, and 3. The two Λ systems are coupled by pump and Stokes fields in a parallel way. This allows a mapping of the qubit states of atoms A and B onto the four states $\psi_{1\pm}$ and $\psi_{3\pm}$ of atom B. After this transfer the two-bit operations can be performed by manipulating atom B alone.

As can be seen from Eq. (123), the single-photon state of the cavity mode is excited during the transfer process. To avoid decoherence, the transfer time T needs to be short compared to the decay time of the cavity. On the other hand, the transfer must be sufficiently slow to guarantee adiabaticity. Both requirements can only be fulfilled in a strongly coupled regime (120).

C. Quantum Networking

An important aspect of quantum information processing is the ability to transmit the wavefunction of qubits over mesoscopic or macroscopic distances. A scheme for an ideal quantum-state transfer between atoms at spatially separated nodes of a network was proposed by Cirac *et al.* (1997), using a Raman transfer of quantum states from an atom to a resonator Stokes field, which is coupled to a transmission line such as an optical fiber. Unlike the case described in the previous subsection, this scheme requires that the two single-photon frequencies be far off resonance, so that the excited state can be adiabatically eliminated. The Raman process generates, in the fiber, a photon wave packet that is directed to a second, strongly coupling resonator containing another atom. When the pump field of the first resonator generates time-symmetric photon pulses, a retarded and time-reversed Stokes field in the second resonator leads to a complete transfer of the photon wave packet to the corresponding atom—without any reflection from the input mirror (Cirac *et al.,* 1997). The possibility for suppressing the reflection for arbitrary photon wave packets (quantum impedance matching) was discussed by Fleischhauer *et al.,* 2000; Lukin *et al.,* 2000).

It was shown by Pellizzari (1997) that state swapping can also be performed by means of adiabatic passage via photonic dark states. In this case the two cavities remain in the vacuum states during the whole operation and the effect of resonator losses is diminished. However, the modes of the optical fiber connecting the two cavities are excited during the transfer process. An interesting extension of the adiabatic-passage idea, given by van Enk *et al.,* (1999), avoids any excitation of fiber modes and thus suppresses the effect of fiber losses.

D. Many-Atom Systems

The disadvantages of single-atom cavity-QED schemes are the need for a strongly coupled cavity and the requirement for extremely close control of individual atoms. As shown by Lukin *et al.* (2000), both drawbacks can be overcome if collective

excitations of an ensemble of atoms are used as qubit states instead of energy levels of individual atoms. If N three-level atoms are placed inside a resonator, with the $1 \rightarrow 2$ transition resonantly coupled by a quantized mode of the resonator and the $2 \rightarrow 3$ transition by a resonant classical Stokes field, the interaction couples only symmetric superpositions:

$$\Psi_1 = \psi_1^1 \psi_1^2 \ldots \psi_1^N, \tag{125a}$$

$$\Psi_3 = \frac{1}{\sqrt{N}} \sum_{j=1}^{N} \psi_1^1 \ldots \psi_3^j \ldots \psi_1^N, \tag{125b}$$

$$\Psi_3^2 = \frac{1}{\sqrt{2N(N-1)}} \sum_{i \neq j=1}^{N} \psi_1^1 \ldots \psi_3^i \ldots \psi_3^j \ldots \psi_1^N. \tag{125c}$$

etc.

In particular, if initially the field is in a state with at most one photon, the relevant eigenstates of the bare system are the total ground state $|\Psi_1, 0\rangle$, which is not affected by the interaction at all; the ground state with one photon in the field $|\Psi_3, 1\rangle$; and the singly excited states $|\Psi_2, 0\rangle$ and $|\Psi_3, 0\rangle$. For the case of two excitations, the coupling involves three more states, etc.

The interaction of the N-atom system with the quantized radiation mode has a family of dark states, i.e., states with no component ψ_2 and zero adiabatic eigenvalue (Parkins *et al.*, 1993; Lukin and Imamoglu, 2000; Fleischhauer *et al.*, 2000). The simplest one is

$$\Phi_0^1 = \cos\theta(t)|\Psi_1, 1\rangle - \sin\theta(t)|\Psi_3, 0\rangle$$

with $\tan\theta(t) = \Omega_{\text{vac}}\sqrt{N}/\Omega(t)$, and in general one has

$$\Phi_0^n = \sum_{k=0}^{n} \sqrt{\frac{n!}{k!(n-k)!}} (-\sin\theta)^k (\cos\theta)^{n-k} \left|\Psi_3^k, n-k\right\rangle.$$

The existence of dark states provides a very elegant way to transfer an arbitrary quantum state of the single-mode field to collective atomic excitations. Adiabatic rotation of the mixing angle θ from 0 to $\pi/2$ leads to a complete and reversible transfer of the photonic excitation to a collective atomic excitation, if the total number of excitations n is less than the number of atoms. If $\theta = 0 \rightarrow \pi/2$ one has, for all $n \leq N$,

$$\Phi_0^n = |\Psi_1\rangle|n\rangle \longrightarrow \left|\Psi_3^n\right\rangle|0\rangle.$$

By contrast with the single-atom case (120), the necessary condition for the adiabatic following of the systems state vector with the dark state is now

$$\frac{\Omega_{\text{vac}}^2 N}{\Gamma} T \gg n.$$

If the number of atoms N is much larger than the number of photons n, this condition can be much more easily fulfilled and does not require strong coupling resonators.

XII. Summary and Outlook

Many contemporary fields in atomic, molecular, and optical physics require preparation of samples in which almost all of the population resides in a preselected target state. Although a variety of methods have been proposed and tried over the years, many of the most successful ones are based on controlling adiabatic time evolution of the quantum system.

The theoretical description of such time dependence is most easily presented with the aid of adiabatic states: if the evolution is adiabatic, then at all times the state vector remains aligned with one of these states. The progress of the changing state vector can be followed by viewing a plot of adiabatic eigenvalues and noting the crossings of diabatic energies.

The experimenter has various guides for the applicability of adiabatic passage—the adiabatic conditions. Typically these require that excitation pulses be strong and smooth and that the interaction act for a "long" time compared with a characteristic atomic time scale. Often this is expressed as the requirement that a time-integrated Rabi frequency be much larger than unity. What typically sets adiabatic techniques apart from other pulsed-excitation techniques is the relative insensitivity of the transfer efficiency to interaction parameters; adiabatic techniques are not sensitive to pulse area, for example.

In simplest form, adiabatic passage can completely invert the population of a two-state system. Numerous extensions have been devised and put to practical use; we have mentioned some of these. When a quantum system of three (or more) states is subjected to two (or more) coherent pulses, to permit adiabatic evolution of a stimulated Raman process, then remarkable and novel effects become possible. These rest on the presence of a "population trapping" quantum superposition state, a concept first appreciated some 30 years ago and described here in some detail, and the use of "counterintuitive" pulse sequences.

Earliest applications of the technique of stimulated Raman adiabatic passage (STIRAP) aimed to produce complete selective excitation of individual rovibrational states of molecules or magnetic sublevels of atoms. We have discussed the basic STIRAP and numerous extensions. Unlike techniques involving only two

quantum states, such procedures can produce population transfer into stable or metastable states. Beyond such simple population transfer uses, we have noted the growing interest in the use of STIRAP and related techniques to the creation of stable superpositions (controlled partial population transfer, with predetermined phases) for a number of applications.

More recently, the response of the fields themselves to such coherent atomic evolution has been considered, and remarkable propagation effects have been demonstrated. For example, inducing an otherwise opaque vapor to allow nearly lossless transmission (electromagnetically induced transparency, or EIT), dramatically slowing pulses of light, and even "stopping photons" for controllable time intervals. These techniques have application, among other things, to the emerging research area of quantum information.

As laser technology continues to improve, and experimenters acquire lasers with ever higher intensity and purer spectral content, one can expect to see imaginative new applications of adiabatic passage to the task of transferring populations between quantum states, of creating novel superposition states, and of modifying pulse propagation in new and novel ways.

XIII. Acknowledgments

This work has been supported by the European Union Research and Training network COCOMO, contract HPRN-CT-1999-00129, by NATO grant 1507-826991, and by Deutsche Forschungsgemeinschaft. NVV has received partial support from the Academy of Finland, project 43336. BWS acknowledges the support of Laserzentrum, University of Kaiserslautern. His work in Germany has been supported, in part, by a Research Award from the Alexander von Humboldt Foundation. His work at Livermore was supported in part under the auspices of the U.S. Department of Energy at Lawrence Livermore National Laboratory under contract W-7405-Eng-48.

XIV. References

Agarwal, G. S. (1993). Coherent population trapping states of a system interacting with quantized fields and the production of the photon statistics matched fields. *Phys. Rev. Lett.* **71,** 1351–1354.

Allen, L., and Eberly, J. H. (1975). "Optical Resonance and Two-level atoms." Dover, New York.

Alzetta, G., Gozzini, A., Moi, L., and Orriols, G. (1976). An experimental method for the observation of RF transitions and laser beat resonances in oriented Na vapour. *Nuovo Cim. B* **36,** 5–20.

Alzetta, G., Moi, L., and Orriols, G. (1979). Nonabsorption hyperfine resonances in a sodium vapour irradiated by a multimode dye-laser. *Nuovo Cim. B* **52,** 2333–2346.

Arimondo, E. (1996). Coherent population trapping in laser spectroscopy. *In* "Progress in Optics XXXV" (E. Wolf, Ed.), pp. 259–356. North-Holland, Amsterdam.

Arimondo, E., and Orriols, G. (1976). Nonabsorbing atomic coherences by coherent two-photon transitions in a three-level optical pumping. *Lett. Nuovo Cim.* **17,** 333–338.

Aspect, A., Armindo, E., Kaiser, R., Vanteenkiste, N., and Cohen-Tannoudji, C. (1988). Laser cooling below the one-photon recoil by velocity-selective coherent population trapping. *Phys. Rev. Lett.* **61,** 826–829.

Aspect, A., Armindo, E., Kaiser, R., Vanteenkiste, N., and Cohen-Tannoudji, C. (1989). Laser cooling below the one-photon recoil energy by velocity-selective coherent population trapping: theoretical analysis. *J. Opt. Soc. Am. B* **6,** 2112–2124.

Autler, S. H., and Townes, C. H. (1955). Stark effect in rapidly varying fields. *Phys. Rev* **100,** 703.

Band, Y. B., and Julienne, P. S. (1991a). Density matrix calculation of population transfer between vibrational levels of Na_2 by stimulated Raman scattering with temporally shifted laser beams. *J. Chem. Phys.* **94,** 5291–5298.

Band, Y. B., and Julienne, P. S. (1991b). Population transfer by multiple stimulated Raman scattering. *J. Chem. Phys.* **95,** 5681–5685.

Band, Y. B., and Julienne, P. S. (1992). Complete alignment and orientation of atoms and molecules by stimulated Raman scattering with temporally shifted lasers. *J. Chem. Phys.* **96,** 3339–3341.

Band, Y. B., and Magnes, O. (1994). Chirped adiabatic passage with temporally delayed pulses. *Phys. Rev. A* **50,** 584–594.

Becker, M., Gaubatz, U., Jones, P. L., and Bergmann, K. (1987). Efficient and selective population of high vibrational levels of Na_2 via a stimulated Raman process. *J. Chem. Phys.* **87,** 5064–5076.

Bergmann, K. (1988). State selection via optical methods. *In* "Atomic and Molecular Beam Methods" (G. Scoles, Ed.), pp. 293–344. Oxford University Press, Oxford.

Bergmann, K., and Demtröder, W. (1971). Inelastic collision cross section for excited molecules: Rotational energy transfer within the $B^1\Pi_u$-state of Na_2 induced by collision with He. *Z. Phys.* **243,** 1–13.

Bergmann, K., and Shore, B. W. (1995). Coherent population transfer. *In* "Molecular Dynamics and Spectroscopy by Stimulated Emission Pumping" (H. L. Dai and R. W. Field, Ed.), pp. 315–73. World Scientific, Singapore.

Bergmann, K., Engelhardt, R., Hefter, U., Hering, P., and Witt, J. (1978). State resolved differential cross sections for rotational transitions in Na_2+Ne(He) collisions. *Phys. Rev. Lett.* **40,** 1446–1450.

Bergmann, K., Theuer, H., and Shore, B. W. (1998). Coherent population transfer among quantum states of atoms and molecules. *Rev. Mod. Phys.* **70,** 1003–1025.

Boller, K. J., Imamoglu, A., and Harris, S. E. (1991). Observation of electromagnetically induced transparency. *Phys. Rev. Lett.* **66,** 2593–2596.

Bordé, C. J. (1989). Atomic interferometry with internal state labeling. *Phys. Lett. A* **140,** 10.

Budker, D., Kimball, D. F., Rochester, S. M., and Yashchuk, V. V. (1999). Nonlinear magneto-optics and reduced group velocity of light in atomic vapor with slow ground state relaxation. *Phys. Rev. Lett.* **83,** 1767–1770.

Carroll, C. E., and Hioe, F. T. (1992). Coherent population transfer via the continuum. *Phys. Rev. Lett.* **68,** 3523–3526.

Carroll, C. E., and Hioe, F. T. (1993). Selective excitation via the continuum and suppression of ionization. *Phys. Rev. A* **47,** 571–580.

Carroll, C. E., and Hioe, F. T. (1995). Excitation using two lasers: effects of continuum-continuum transitions. *Phys. Lett. A* **199,** 145–150.

Carroll, C. E., and Hioe, F. T. (1996). Selective excitation and structure in the continuum. *Phys. Rev. A* **54,** 5147–5151.

Cerboneschi, E., and Arimondo, E. (1995). Transparency and dressing for optical pulse pairs through a double-lambda absorbing medium. *Phys. Rev. A* **52,** R1823–R1826.

Chu, S. (1998). Nobel lecture: The manipulation of neutral particles. *Rev. Mod. Phys.* **70,** 685–706.

Cirac, J. I., Zoller, P., Kimble, H. J., and Mabuchi, H. (1997). Quantum state transfer and entanglement distribution among distant nodes in a quantum network. *Phys. Rev. Lett.* **78,** 3221–3224.

Cohen-Tannoudji, C. N. (1998). Nobel lecture: Manipulating atoms with photons. *Rev. Mod. Phys.* **70,** 707–720.

Coulston, G. W., and Bergmann, K. (1992). Population transfer by stimulated Raman scattering with delayed pulses: Analytical results for multilevel systems. *J. Chem. Phys.* **96,** 3467–3495.

Crim, F. F. (1984). Selective excitation studies of unimolecular reaction dynamics. *Annu. Rev. Phys. Chem.* **35,** 657–691.

Crisp, M. D. (1973). Adiabatic-following approximation. *Phys. Rev. A* **8,** 2128–2135.

Dai, H. C., and Field, R. W. (1995). "Molecular Dynamics and Spectroscopy by Stimulated Emission Pumping." World Scientific, Singapore.

Danileiko, M. V., Romanenko, V. I., and Yatsenko, L. P. (1994). Landau–Zener transitions and population transfer in a three-level system driven by two delayed laser pulses. *Opt. Commun.* **109,** 462–466.

Davis, J. P., and Pechukas, P. (1976). Nonadiabatic transitions induced by a time-dependent Hamiltonian in the semiclassical/adiabatic limit: The two-state case. *J. Chem. Phys.* **64,** 3129–3137.

Demkov, Y. N., and Kunike, M. (1969). Hypergeometric models of the two-state approximation in the theory of atomic collisions. *Vestn. Leningr. Univ. Fiz. Khim.* **16,** 39–45 (in Russian).

Demtröder, W., McClintock, M., and Zare, R. N. (1969). Spectroscopy of Na_2 using laser-induced fluorescence. *J. Chem. Phys.* **51,** 5495–5509.

Dittmann, P., Pesl, F. P., Martin, J., Coulston, G. W., He, G. Z., and Bergmann, K. (1992). The effect of vibrational excitation ($3 \leq v' \leq 19$) on the reaction $Na_2(v') + Cl \rightarrow NaCl + Na^*$. *J. Chem. Phys.* **97,** 9472–9475.

Drese, K., and Holthaus, M. (1998). Perturbative and nonperturbative processes in adiabatic population transfer. *Eur. Phys. J. D* **3,** 73–86.

Dykhne, A. M. (1962). Adiabatic perturbation of discrete spectrum states. *Sov. Phys. JETP* **14,** 941.

Eberly, J. H., Pons, M. L., and Haq, H. R. (1994). Dressed-field pulses in an absorbing medium. *Phys. Rev. Lett.* **72,** 56–59.

Einstein, A. (1917). Zur Quantentheorie de Strahlung. *Phys. Z.* **18,** 121.

Ekers, A., Kaufmann, O., Bergmann, K., Alnis, J., and Klavins, J. (1999a). Vibrational dependence of the Na_3^+-formation by associate ionization of $Na_3(P_{3/2}) + Na_2$ ($A\,^1\Sigma_u^+, v''$). *Chem. Phys. Lett.* **304,** 69–72.

Ekers, A., Kaufmann, O., Keil, M., and Bergmann, K. (1999b). Associative ionization in collision of electronically excited Na atoms with vibrationally excited $Na_2(v'')$ molecules. *Eur. Phys. J. D* **7,** 65–71.

Elk, M. (1995). Adiabatic transition histories of population transfer in the Lambda system. *Phys. Rev. A* **52,** 4017–4022.

Esslinger, T., Sander, F., Weidemüller, M., Hemmerich, A., and Hänsch, T. W. (1996). Subrecoil laser cooling with adiabatic transfer. *Phys. Rev. Lett.* **76,** 2432–2435.

Fano, U. (1961). Effects of configuraton interaction on intensities and phase shifts. *Phys. Rev.* **124,** 1866–1878.

Fano, U., and Cooper, J. W. (1968). Spectral distribution of atomic oscillator strengths. *Rev. Mod. Phys.* **41,** 441.

Featonby, P. D., Summy, G. S., Martin, J. L., Wu, H., Zetie, K. P., Foot, C. J., and Burnett, K. (1996). Adiabatic transfer for atomic interferometry. *Phys. Rev. A* **53,** 373–380.

Featonby, P. D., Summy, G. S., Webb, C. L., Godun, R. M., Oberthaler, M. K., Wilson, A. C., Foot, C. J., and Burnett, K. (1998). Separated-path Ramsey atom interferometer. *Phys. Rev. Lett.* **81,** 495–499.

Fewell, M. P., Shore, B. W., and Bergmann, K. (1997). Coherent population transfer among three states: Full algebraic solutions and the relevance of non adiabatic processes to transfer by delayed pulses. *Austral. J. Phys.* **50,** 281–304.

Fleischhauer, M., Keitel, C. H., Narducci, L. M., Scully, M. O., Zhu, S.-Y., and Zubairy, M. S. (1992). Lasing without inversion: Interference of radiatively broadened resonances in dressed atomic systems. *Opt. Commun.* **94,** 599.

Fleischhauer, M. (1994). Correlation of high-frequency phase fluctuations in electromagnetically induced transparency. *Phys. Rev. Lett.* **72,** 989–992.

Fleischhauer, M., and Lukin, M. D. (2000). Dark-state polaritons in electromagnetically induced transparency. *Phys. Rev. Lett.* **84,** 5094–5097.

Fleischhauer, M., and Manka, A. S. (1996). Propagation of laser pulses and coherent population transfer in dissipative three-level systems: An adiabatic dressed-state picture. *Phys. Rev. A* **54,** 794–803.

Fleischhauer, M., Yelin, S. F., and Lukin, M. D. (2000). How to trap photons? Storing single-photon quantum states in collective atomic excitations. *Opt. Commun.* **179,** 395–410.

Frishman, E., and Shapiro, M. (1996). Reversibility of bound-to-continuum transitions induced by a strong short laser pulse and the semiclassical uniform approximation. *Phys. Rev. A* **54,** 3310–3321.

Garraway, B. M., and Suominen, K.-A. (1998). Adiabatic passage by light-induced potentials in molecules. *Phys. Rev. Lett.* **80,** 932–935.

Gaubatz, U., Rudecki, P., Becker, M., Schiemann, S., Külz, M., and Bergmann, K. (1988). Population switching between vibrational levels in molecular beams. *Chem. Phys. Lett.* **149,** 463–468.

Gaubatz, U., Rudecki, P., Schiemann, S., and Bergmann, K. (1990). Population transfer between molecular vibrational levels by stimulated Raman scattering with partially overlapping laser fields. A new concept and experimental results. *J. Chem. Phys.* **92,** 5363–5376.

Glushko, B., and Kryzhanovsky, B. (1992). Radiative and collisional damping effects on efficient population transfer in a three-level system driven by two delayed laser pulses. *Phys. Rev. A* **46,** 2823–2830.

Godun, R. M., Webb, C. L., Oberthaler, M. K., Summy, G. S., and Burnett, K. (1999). Efficiencies of adiabatic transfer in a multistate system. *Phys. Rev. A* **59,** 3775–3781.

Goldner, L. S., Gerz, C., Spreeuw, R. J. C., Rolston, S. L., Westbrook, C. I., Phillips, W. D., Marte, P., and Zoller, P. (1994a). Momentum transfer in laser-cooled cesium by adiabatic passage in a light field. *Phys. Rev. Lett.* **72,** 997–1000.

Goldner, L. S., Gerz, C., Spreeuw, R. J. C., Rolston, S. L., Westbrook, C. I., Phillips, W. D., Marte, P., and Zoller, P. (1994b). Coherent transfer of photon momentum by adiabatic following in a dark state. *Quantum Opt.* **6,** 387–389.

Goral, K., Gajda, M., and Rzazewski, K. (2000). Multi-mode dynamics of a coupled ultracold atomic-molecular system. *Phys. Rev. Lett.* **86,** 1397–1401.

Gottwald, E., Mattheus, A., Schinke, R., and Bergmann, K. (1986). Angularly resolved vibrational excitation in Na_2-He collisions. *J. Chem. Phys.* **84,** 756–763.

Gottwald, E., Mattheus, A., Schinke, R., and Bergmann, K. (1987). Resolution of supernumerary rotational rainbows in Na_2-He-Ne, Ar collisions. *J. Chem. Phys.* **86,** 2685–2688.

Gray, H. R., Whitley, R. M., and Stroud, C. R. (1978). Coherent trapping of atomic populations. *Opt. Lett.* **3,** 218–220.

Grobe, R., Hioe, F. T., and Eberly, J. H. (1994). Formation of shape-preserving pulses in a nonlinear adiabatically integrable system. *Phys. Rev. Lett.* **73,** 3183–3186.

Guérin, S., and Jauslin, H. R. (1998). Two-laser multiphoton adiabatic passage in the frame of the Floquet theory. Applications to (1+1) and (2+1) STIRAP. *Eur. Phys. J. D* **2,** 99–113.

Guérin, S., Yatsenko, L. P., Halfmann, T., Shore, B. W., and Bergmann, K. (1998). Stimulated hyper-Raman adiabatic passage. II. Static compensation of dynamic Stark shifts. *Phys. Rev. A* **58,** 4691–4704.

Guérin, S., Jauslin, H. R., Unanyan, R. G., and Yatsenko, L. P. (1999). Floquet perturbative analysis for STIRAP beyond the rotating wave approximation. *Optics Express* **4,** 84–90.

Halfmann, T., and Bergmann, K. (1996). Coherent population transfer and dark resonances in SO_2. *J. Chem. Phys.* **104,** 7068–7072.

Halfmann, T., Yatsenko, L. P., Shapiro, M., Shore, B. W., and Bergmann, K. (1998). Population trapping and laser-induced continuum structure in helium: Experiment and theory. *Phys. Rev. A* **58,** R46–R49.

Hamilton, C. H., Kinsey, J. L., and Field, R. W. (1986). Stimulated emission pumping: New methods in spectroscopy and molecular dynamics. *Annu. Rev. Phys. Chem.* **37,** 493–524.

Harris, S. E., Field, J. E., and Imamoglu, A. (1990). Nonlinear optical processes using electromagnetically induced transparency. *Phys. Rev. Lett.* **64,** 1107–1110.

Harris, S. E. (1993). Electromagnetically induced transparency with matched pulses. *Phys. Rev. Lett.* **70,** 552–555.

Harris, S. E. (1994). Normal modes for electromagnetically induced transparency. *Phys. Rev. Lett* **72,** 52–55.

Harris, S. E. (1997). Electromagnetically induced transparency. *Phys. Today* **50,** 36–42.

Harris, S. E. (2000). Pondermotive forces with slow light. *Phys. Rev. Lett.* **85,** 4032–5.

Harris, S. E., and Hau, L. V. (1999). Nonlinear optics at low light levels. *Phys. Rev. Lett.* **82,** 4611–4614.

Harris, S. E., and Luo, Z. F. (1995). Preparation energy for electromagnetically induced transparency. *Phys. Rev. A* **52,** R928–R931.

Hau, L. V., Harris, S. E., Dutton, Z., and Behroozi, C. H. (1999). Light speed reduction to 17 metres per second in an ultracold atomic gas. *Nature* **397,** 594–598.

He, G.-Z., Kuhn, A., Schiemann, S., and Bergmann, K. (1990). Population transfer by stimulated Raman scattering with delayed pulses and by the stimulated-emission pumping method: a comparative study. *J. Opt. Soc. Am. B* **7,** 1960–1969.

Hefter, U., Jones, P., Bergmann, K., and Schinke, R. (1981). Resolution of supernumerary rotational rainbows in state-to-state Na_2-Ne scattering. *Phys. Rev. Lett.* **46,** 915–918.

Hefter, U., Eichert, J., and Bergmann, K. (1985). An optically pumped iodine supersonic beam laser. *Opt. Commun.* **52,** 330–535.

Hefter, U., Ziegler, G., Mattheus, A., Fischer, A., and Bergmann, K. (1986). Preparation and detection of molecular alignment with high state selectivity by saturated optical pumping in beams. *J. Chem. Phys.* **85,** 286–302.

Hemmer, P. R., Katz, D. P., Donoghue, J., Cronin-Golomb, M., Shahriar, M. S., and Kumar, P. (1995). Efficient low-intensity optical phase conjugation based on coherent population trapping in sodium. *Opt. Lett.* **20,** 982–984.

Hennrich, M., Legero, T., Kuhn, A., and Rempe, G. (2000). Vacuum-stimulated Raman scattering based on adiabatic passage in a high-finesse optical cavity. *Phys. Rev. Lett.* **85,** 4872–4875.

Hioe, F. T. (1984). Solution of Bloch equations involving amplitude and frequency modulations. *Phys. Rev. A* **30,** 2100–2103.

Hioe, F. T., and Carroll, C. E. (1988). Coherent population trapping in N-level quantum systems. *Phys. Rev. A* **37,** 3000–3005.

Imamoglu, A., and Harris, S. E. (1989). Lasers without inversion: interference of dressed lifetime-broadened states. *Opt. Lett.* **14,** 1344–1346.

Jaĭn, M. (1994). Excess noise correlation using population-trapped atoms. *Phys. Rev. A* **50,** 1899–1902.

Javanainen, J., and Mackie, M. (1998). Probability of photoassociation from a quasicontinuum approach. *Phys. Rev. A* **58,** R789–R792.

Javanainen, J., and Mackie, M. (1999). Coherent photoassociation of a Bose-Einstein condensate. *Phys. Rev. A* **59,** R3186–R3189.

Jones, P. L., Gaubatz, U., Hefter, U., Wellegehausen, B., and Bergmann, K. (1983). An optically pumped sodium-dimer supersonic beam laser. *Appl. Phys. Lett.* **42,** 222–224.

Kallush, S., and Band, Y. B. (2000). Short-pulse chirped adiabatic population transfer in diatomic molecules. *Phys. Rev. A* **61,** 041401.

Kasapi, A., Jain, M., Yin, G. Y., and Harris, S. E. (1995). Electromagnetically induced transparency: Propagation dynamics. *Phys. Rev. Lett.* **74,** 2447–2450.

Kasevich, M., and Chu, S. (1991). Atomic interferometry using stimulated Raman transitions. *Phys. Rev. Lett.* **67,** 181–184.

Kasevich, M., and Chu, S. (1992). Laser cooling below a photon recoil with three-level atoms. *Phys. Rev. Lett.* **69,** 1741–1744.

Kasevich, M., Weiss, D. S., Riis, E., Moler, K., Kasapi, S., and Chu, S. (1991). Atomic velocity selection using stimulated Raman transitions. *Phys. Rev. Lett.* **66,** 2297–2300.

Kash, M. M., Sautenkov, V. A., Zibrov, A. S., Hollberg, L., Welch, G. R., Lukin, M. D., Rostovtsev, Y., Fry, E. S., and Scully, M. O. (1999). Ultraslow group velocity and enhanced nonlinear optical effects in a coherently driven hot atomic gas. *Phys. Rev. Lett.* **82,** 5229–5232.

Kaufmann, O., Ekers, A., Gebauer-Rochholz, Ch., Mettendorf, K. U., Keil, M., and Bergmann, K. (2001). Dissociative charge transfer from highly excited Na Rydberg atoms to vibrationally excited Na_2 molecules. *Int. J. Mass Spectr.* in press.

Keil, M., Kolling, T., Bergmann, K., and Meyer, W. (1999). Dissociative attachment of low energy electrons to vibrationally excited Na_2-molecules using a novel photoelectron source. *Eur. Phys. J. D* **7,** 55–64.

Kittrell, C., Abramson, E., Kinsey, J. L., McDonald, S. A., Reisner, D. E., Field, R. W., and Katayama, D. H. (1981). Selective vibrational excitation by stimulated emission pumping. *J. Chem. Phys.* **75,** 2056–2059.

Knight, P. L. (1984). Laser-induced continuum structure. *Commun. Atomic Mol. Phys.* **15,** 193–214.

Knight, P. L., Lauder, M. A., and Dalton, B. J. (1990). Laser-induced continuum structure. *Phys. Rep.* **190,** 1–61.

Kobrak, M. N., and Rice, S. A. (1998a). Coherent population transfer via a resonant intermediate state: The breakdown of adiabatic passage. *Phys. Rev. A* **57,** 1158–1163.

Kobrak, M. N., and Rice, S. A. (1998b). Selective photochemistry via adiabatic passage: An extension of stimulated Raman adiabatic passage for degenerate final states. *Phys. Rev. A* **58,** 2885–2894.

Kobrak, M. N., and Rice, S. A. (1998c). Equivalence of the Kobrak- Rice photoselective adiabatic passage and the Brumer-Shapiro strong field methods for control of product formation in a reaction. *J. Chem. Phys.* **109,** 1–10.

Kuhn, A., Coulston, G., He, G. Z., Schiemann, S., Bergmann, K., and Warren, W. S. (1992). Population transfer by stimulated Raman scattering with delayed pulses using spectrally broad light. *J. Chem. Phys.* **96,** 4215–4223.

Kuhn, A., Steuerwald, S., and Bergmann, K. (1998). Coherent population transfer in NO with pulsed lasers: The consequences of hyperfine structure, doppler broadening and electromagnetically induced absorption. *Eur. Phys. J. D* **1,** 57–70.

Kuklinski, J. R., Gaubatz, U., Hioe, F. T., and Bergmann, K. (1989). Adiabatic population transfer in a three-level system driven by delayed laser pulses. *Phys. Rev. A* **40,** 6741–6744.

Kulin, S., Saubamea, B., Peik, E., Lawall, J., Hijmans, T. W., Leduc, M., and Cohen-Tannoudji, C. (1997). Coherent manipulation of atomic wave packets by adiabatic transfer. *Phys. Rev. Lett.* **78,** 4185–4188.

Kurzel, R. B., and Steinfeld, J. I. (1970). Energy-transfer processes in monochromatically excited iodine molecules. III. Quenching and multiquantum transfer from $v' = 43$. *J. Chem. Phys.* **53,** 3293–3303.

Külz, M., Kortyna, A., Keil, M., Schellhaass, B., and Bergmann, K. (1993). Vibrational dependence of negative-ion formation by dissociative attachment of low-energy electrons. *Phys. Rev. A* **48,** 4015–4018.

Külz, M., Kortyna, A., Keil, M., Schellhaass, B., and Bergmann, K. (1995). On the vibrational dependence of electron impact ionization of diatomic molecules. *Z. Phys. D* **33,** 109–117.

Külz, M., Keil, M., Kortyna, A., Schellhaass, B., Hauck, J., Bergmann, K., Meyer, W., and Weyh, D. (1996). Dissociative attachment of low-energy electrons to state-selected diatomic molecules. *Phys. Rev. A* **53,** 3324–3334.

Kylstra, N. J., Paspalakis, E., and Knight, P. L. (1998). Laser-induced continuum structure in helium: ab initio non-perturbative calculations. *J. Phys. B* **31,** L719–L728.

Laine, T. A., and Stenholm, S. (1996). Adiabatic processes in three-level systems. *Phys. Rev. A* **53,** 2501–2512.

Landau, L. D. (1932). Zur Theorie der Energie übertragung II. *Phys. Z. Sowjetunion* **2,** 46.

Lange, W., and Kimble, H. J. (2000). Dynamic generation of maximally entangled photon multiplets by adiabatic passage. *Phys. Rev. A* **61,** 063817.

Law, C. K., and Eberly, J. H. (1996). Arbitrary control of a quantum electromagnetic field. *Phys. Rev. Lett.* **76,** 1055–1058.

Law, C. K., and Eberly, J. H. (1998). Synthesis of arbitrary superposition of Zeeman states in an atom. *Opt. Express* **2,** 368–371.

Law, C. K., and Kimble, H. J. (1997). Deterministic generation of a bit-stream of single-photon pulses. *J. Mod. Opt.* **44,** 2067–2074.

Lawall, J., and Prentiss, M. (1994). Demonstration of a novel atomic beam splitter. *Phys. Rev. Lett.* **72,** 993–996.

Lawall, J., Bardou, F., Saubamea, B., Shimizu, K., Leduc, M., Aspect, A., and Cohen-Tannoudji, C. (1994). Two-dimensional subrecoil laser cooling. *Phys. Rev. Lett.* **73,** 1915–1918.

Lawall, J., Kulin, S., Saubaméa, B., Bigelow, N., Leduc, M., and Cohen-Tannoudji, C. (1995). Three-dimensional laser cooling of helium beyond the single-photon recoil limit. *Phys. Rev. Lett.* **75,** 4194–4197.

Lawall, J., Kulin, S., Saubamea, B., Bigelow, N., Leduc, M., and Cohen-Tannoudji, C. (1996). Subrecoil laser cooling into a single wavepacket by velocity-selective coherent population trapping followed by adiabatic passage. *Laser Phys.* **6,** 153–158.

Lindinger, A., Verbeek, M., and Rubahn, H.-G. (1997). Adiabatic population transfer by acoustooptically modulated laser beams. *Z. Phys. D* **39,** 93–100.

Liu, C., Dutton, Z., Pehroozi, C. H., and Hau, L. V. (2001). Observation of coherent optical information storage in an atomic medium using halted light pulses. *Nature* **409,** 490–493.

Lounis, B., and Cohen-Tannoudji, C. (1992). Coherent population trapping and Fano profiles. *J. Phys. II (France)* **2,** 579.

Loy, M. M. T. (1974). Observation of population inversion by optical adiabatic rapid passage. *Phys. Rev. Lett.* **32,** 814–817.

Lukin, M. D., and Imamoglu, A. (2000). Nonlinear optics and quantum entanglement of ultraslow single photons. *Phys. Rev. Lett.* **84,** 1419–1422.

Lukin, M. D., Fleischhauer, M., Zibrov, A. S., Robinson, H. G., Velichansky, V. L., Hollberg, L., and Scully, M. O. (1997). Spectroscopy in dense coherent media: Line narrowing and interference effects. *Phys. Rev. Lett.* **79,** 2959–2962.

Lukin, M. D., Yelin, S. F., and Fleischhauer, M. (2000). Entanglement of atomic ensembles by trapping correlated photon states. *Phys. Rev. Lett.* **84,** 4232–4235.

Mackie, M., and Javanainen, J. (1999). Quasicontinuum modeling of photoassociation. *Phys. Rev. A* **60,** 3174–3187.

Mackie, M., Kowalski, R., and Javanainen, J. (2000). Bose-stimulated Raman adiabatic passage in photoassociation. *Phys. Rev. Lett.* **84,** 3803–3806.

Malinovsky, V. S., and Tannor, D. J. (1997). Simple and robust extension of the stimulated Raman adiabatic passage technique to N-level systems. *Phys. Rev. A* **56,** 4929–4937.

Marangos, J. P. (1998). Electromagnetically induced transparency. *J. Mod. Opt.* **45,** 471–503.

Marte, P., Zoller, P., and Hall, J. L. (1991). Coherent atomic mirrors and beam splitters by adiabatic passage in multilevel systems. *Phys. Rev. A* **44,** 4118–4121.

Martin, J., Shore, B. W., and Bergmann, K. (1995). Coherent population transfer in multilevel systems with magnetic sublevels. II. Algebraic analysis. *Phys. Rev. A* **52,** 583–593.

Martin, J., Shore, B. W., and Bergmann, K. (1996). Coherent population transfer in multilevel systems with magnetic sublevels. III. Experimental results. *Phys. Rev. A* **54,** 1556–1569.

Matsko, A., Rostovstsev, Y. V., Fleischhauer, M., and Scully, M. O. (2001). Anomalous Brillouin scattering via ultra-slow light. *Phys. Rev. Lett.,* in press.

Mattheus, A., Fischer, A., Ziegler, G., Gottwald, E. E., and Bergmann, K. (1986). Experimental proof of $\Delta m \ll J$ propensity rule in rotationally inelastic differential scattering. *Phys. Rev. Lett.* **56,** 712–715.

Meier, W., Ahlers, G., and Zacharias, H. (1986). State selective population of H_2 ($v' = 1$, $J' = 1$) and D_2 ($v' = 1$, $J' = 2$) and rotational relaxation in collisions with H_2, D_2, and He. *J. Chem. Phys.* **85,** 2599–2608.

Messiah, A. (1962). "Quantum Mechanics." North-Holland, New York.

Milner, V., and Prior, Y. (1998). Multilevel dark states: Coherent population trapping with elliptically polarized incoherent light. *Phys. Rev. Lett.* **80,** 940–943.

Morigi, G., Featonby, P., Summy, G., and Foot, C. (1996). Calculation of the efficiencies and phase shifts associated with an adiabatic transfer atom interferometer. *Quant. Semiclass. Opt.* **8,** 641–653.

Morris, J. R., and Shore, B. W. (1983). Reduction of degenerate two-level excitation to independent two-state systems. *Phys. Rev. A* **27,** 906–912.

Nakajima, T. (1999). Population transfer in N-level systems assisted by dressing fields. *Phys. Rev. A* **59,** 559–568.

Nakajima, T., and Lambropolous, P. (1996). Population transfer through an autoionizing state by pulse delay. *Z. Phys. D* **36,** 17–22.

Nakajima, T., Elk, M., Zhang, J., and Lambropoulos, P. (1994). Population transfer through the continuum. *Phys. Rev. A* **50,** R913–R916.

Newton, R. G., and Young, B.-L. (1968). Measurability of the spin density matrix. *Ann. Phys. (New York)* **49,** 393–402.

Oreg, J., Hioe, F. T., and Eberly, J. H. (1984). Adiabatic following in multilevel systems. *Phys. Rev. A* **29,** 690–697.

Oreg, J., Bergmann, K., Shore, B. W., and Rosenwaks, S. (1992). Population transfer with delayed pulses in four-state systems. *Phys. Rev. A* **45,** 4888–4896.

Orr, B. J., Haub, J. G., and Haines, R. (1984). Time-resolved infrared-ultraviolet double-resonance studies of rotational relaxation in D_2CO. *Chem. Phys. Lett.* **107,** 168.

Parkins, A. S., and Kimble, H. J. (1999). Quantum state transfer between motion and light. *J. Opt. B* **1,** 496–504.

Parkins, A. S., Marte, P., Zoller, P., and Kimble, H. J. (1993). Synthesis of arbitrary quantum states via adiabatic transfer of Zeeman coherence. *Phys. Rev. Lett.* **71,** 3095–3098.

Parkins, A. S., Marte, P., Zoller, P., Carnal, O., and Kimble, H. J. (1995). Quantum-state mapping between multilevel atoms and cavity light fields. *Phys. Rev. A* **51,** 1578–1796.

Paspalakis, E., and Knight, P. L. (1998). Population transfer via an autoionizing state with temporally delayed chirped laser pulses. *J. Phys. B* **31,** 2753–2767.

Paspalakis, E., Protopapas, M., and Knight, P. L. (1997). Population transfer through the continuum with temporally delayed chirped laser pulses. *Opt. Commun.* **142,** 34–40.

Paspalakis, E., Protopapas, M., and Knight, P. L. (1998). Time-dependent pulse and frequency effects in population trapping via the continuum. *J. Phys. B* **31,** 775–794.

Pellizzari, T. (1997). Quantum networking with optical fibres. *Phys. Rev. Lett.* **79,** 5242–5245.

Pellizzari, T., Gardiner, S. A., Cirac, J. I., and Zoller, P. (1995). Decoherence, continuous observation, and quantum computing: A cavity QED model. *Phys. Rev. Lett.* **75,** 3788–3791.

Pesl, F. (1999). Ph.D. thesis. University of Kaiserslautern, Kaiserslautern, Germany.

Phillips, W. D. (1998). Nobel lecture: Laser cooling and trapping of neutral atoms. *Rev. Mod. Phys.* **70,** 721–742.

Phillips, D. F., Fleischhauer, A., Mair, A., Walsworth, R. L., and Lukin, M. D. (2001). Storage of light in atomic vapor. *Phys. Rev. Lett.* **86,** 783–786.

Pillet, P., Valentin, C., Yuan, R.-L., and Yu, J. (1993). Adiabatic population transfer in a multilevel system. *Phys. Rev. A* **48,** 845–848.

Rickes, T., Yatsenko, L. P., Steuerwald, S., Halfmann, T., Shore, B. W., Vitanov, N. V., and Bergmann, K. (2000). Efficient adiabatic population transfer by two-photon excitation assisted by a laser-induced Stark shift. *J. Chem. Phys.* **113,** 534–546.

Riehle, F., Kisters, T., Witte, A., Helmcke, J., and Bord, C. J. (1991). Optical Ramsey spectroscopy in a rotating frame: Sagnac effect in a matter-wave interferometer. *Phys. Rev. Lett.* **67,** 177–180.

Rodriguez, M., Garraway, B. M., and Suominen, K.-A. (2000). Tailoring of vibrational state populations with light-induced potentials in molecules. *Phys. Rev. A* **62,** 53413.

Romanenko, V. I., and Yatsenko, L. P. (1997). Adiabatic population transfer in the three-level lambda-system: Two-photon lineshape. *Opt. Commun.* **140,** 231–236.

Rubahn, H.-G., and Bergmann, K. (1990). Effect of laser-induced vibrational bond stretching in atom-diatom collisions. *Annu. Rev. Phys. Chem.* **41,** 735–773.

Rubahn, H.-G., Konz, E., Schiemann, S., and Bergmann, K. (1991). Alignment of electronic angular momentum by stimulated Raman scattering with delayed pulses. *Z. Phys. D* **22,** 401–406.

Schiemann, S., Kuhn, A., Steuerwald, S., and Bergmann, K. (1993). Efficient coherent population transfer in NO molecules using pulsed lasers. *Phys. Rev. Lett.* **71,** 3637–3640.

Series, G. W. (1978). A semiclassical approach to radiation problems. *Phys. Rep.* **43,** 1–41.

Shore, B. W. (1990). "The Theory of Coherent Atomic Excitation." Wiley, New York.

Shore, B. W. (1995). Examples of counter-intuitive physics (atomic and molecular excitation). *Contemp. Phys.* **36,** 15–28.

Shore, B. W., Bergmann, K., Oreg, J., and Rosenwaks, S. (1991). Multilevel adiabatic population transfer. *Phys. Rev. A* **44,** 7442–7447.

Shore, B. W., Bergmann, K., Kuhn, A., Schiemann, S., Oreg, J., and Eberly, J. H. (1992a). Laser-induced population transfer in multistate systems: A comparative study. *Phys. Rev. A* **45,** 5297–5300.

Shore, B. W., Bergmann, K., and Oreg, J. (1992b). Coherent population transfer: stimulated Raman adiabatic passage and the Landau-Zener picture. *Z. Phys. D* **23,** 33–39.

Shore, B. W., Martin, J., Fewell, M. P., and Bergmann, K. (1995). Coherent population transfer in multilevel systems with magnetic sublevels. I. Numerical studies. *Phys. Rev. A* **52,** 566–582.

Smith, A. V. (1992). Numerical studies of adiabatic population inversion in multilevel systems. *J. Opt. Soc. Am. B* **9,** 1543–1551.

Solá, I. R., Malinovsky, V. S., and Tannor, D. J. (1999). Optimal pulse sequences for population transfer in multilevel systems. *Phys. Rev. A* **60,** 3081–3090.

Solá, I. R., Santamaría, J., and Malinovsky, V. S. (2000). Efficiency and robustness of adiabatic passage by light-induced potentials. *Phys. Rev. A* **61,** 043413.

Steane, A. (1998). Quantum computing. *Rep. Prog. Phys.* **61,** 117–173.

Suominen, K.-A., and Garraway, B. M. (1992). Population transfer in a level-crossing model with two time scales. *Phys. Rev. A* **45,** 374–386.

Süptitz, W., Duncan, B. C., and Gould, P. L. (1997). Efficient 5d excitation of trapped Rb atoms using pulses of diode-laser light in the counterintuitive order. *J. Opt. Soc. Am. B* **14,** 1001–1008.

Theuer, H., and Bergmann, K. (1998). Atomic beam deflection by coherent momentum transfer and the dependence on weak magnetic fields. *Eur. Phys. J. D* **2,** 279–289.

Theuer, H., Unanyan, R. G., Habscheid, C., Klein, K., and Bergmann, K. (1999). Novel laser controlled variable matter wave beamsplitter. *Opt. Express* **4,** 77–83.

Unanyan, R., Fleischhauer, M., Shore, B. W., and Bergmann, K. (1998a). Robust creation and phase-sensitive probing of superposition states via stimulated Raman adiabatic passage (STIRAP) with degenerate dark states. *Opt. Commun.* **155,** 144–154.

Unanyan, R. G., Vitanov, N. V., and Stenholm, S. (1998b). Suppression of incoherent ionization in population transfer via continuum. *Phys. Rev. A* **57,** 462–466.

Unanyan, R. G., Shore, B. W., and Bergmann, K. (1999). Laser-driven population transfer in four-level atoms: Consequences of non-Abelian geometrical adiabatic phase factors. *Phys. Rev. A* **59,** 2910–2919.

Unanyan, R. G., Vitanov, N. V., Shore, B. W., and Bergmann, K. (2000a). Coherent properties of a tripod system coupled via a continuum. *Phys. Rev. A* **61,** 043408.

Unanyan, R., Guerin, S., Shore, B. W., and Bergmann, K. (2000b). Efficient population transfer by delayed pulses despite coupling ambiguity. *Eur. Phys. J. D* **8,** 443–449.

Unanyan, R. G., Guérin, S., and Jauslin, H. R. (2000c). Coherent population trapping under bichromatic fields. *Phys. Rev. A* **62,** 043407.

Valentin, C., Yu, J., and Pillet, P. (1994). Adiabatic transfer In $J \rightarrow J$ and $J \rightarrow J - 1$ transitions. *J. Phys. II (France)* **4,** 1925–1937.

van Enk, S. J., Kimble, H. J., Cirac, J. I., and Zoller, P. (1999). Quantum communication with dark photons. *Phys. Rev. A* **59,** 2659–2664.

Vardi, A., and Shapiro, M. (1996). Two-photon dissociation/ionization beyond the adiabatic approximation. *J. Chem. Phys.* **104,** 5490–5496.

Vardi, A., Abrashkevich, D., Frishman, E., and Shapiro, M. (1997). Theory of radiative recombination with strong laser pulses and the formation of ultracold molecules via stimulated photorecombination of cold atoms. *J. Chem. Phys.* **107,** 6166–6174.

Vardi, A., Shapiro, M., and Bergmann, K. (1999). Complete population transfer to and from a continuum and the radiative association of cold Na atoms to produce translationally cold Na_2 molecules in specific vib-rotational states. *Opt. Express* **4,** 91–106.

Vitanov, N. V. (1995). Complete population return in a two-state system driven by a smooth asymmetric pulse. *J. Phys. B* **28,** L19–L22.

Vitanov, N. V. (1998a). Adiabatic population transfer by delayed laser pulses in multistate systems. *Phys. Rev. A* **58,** 2295–2309.

Vitanov, N. V. (1998b). Analytic model of a three-state system driven by two laser pulses on two-photon resonance. *J. Phys. B* **31,** 709–725.

Vitanov, N. V. (1999). Pulse-order invariance of the initial-state population in multistate chains driven by delayed laser pulses. *Phys. Rev. A* **60,** 3308–3310.

Vitanov, N. V. (2000). Measuring a coherent superposition of multiple states. *J. Phys. B* **33,** 2333–2346.

Vitanov, N. V. (2001). Two-photon line width in stimulated Raman adiabatic passage. To be published.

Vitanov, N. V., and Knight, P. L. (1995). Coherent excitation by asymmetric pulses. *J. Phys. B* **28,** 1905–1920.

Vitanov, N. V., and Stenholm, S. (1996). Non-adiabatic effects in population transfer in three-level systems. *Opt. Commun.* **127,** 215–222.

Vitanov, N. V., and Stenholm, S. (1997a). Properties of stimulated Raman adiabatic passage with intermediate-level detuning. *Opt. Commun.* **135,** 394–405.

Vitanov, N. V., and Stenholm, S. (1997b). Analytic properties and effective two-level problems in stimulated Raman adiabatic passage. *Phys. Rev. A* **55,** 648–660.

Vitanov, N. V., and Stenholm, S. (1997c). Population transfer by delayed pulses via continuum states. *Phys. Rev. A* **56,** 741–747.

Vitanov, N. V., and Stenholm, S. (1997d). Population transfer via a decaying state. *Phys. Rev. A* **56,** 1463–1471.

Vitanov, N. V., and Stenholm, S. (1999). Adiabatic population transfer via multiple intermediate states. *Phys. Rev. A* **60,** 3820–3832.

Vitanov, N. V., Shore, B. W., and Bergmann, K. (1998). Adiabatic population transfer in multistate chains via dressed intermediate states. *Eur. Phys. J. D* **4,** 15–29.

Vitanov, N. V., Suominen, K.-A., and Shore, B. W. (1999). Creation of coherent atomic superpositions by fractional stimulated Raman adiabatic passage. *J. Phys. B* **32,** 4535–4546.

Vitanov, N. V., Shore, B. W., Unanyan, R. G., and Bergmann, K. (2000). Measuring a coherent superposition. *Opt. Commun.* **179,** 73–83.

Vitanov, N. V., Halfmann, T., Shore, B. W., and Bergmann, K. (2001). Laser-induced population transfer by adiabatic passage techniques. *Annu. Rev. Phys. Chem.* **52,** 763–809.

Webb, C. L., Godun, R. M., Summy, G. S., Oberthaler, M. K., Featonby, P. D., Foot, C. J., and Burnett, K. (1999). Measurement of Berry's phase using an atom interferometer. *Phys. Rev. A* **60,** R1783–R1786.

Weitz, M., Young, B. C., and Chu, S. (1994a). Atomic interferometer based on adiabatic population transfer. *Phys. Rev. Lett.* **73,** 2563–2566.

Weitz, M., Young, B. C., and Chu, S. (1994b). Atom manipulation based on delayed laser pulses in three- and four-level systems: Light shifts and transfer efficiencies. *Phys. Rev. A* **50,** 2438–2444.

Weitz, M., Heupel, T., and Hänsch, T. W. (1996). Multiple beam atomic interferometer. *Phys. Rev. Lett.* **77,** 2356–2359.

Williams, C. P., and Clearwater, S. H. (1997). "Explorations in Quantum Computing." Springer-Verlag, Berlin.

Yatsenko, L. P., Unanyan, R. G., Bergmann, K., Halfmann, T., and Shore, B. W. (1997). Population transfer through the continuum using laser-controlled Stark shifts. *Opt. Commun.* **135,** 406–412.

Yatsenko, L. P., Guerin, S., Halfmann, T., Boehmer, K., Shore, B. W., and Bergmann, K. (1998). Stimulated hyper-Raman adiabatic passage. I. The basic problem and examples. *Phys. Rev. A* **58,** 4683–4690.

Yatsenko, L. P., Halfmann, T., Shore, B. W., and Bergmann, K. (1999a). Photoionization suppression by continuum coherence: Experiment and theory. *Phys. Rev. A* **59,** 2926–2947.

Yatsenko, L. P., Shore, B. W., Halfmann, T., Bergmann, K., and Vardi, A. (1999b). Source of metastable H(2s) atoms using the Stark chirped rapid-adiabatic-passage technique. *Phys. Rev. A* **60,** R4237–R4240.

Zener, C. (1932). Non-adiabatic crossing of energy levels. *Proc. R. Soc. London Ser. A* **137,** 696–969.

Ziegler, G., Rädle, M., Pütz, O., Jung, K., Ehrhardt, H., and Bergmann, K. (1987). Rotational rainbows in electron scattering. *Phys. Rev. Lett.* **58,** 2642–2645.

Ziegler, G., Kumar, S. V. K., Dittmann, P., and Bergmann, K. (1988). Effect of vibrational bond stretching in rotationally inelastic electron-molecule scattering. *Z. Phys. D* **10,** 247–252.